UNIVERSITÉ DU QUÉBEC À MONTRÉAL

LINKING ECOSYSTEM METABOLISM AND GREENHOUSE GAS DYNAMICS IN NORTHERN LAKES

THESIS

PRESENTED

AS PARTIAL REQUIREMENT

OF THE DOCTORAT OF BIOLOGY

BY

MATTHEW J. BOGARD

MAY 2017

UNIVERSITÉ DU QUÉBEC À MONTRÉAL

LIENS ENTRE LE MÉTABOLISME DES ÉCOSYSTÈMES ET LA DYNAMIQUE DES GAZ À EFFET DE SERRE DANS LES LACS DU NORD

THÈSE

PRESENTÉE

COMME EXIGENCE PARTIELLE

DU DOCTORAT EN BIOLOGIE

PAR

MATTHEW J. BOGARD

MAI 2017

ACKNOWLEDGEMENTS

Writing this section has been an incredibly humbling experience. I have received a mountain of support from many wonderful people in my life, as well as multiple funding agencies, without which this project would not have been possible.

First, I thank the funding agencies that have supported me directly (NSERC, UQAM, FQRNT-GRIL, SCL) and have supported me through the funding of the del Giorgio lab and CarBBAS research program (NSERC, Hydro-Québec), thank you for making this possible.

I thank my supervisor Paul del Giorgio for his guidance, academic and financial support, encouragement, and enthusiasm. Paul, thank you for your honest and open minded scientific approach, and for always pushing to make each of my chapters as thorough and meaningful as possible. You are a remarkable scientist and person, and it has been a privilege to work with you. Next, I thank my committee members and examiners (Chris Solomon, Yves Prairie, David Bird, Bill Taylor and Paul Hanson) for all taking the time to read my work and for providing such thoughtful and excellent feedback. I thank Yves also for his open door and willingness to help me through some of the technical aspects of my project, and Alison Derry for her support and generous partnership on the mesocosm experiment. I thank the GRIL-UQAM professors (Alison, Yves, plus Dolors Planas, Beatrix Beisner, David Bird) for the use of their spaces and equipment, and most importantly for working so hard to make the UQAM-GRIL a fun, respectful, and exciting group. The GRIL staff (Claudette Blanchard, Marie-Andrée Fallu, P.O. Benoit, and Katherine Velghe) and the U. de M.-SBL staff (Roxane Maranger, Jacques Mercier, and Eric Valiquette) have helped me greatly along the way, and I thank them for their support. I thank Tom Battin of the EPFL for his incredible generosity, and his team for supporting and welcoming me during my visit to the SBER lab. This was truly a once in a lifetime opportunity, both scientifically and personally.

I would have been lost without all the support and guidance from my friends and colleagues in the del Giorgio lab: Thank you to Dominic Vachon, Nicolas Fortin St. Gelais, Carolina Garcia Chaves, Adam Heathcote, Erin Hotchkiss, Karelle Desrosiers, Marie Gerardin, JF Lapierre, Francois Guillemette, Juan Pablo Nino Garcia, Marilyne Robidoux, Clara Ruiz Gonzalez, Terhi Rasilo, Ryan Hutchins, Shoji Thottathil, Ming-Feng Li, Julia Jakobssen, Roy Nahas, Audrey Campeau, Lennie Boutet, Katherie Deschamps, Mathieu Dumais, Julien, Simon Gauthier Fauteaux, Marie-Eve Ferland, and especially Alice Parkes and Annick St. Pierre, for keeping the wheels on the wagon through their incredible commitment and hard work. I thank my collaborators Dom, Nico, Lennie, and Caro for their scientific input and contributions of time and data in 3 of my chapters. An extra special thanks to Rich Vogt for his long standing friendship prior to and during his time with the CarBBAS group, and to Tonya delSontro and Cynthia Soued for their kindness and support; the

three of you have been there to listen and help me through many challenging aspects of this work. You have been wonderful friends and I really appreciate everything you have done for me. To the entire CarBBAS group, you have generously shared your time, knowledge, cultures, and I thank you for making the past 5 years a lot of fun.

I thank Jacob Ziegler for being such a great friend, climbing partner, and technical resource over the years, as well as Peter Leavitt for his support and mentorship; Peter, you have always been there for me, and I am incredibly grateful for this. I am also indebted to David Butman for his support and understanding during the late stages of this writing process.

Finally, my family has supported me every step of the way. Mom, Dad, Brenda, and Bill, I don't even know where to begin; you have helped us get through this, in every way possible, and I cannot thank you enough. I love you all and am so grateful for your help and support. Mom, thanks also for being such a great friend and for always being there to talk, this means more to me than you know. Lecia, William, Jon, Andrea, John, Amanda and Kurt, thank you all for the support; we are so fortunate to have you in our lives. Your visits, phone calls, hand-me-downs, babysitting, and most importantly your love and encouragement over the years have been an amazing gift. Of course, I cannot forget my nieces and nephews; Meg, Evie, Nicholas and Liam, thank you for your love and joy, your face time calls, and not to mention, inspirational dance videos! You are truly an amazing family, and having you in my life is a remarkable gift; I love you all so much.

Most importantly, my wife Holly and children Kalani and Lev have provided me with unwavering love, support, encouragement, and have kept my life as balanced as possible throughout this process. Holly, you are such a strong, intelligent, and beautiful person. You are an amazing source of knowledge, adventure, and inspiration. You pour everything you have into caring for our family and have sacrificed so much for me to pursue this degree, words cannot capture my gratitude. We have been through so much together, especially in the past 5 years, and the fact that I have you to share it all with is the best part of the journey. Thank you for inspiring me to always strive for improvement in my life. Kalani and Lev, the joy and happiness you bring me is truly remarkable and has helped me immensely through the challenging parts of this program. There are many perks to being a graduate student, and one of the greatest has been the flexibility to be so present in your lives. Watching you grow and discover the world over the years is one of the most precious experiences I may ever have. At the same time, you have made me grow and discover the world too, in ways I could never have expected. Thank you for bringing such new and profound meaning to my life.

DEDICATION

I dedicate this work to my family; Holly, Kalani, and Lev. Thank you for being the light in my life. I love you.

TABLE OF CONTENTS

ACKNOWLEDGEMENTS i
DEDICATION iii
TABLE OF CONTENTS v
LIST OF FIGURES xi
LIST OF TABLES xv
RÉSUMÉ xvii
SUMMARY xix
INTRODUCTION 1
0.1 Context 1
0.1.1 Boreal lakes in the global C cycle 2
0.1.2 The role of lake metabolism in shaping patterns of GHG flux 2
0.2 Thesis Objectives 6
0.3 General Approach 9
0.3.1 Measuring gas dynamics and lake metabolism 9
0.3.2 Mesocosm experiment 10
0.3.3 Lake sampling 10
CHAPTER I
USING OXYGEN STABLE ISOTOPES TO QUANTIFY ECOSYSTEM METABOLISM IN NORTHERN LAKES 13
1.1 ABSTRACT 15
1.2 INTRODUCTION 17
1.2.1 Description of the oxygen isotopic approach 22
1.2.2 Uncertainties linked to the isotopic approach 27
1.3 MATERIALS AND METHODS 31
1.3.1 Sensitivity analyses 31

1.3.2 Field validation 32
1.3.3 Field and laboratory methods 34
1.3.4 Quantification of air/water gas exchange and fluxes 35
1.3.5 Estimating mesocosm and lake α_C values 36
1.3.6 Error analyses 37
1.4 RESULTS AND DISCUSSION 35
1.4.1 Results and implications of sensitivity analyses 39
1.4.2 Model performance and comparisons in mesocosm experiments 43
1.4.3 Model performance and comparison in lakes 48
1.4.4 Assessing uncertainties in model parameters 61
1.4.5 Summary and Conclusions 63
1.5 ACKNOWEDGEMENTS 67
1.6 SUPPLEMENTARY INFORMATION 69
1.6.1 Supplement 1: Photomineralization experiment 69
1.6.2 Supplement 2: Sensitivity Analyses 71
1.6.3 Supplement 3: Mesocosm experiment 72
CHAPTER II
EMERGENT PATTERNS IN ECOSYSTEM METABOLISM ACROSS BOREAL LAKES 75
2.1 ABSTRACT 77
2.2 INTRODUCTION 79
2.3 METHODS 83
2.3.1 Study area and sampling approach 83
2.3.2 Climate and catchment characteristics 83
2.3.3 Lake physical and morphometric characteristics 86
2.3.4 Laboratory analyses 87
2.3.5 NEP and gas flux 87
2.3.6 Stable isotopic estimates of GPP, R, and GPP:R 88
2.3.7 Statistical methods 92

2.4 RESULTS 95
2.4.1 Cross-lake and inter-regional patterns in lake metabolism 95
2.4.2 Limnological predictors of lake metabolism 98
2.4.3 Combined catchment and lake predictors of metabolism 100
2.5 DISCUSSION 107
2.5.1 Whole-lake versus habitat-specific lake metabolism 108
2.5.2 Trends in lake metabolism along DOC and light gradients 113
2.5.3 Temperature effects on lake metabolism 115
2.5.4 Mechanisms underpinning landscape patterns of lake metabolism . 116
2.6 ACKNOWLEDGEMENTS 119
2.7 SUPPLEMENTARY INFORMATION 121
2.7.1 Supplementary Figures 121
2.7.2 Supplementary Tables 123
CHAPTER III
THE ROLE OF METABOLISM IN MODULATING CO_2 FLUXES IN BOREAL LAKES 127
3.1 ABSTRACT 129
3.2 INTRODUCTION 131
3.3 METHODS 137
3.3.1 Study Area and Sampling Approach 137
3.3.2 Climate and Catchment Characteristics 140
3.3.3 Laboratory Analyses 140
3.3.4 Isotopic Analyses 141
3.3.5 Calculating Gas Flux and NEP 142
3.3.6 Isotopic estimates of GPP : R 144
3.3.7 Lake CO_2 Excess Emissions and Mass Balance Calculations 146
3.3.8 Statistical Methods 147
3.4 RESULTS 149
3.4.1 Patterns of CO_2 and metabolic dynamics 149
3.4.2 Categorizing lakes by NEP and CO_2 flux 153

3.4.3 Differentiating the 3 categories of lakes 157
3.4.4 Deviation of CO_2 flux from NEP ($\Delta_{emissions}$) 159
3.4.5 Exploring the drivers of $\Delta_{emissions}$ 159
3.5 DISCUSSION 165
3.5.1 CO_2 fluxes track metabolism in most lakes 166
3.5.2 Methodological effects on $\Delta_{emissions}$ variability 167
3.5.3 Patterns of excess CO_2 flux – predominance in autotrophic outgassing lakes 168
3.5.4 Catchment structure shapes the CO_2-NEP relationship 170
3.5.5 Sources of excess CO_2 flux 171
3.5.6 Implications for regional C balances 176
3.6 ACKNOWLEDGEMENTS 179
3.7 SUPPORTING INFORMATION 181
3.7.1 Supporting Figures 181
3.7.2 Supporting Tables 188
3.7.3 Supporting Text S3.1: Exploring the validity of methodological assumptions 189
CHAPTER IV
OXIC WATER COLUMN METHANOGENESIS AS A MAJOR COMPONENT OF AQUATIC CH_4 FLUXES 193
4.1 ABSTRACT 195
4.2 INTRODUCTION 197
4.3 RESULTS 201
4.3.1 CH_4 dynamics in experimental enclosures 201
4.3.2 Linking CH_4 production to algal dynamics 204
4.3.3 Identifying the biochemical source of CH_4 207
4.3.4 Rates of oxic water-column methanogenesis 210
4.3.5 Oxic water methanogenesis in a whole-lake perspective 210
4.4 DISCUSSION 213
4.5 METHODS 223

4.5.1 Study site 223
4.5.2 Experimental design 223
4.5.3 Limnological measurements 224
4.5.4 CH_4 chamber flux estimates 225
4.5.5 Isotopic analyses 226
4.5.6 Numerical methods 227
4.5.7 Apparent isotopic fractionation of methanogenesis 228
4.5.8 Mesocosm mass balances 230
4.5.9 Whole-Lake CH_4 dynamics 231
4.5.10 Data compilation for meta-analysis 233
4.6 CONCLUDING NOTES 235
4.6.1 Acknowledgements 235
4.6.2 Author contributions 235
4.6.3 Competing Financial Interests 236
4.7 SUPPLEMENTARY INFORMATION 237
4.7.1 Supplementary Figures 237
4.7.2 Supplementary Tables 242
4.7.3 Supplementary Notes 247
4.7.4 Supplementary Methods: Estimates of cross-membrane CH_4 flux... 249
GENERAL CONCLUSIONS 253
5.1 Key contributions 253
5.2 Implications 257
REFERENCES 261

LIST OF FIGURES

Figure Page

0.1. Overall thesis objective, and chapter specific themes. 8
1.1. Schematic representation of lake oxygen and $\delta^{18}O$ dynamics involved in the oxygen isotope metabolic approach. 20
1.2. Sensitivity analyses investigating how the simultaneous manipulation of model input terms alters estimates of respiration (R) and gross primary production (GPP) in the $\delta^{18}O$ isotopic mass balance model. 42
1.3. Oxygen and metabolic patterns in the experimental enclosures. 46
1.4. Biplot of dissolved oxygen (DO) departure from equilibrium with the atmosphere versus DO isotopic signature ($\delta^{18}O$) for the two study lakes. 49
1.5. High frequency (hourly) mixed layer measurements for Lac Croche (red) and Simoncouche (blue). 52
1.6. Physico-chemical conditions in Lac Simoncouche (a, b, c) and Lac Croche (d, e, f) during the 2011 ice-free season. 53
1.7. Relative contribution of epilimnetic metabolism as a function of the ratio of mixed layer depth (Z_{mix}) to euphotic zone depth (Z_{eu}). 54
1.8. Temporal patterns in ecosystem metabolism in (a) Lac Croche and (b) Simoncouche. 59
S1.2. Sensitivity analysis investigating how the independent manipulation of model input terms alters estimates of respiration (R) and gross primary production (GPP) in the $\delta^{18}O$ isotopic mass balance model. 71
S1.3.1. Diel wind speeds (a) were used to estimate (b) the air water gas exchange coefficient (k_{O2}) for weeks 2 and 5 (white and black circles respectively)..... 72
S1.3.2. Vertical profiles of physico-chemical conditions during week 2 of the mesocosm experiment. 73

2.1. Landscape-level shifts in lake ecosystem metabolism throughout north-eastern Canada. 85
2.2. Direct drivers of lake ecosystem metabolism. 99
2.3. Hierarchical control of landscape-level metabolic variability in northern lakes. ..... .106
2.4. Ecosystem-scale metabolic patterns deviate from community assessments in northern lakes. 111
S2.1. Histograms depicting the distribution of surface-water metabolism in our study lakes. 121
S2.2. Principal components analysis (PCA) summarizing the relationship among landscape characteristics of individual lake catchments. 122
3.1. Histogram of (a) surface water pCO_2, (b) daily air-water CO_2 flux, (c) rates of net ecosystem production (NEP), and (d) the ratio of GPP : R. 151
3.2. How partial pressure of CO_2 (pCO_2) relates to indicies of lake metabolism and C cycling in the surface mixed layer of boreal lakes. 152
3.3. Comparing patterns of aerobic metabolism and biotic CO_2 production to surface emissions from boreal lakes. 155
3.4. Environmental and limnological conditions associated with each lake Group from Fig. 3.3a (Auto + out = net autotrophic and CO_2 out-gassing, Het + Out = net heterotrophic and CO_2 out-gassing, Auto + In = net autotrophic and CO_2 ingassing). 158
3.5. Predictors of excess CO_2 emissions ($\Delta_{emissions}$; Fig. 3.3) were assessed using partial least squares regression analysis (PLS) on a subset of boreal lakes (n = 155). 161
3.6. For the same subset of lakes examined in Fig. 3.2c (n = 68), we compared $\delta^{13}C$-CO_2 and the deviation of CO_2 flux rates from the metabolic reference line ($\Delta_{emissions}$; see Fig. 3.3a). 164
3.7. Mass balance calculation estimating the hypothetical pCO_2 needed for incoming water in order to sustain the observed $\Delta_{emissions}$ rates (i.e., rates of lake CO_2 emissions exceeding rates of NEP, as presented in Fig. 3.3a). ... 174
3.8. Environmental and limnological conditions associated with lakes for which mass-balance derived pCO_2 of incoming water was within, or above a reasonable range based on known ranges of stream- and groundwater pCO_2 (see Fig. 3.7). ..... .175
S3.1. Physical conditions in boreal sampling regions. 181
S3.2. Isotopic composition of boreal lake surface water. 182
S3.3. Replotting of Fig. 3.3a from main text, but with untransformed axes. 183

S3.4. Exploring hourly summertime gas dynamics using previously published data (Vachon and del Giorgio, 2014) from two of our northern Canadian lakes (Lac Croche, white fill; Lac Simoncouche, blue fill). 184
S3.5. Patterns of isotopically-derived metabolic balance estimates (ratio of gross primary production to respiration; GPP : R) for surface waters of Lac Simoncouche, one of two reference lakes described in Fig. S3.3. 186
S3.6. Summertime CO_2 dynamics based on previously published data (Vachon and del Giorgio, 2014) from two of our northern Canadian lakes (presented in Fig. S3.3; Lac Croche, white fill; Lac Simoncouche, blue fill). 187
4.1. Surface water CH_4 dynamics in experimental enclosures. 203
4.2. Linking pelagic ecosystem metabolism and CH_4 dynamics. 206
4.3. Assessing the biochemical source of pelagic CH_4. 208
4.4. Linking dissolved CH_4 and algal biomass across diverse open-water aquatic ecosystems. 219
S4.1. Mesocosm water-column profiles. 237
S4.2. Daily atmospheric gas-exchange dynamics for the mesocosms and the lake. 239
S4.3. Daily average weather patterns recorded at the field station near Lac Cromwell. 240
S4.4. Mesocosm methane oxidation (MOX) dynamics..... 241

LIST OF TABLES

Table Page

1.1. Experimentally derived isotopic fractionation factors (α_{photo}) associated with dissolved O_2 uptake and changes in isotopic signature ($\delta^{18}O$-O_2) during the photo-oxidation of dissolved organic matter. 24

2.1. Regional correlations between metabolism and environmental characteristics. 97

2.2. Summary of the top multiple regression models predicting lake GPP, R, GPP:R, and NEP from a combination of lake and catchment characteristics..... 102

S2.1. Multiple regression results including models of GPP and R. 123

S2.2. Multiple regression results including models of GPP:R and NEP. 125

3.1. Regional, catchment, and lake-specific environmental characteristics associated with eastern Canadian boreal lakes (n = 187) sampled in this study. 139

3.2. Top limnological and environmental predictors of $\Delta_{emissions}$ (mg C m^{-2} d^{-1}) for Canadian boreal lakes (n = 139). 162

S3.1. Correlation strength of lake water d-excess (‰) to individual environmental variables. 188

4.1. Greenhouse gas dynamics in Lac Cromwell. 212

S4.1. Estimates of zooplankton CH_4 release in ambient enclosures. 242

S4.2. Mass balance estimates of methanogenesis in ambient enclosures. 243

S4.3. Raw data and assembly methods for open-water CH_4 and chlorophyll a (chl a) meta-analysis. 244

RÉSUMÉ

Les lacs nordiques fournissent de nombreux services écosystémiques à l'humanité, dont l'un est de soutenir l'effet de serre planétaire via leurs émissions de dioxyde de carbone (CO_2) et de méthane (CH_4) vers l'atmosphère. Malgré l'importance grandissante de ce phénomène, nous ne comprenons toujours pas clairement le rôle que jouent les réseaux trophiques aquatiques dans la régulation des flux de gaz à effet de serre (GES), en grande partie parce que les mesures de métabolisme à l'échelle de l'écosystème sont rares pour cette vaste région du globe. Cette lacune constitue un obstacle majeur à notre interprétation mécaniste du cycle aquatique des GES. Pour aider à surmonter ce problème, cette thèse explore collectivement les tendances du métabolisme des écosystèmes et le lien entre les réseaux trophiques et la dynamique des GES dans les lacs nordiques.

Dans le chapitre 1, nous quantifions le métabolisme des lacs en utilisant une approche puissante, mais sous-utilisée, reposant sur le bilan de masse isotopique de l'oxygène. Nous examinons d'abord la théorie et la méthodologie de cette approche pour ensuite la tester à l'aide d'une simulation, une expérience in-situ et ce, dans deux lacs aux caractéristiques limnologiques distinctes. Nous concluons qu'avec une compréhension suffisante des caractéristiques physiques des lacs, cette approche isotopique de l'oxygène peut efficacement capturer les taux spatialement et temporellement intégrés de production primaire brute (PPB) et de respiration (R) des écosystèmes dans les lacs nordiques oligotrophiques et mesotrophiques.

Dans le chapitre 2, nous appliquons cette approche isotopique de l'oxygène pour une série de lacs présents sur un vaste territoire (~ 10^6 km^2) représentant divers paysages boréaux canadiens. Nous montrons que les taux volumétriques de PPB et R de ces lacs sont fortement influencés par la teneur en carbone organique dissous (COD) et l'azote total (modulé par la morphométrie du lac et sa position géographique) et non par la disponibilité de la lumière, contrairement aux études précédentes montrant l'importance de la lumière sur le métabolisme à l'échelle de l'habitat. Nous montrons que la productivité nette de l'écosystème (PNE = PPB - R) et le rapport PPB:R augmentent avec la température en raison de l'augmentation de PPB mais pas de R, ce qui dévie des attentes. Nous relions ces facteurs directs de PPB, R et finalement PNE aux changements du climat et à la structure du bassin versant dans le paysage, soulignant que la PNE des lacs nordiques est soumise à des contrôles multiples et souvent opposés qui n'auraient pu être définis par des approches conventionnelles. Les effets opposés de la température et du COD sur la PNE mettent en évidence cette conclusion, qui suggère que des augmentations simultanées de ces deux facteurs pourraient ne pas affecter la PNE lors de futurs scénarios de changements climatiques.

Nous montrons au chapitre 3 que les structure spatiales de PNE des lacs nordiques varient grandement, tant en ce qui concerne leurs taux que leurs couplages avec les flux de CO_2. Nous identifions un grand sous-ensemble (~ 1/3) de lacs qui sont nettement autotrophes (PPB > R), mais qui sont encore sursaturés et qui émettent du CO_2 vers l'atmosphère. Combinés avec d'autres informations, ces résultats indiquent que la variabilité au niveau du paysage de la régulation des émissions de CO_2 (via les processus hydrologiques externes et les processus internes aérobiques et anaérobiques) est plus diversifiée qu'on ne le pensait auparavant.

Enfin, le chapitre 4 explore plus en détail les liens entre les processus aérobiques et anaérobiques dans les habitats oxiques de la colonne d'eau des lacs et des implications sur le cycle du CH_4. Nous utilisons une approche expérimentale pour montrer qu'une fraction importante (~ 20%) des émissions de CH_4 d'un petit lac nordique provient de la colonne d'eau oxique. Des manipulations expérimentales montrent que les taux d'émission sont étroitement liés à la dynamique des algues et que le CH_4 est probablement produit principalement à partir de la méthanogenèse acétoclastique. Ces résultats remettent en question la compréhension globale actuelle de la dynamique du CH_4 aquatique, qui suppose que la méthanogenèse est exclusive aux sédiments anoxiques et aux eaux profondes des lacs.

Lorsque les résultats de chaque chapitre sont réunis, nous observons que les structures du métabolisme et des flux de GES de source biologique dans les lacs nordiques sont plus complexes qu'on ne le pensait auparavant: Les réseaux alimentaires jouent un rôle plus diversifié que prévu dans la modulation des flux de CO_2 et la PNE s'écartent souvent, à l'échelle de l'écosystème, des attentes théoriques et spécifiques aux communautés. De plus, ces résultats mettent en évidence la rétroaction sous-estimée entre la PNE et la production anaérobique de GES (même dans les habitats oxiques) qui restreint la capacité globale des puits de carbone des lacs autotrophes. Les méthodes et les résultats présentés dans cette thèse devraient aider à comprendre et prédire les réponses du cycle du carbone dans les lacs nordiques face aux changements généralisés des caractéristiques physico-chimiques des lacs causés par l'intensification des activités anthropiques.

Mots clés: CO_2, méthane, métabolisme des lacs, production primaire brute, respiration, productivité nette de l'écosystème

SUMMARY

Northern lakes provide many ecosystem services to humanity, one of which is supporting the planetary greenhouse effect via the flux of carbon dioxide (CO_2) and methane (CH_4) to the atmosphere. Despite the broader importance of this phenomenon, we lack a clear understanding of the role that lake food webs play in regulating aquatic greenhouse gas (GHG) fluxes, in large part because ecosystem-scale metabolic measurements are scarce for this vast region of the world. This knowledge gap represents a major bottleneck to our mechanistic interpretation of aquatic GHG cycling. To help overcome this problem, this thesis collectively explores patterns of ecosystem metabolism and the link between food webs and GHG dynamics in northern lakes.

In chapter 1, we quantify lake metabolism using a powerful, but under-applied, oxygen isotopic mass balance approach. We review the theory and methodology underlying this approach and test it in a simulation, an *in-situ* experiment, and in two limnologically-diverse lakes. We conclude that with sufficient understanding of lake physical characteristics, the oxygen isotopic approach can effectively capture spatio-temporally integrated rates of ecosystem gross primary production (GPP) and respiration (R) in northern lakes of low to moderate trophic status.

In chapter 2, we apply the oxygen isotopic approach to lakes across a vast ($\sim 10^6$ km^2) and diverse tract of the boreal Canadian landscape. We show that northern lake GPP and R is most strongly driven by lake total nitrogen (TN) and dissolved organic carbon (DOC) content (modulated by lake morphometry and geographic position), and not by light availability, despite previous work showing important effects of light on metabolism within individual habitats. We show that ecosystem-scale net ecosystem production (NEP = GPP - R) and GPP:R increases with temperature due to increased GPP but not R, thus deviating from expectations. We link these drivers of GPP, R, and ultimately NEP to shifts in climate and catchment structure throughout the landscape, highlighting the fact that ecosystem NEP of northern lakes is under multiple, often opposing controls that are not always easy to predict based on first principles or on patterns drawn from other systems. The opposing temperature and DOC effects on NEP highlight this conclusion, suggesting that simultaneous increases in each may not change NEP under scenarios of future change.

We show in chapter 3 that patterns of NEP vary widely, both in their rates and coupling to lake CO_2 fluxes. We identify a large subset (~1/3) of lakes that are net autotrophic (GPP > R), but still supersaturated in, and emitting CO_2 to the atmosphere. Paired with additional information, these patterns indicate that

landscape level variability in the regulation of boreal lake CO_2 emissions *via* external hydrologic, in-lake aerobic, and anaerobic processes is more diverse than previously thought.

Finally, chapter 4 explores in greater detail the connections between aerobic and anaerobic processes in oxic, open water habitats, and the implications for lake CH_4 cycling: We use an experimental approach to show an important fraction (~20%) of summertime CH_4 emissions from a small northern lake are derived from the oxic water column. Experimental manipulations show that emission rates are closely linked to algal growth and NEP, and CH_4 is likely produced mostly from acetoclastic methanogenesis. These findings challenge the current global understanding of aquatic CH_4 dynamics, which assumes methanogenesis is exclusive to anoxic lake sediments and bottom waters.

When the results from each chapter are taken together, we see that patterns of metabolism and biotic GHG fluxes in northern lakes are more complex than previously thought: Lake food webs play a broader than expected role in shaping CO_2 fluxes, and the drivers and sensitivity of lake NEP often deviate, at the ecosystem scale, away from theoretical and community-specific expectations. At the same time, these findings highlight the underappreciated feedback between lake NEP and anaerobic GHG production (even in oxic habitats) that serves to restrict the overall C sink strength of autotrophic lakes. Moving forward, the methods and findings presented in this thesis should help in efforts to both track and predict the responses of northern lake C cycling to widespread changes in physico-chemical lake characteristics linked to intensifying anthropogenic activities.

Keywords: CO_2, methane, lake metabolism, gross primary production, respiration, net ecosystem production

INTRODUCTION

0.1 Context

0.1.1 Northern lakes in the global carbon cycle

Traditionally, freshwater ecosystems were considered passive transmitters of carbon (C) from land to the ocean, and thus were excluded from studies of global C dynamics (e.g., Falkowski et al. 2000). Recent syntheses have fundamentally revised this understanding by highlighting that only half the land-derived C entering freshwater systems actually reaches the ocean, with inland waters actively burying, mineralizing, and transforming the C-pool in transit (Cole et al. 2007; Battin et al. 2009). Freshwater ecosystems process a disproportionate quantity of C relative to their small global distribution (Downing et al. 2006; Prairie 2008), to the extent that global freshwater carbon dioxide (CO_2) and methane (CH_4) evasion and C burial is on the same order of magnitude as other important C fluxes including anthropogenic fossil fuel emissions, deforestation, and oceanic CO_2 uptake (Tranvik et al. 2009; Bastviken et al. 2011).

The boreal biome contains 50% of the planet's terrestrial C pool primarily in peatlands and soils, with 5-15% aboveground in vegetation (Gorham 1991; Benoy et al. 2007). The fate of this C pool is largely determined in boreal waters. Lakes and ponds alone occupy up to 20% of the boreal land surface in some regions (Algesten et al. 2004; Teodoru et al. 2009), compared to a global mean of 3% (Downing et al.

2006). Consequently, the extensive boreal land-water interface facilitates tremendous loading of terrestrial organic C (OC). Between 30-80% of OC entering freshwaters is decomposed or buried, and the remainder is released to coastal waters (Molot and Dillon 1996; Algesten et al. 2004; Weyhenmeyer et al. 2012). Intense OC mineralization generates massive amounts of CO_2 and CH_4, which evade from freshwaters to the atmosphere in the process (Cole et al. 1994; Bastviken et al. 2011; Raymond et al. 2013), making boreal aquatic systems an important component of the global C cycle through their role in sustaining atmospheric GHG pools.

0.1.2 The role of lake metabolism in shaping patterns of GHG flux

Accurate measurements of lake metabolism provide crucial information on the role that aquatic food webs play in the energetics and flow of materials through a given ecosystem. Such measurements also provide critical information on the mechanistic underpinnings of lake GHG dynamics, however a number of obstacles presently limit our understanding of the patterns and controls shaping metabolic connection to lake GHG fluxes:

The first major obstacle in linking lake metabolism and GHG emissions lies in determining the net metabolic balance of northern lakes. In principle, where gross primary production (GPP) exceeds ecosystem respiration (R), or vice versa, the food web should represent a net sink, or source of CO_2 in any aquatic ecosystem (Odum 1956; Duarte and Prairie 2005). In reality, a number of methodological discrepancies (reviewed by Staehr et al. 2012a) complicate our interpretation of the rates and net

metabolic balance of northern lakes. Prairie et al. (2002) found that the method used to assess net metabolism, either as a unitless ratio (GPP:R) or as net ecosystem production (NEP = GPP – R) can strongly influence the interpretation of patterns, rates, and controls of lake metabolism. Others have noted that the widely used ^{14}C-radiolabeled dissolved inorganic C (DIC) incubations can underestimate GPP and thus GPP:R (Bender et al. 1987b; Carignan et al. 2000; Luz et al. 2002). Assessing net metabolism based on combinations of data derived from DO and ^{14}C-DIC based incubations may also introduce error during stoichiometric conversion (Carignan et al. 2000). The prevailing approach to assessing metabolism in boreal lakes has been to use bottle incubations of isolated water samples (e.g., Carrignan et al. 2000; Ask et al. 2012; Kankaala et al. 2013). These have generated great insight into community level dynamics, but do not necessarily reflect whole-system metabolic rates or balances, because they do not integrate through extended periods of time, nor across different spatial habitats (Dubois et al. 2009; Quay et al. 2010). Taken together, an assessment of northern lake metabolism using consistent, ecosystem-scale methodology would greatly improve our current understanding of lake food web functioning and its role in the aquatic C cycle.

A second major challenge lies in defining how climatic and catchment-scale drivers transmit an effect on GPP, R, and ultimately the metabolic balance of northern lakes. Many studies have collectively advanced our understanding of the connection between in-lake conditions (e.g., light environment, nutrient and DOC concentrations, trophic structure) and community metabolism, largely focusing on plankton (e.g., del

Giorgio and Peters 1994; Nurnberg and Shaw 1999; Cottner and Biddanda 2002; Pace and Prairie 2005; Sand-Jensen and Staehr 2009). Studies have also explored the connections between metabolism and both the physical structure of lakes (Fee et al. 1992; Kelly et al. 2001; Staehr et al. 2012a; Obrador et al. 2014), and the effect of hydrologic residence time on metabolism (del Giorgio and Peters 1994; Schindler et al. 1996; Berggren et al. 2009; Solomon et al. 2013). Decades of evidence has shown a strong connection between lake physico-chemical characteristics and both natural and human-induced variability in catchment features (topography, vegetative cover; catchment lake position) and climatic characteristics (patterns of temperature, precipitation, and solar radiation). Studies have in-turn highlighted the ultimate connection between these external features and patterns of biotic C cycling at the community level (e.g., Schindler et al. 1996; Jankowski et al. 2014; Lapierre et al. 2015). Yet at the whole-ecosystem level, metabolic responses to changes in external forcing are not well defined (Cross et al. 2015), especially for aquatic NEP; which may not follow expected theoretical or community-specific expectations (Rodriguez et al. 2016; Vasconcelos et al. et al. 2016; Vesterinen et al. 2016). To address this knowledge gap, we need a broad-scale investigation of whole-lake metabolism spanning diverse terrestrial habitats and climatic conditions.

Third, our appreciation of the relative importance of external (catchment-derived) versus internal support of air-water GHG flux is limited. Studies have typically attempted to distinguish each contribution indirectly using multiple techniques; with DIC mass balancing, isotopic analyses, correlations with proxies of

lake trophic status or soil water, or comparison of whole-ecosystem CO_2 fluxes with community level estimates of pelagic metabolism (Jones et al. 2001; Duarte and Prairie 2005; McCallister and del Giorgio 2008; Dubois et al. 2009; Humborg et al. 2010; Lapierre and del Giorgio 2012; Maberly et al. 2013; McDonald et al. 2013; Weyhenmeyer et al. 2015). These studies have differed in their interpretation of the importance of lake metabolism as a driver of lake CO_2 flux, pointing to the likely wide-ranging and variable relationship between metabolism and CO_2 flux, analogous to that which can occur within a given lake over time due to hydrologic flushing of catchments (Vachon and del Giorgio 2014; Vachon et al. 2016) and experimentally induced shifts in lake NEP (Wilkinson et al. 2016). Perhaps most importantly, the widespread environmental drivers of variability controlling the relationship between metabolism and lake GHG flux are poorly defined, but must be understood if we are to better appreciate the mechanisms underlying broad-scale patterns in aquatic GHG flux.

Lastly, it is unclear how pelagic anaerobic processes shape aquatic GHG fluxes. Production of CH_4 in oxic pelagic zones has only been considered in a handful of lake studies (Oremland 1979; Schmidt and Conrad 1993; Schulz et al. 2001; Grossart et al. 2011; Berg et al. 2013;Tang et al. 2014), because the notion that methanogenesis is exclusive to anoxic environments has historically precluded the search for methanogen existence and activity in oxic environments. It is now clear that CH_4 is produced in many diverse, oxic environments (Scranton and Brewer 1977; Karl et al. 2008; Damm et al. 2010; Angel et al. 2011; Grossart et al. 2011),

possibly in microanoxic habitats on algae and particulate organic matter (POM) (Karl and Tilbrook 1994; Schulz et al. 2001; Grossart et al. 2011), in anoxic guts of metazoans (Oremland 1979; de Angelis and Lee 1994), but also possibly via unidentified aerobic archaea (Paganin et al. 2013), or by bacteria that release CH_4 during the breakdown of methylated compounds (Karl et al. 2008; Damm et al. 2010; Florez-Leiva et al. 2013). Little is known about these pathways and to what extent they occur in pelagic lake water. Pelagic CH_4 production may represent an important energetic coupling between auto- and heterotrophic plankton if algal C is converted to CH_4. It may also generate a unique source of OC that fuels aerobic respiration and CO_2 production if it is subsequently consumed by methane oxidizing bacteria (MOB). Therefore, pelagic methanogenesis may supply both DOC and GHGs to the water column and constitute a yet-unestablished link between pelagic anaerobic metabolism and lake GHG dynamics.

These issues each represent fundamental gaps in our understanding of lake metabolism that collectively limit our mechanistic appreciation of GHG cycling in lakes. Here, I attempt to address each of these issues, as outlined below.

0.2 Thesis Objectives

The main goal of this thesis is to provide a better mechanistic understanding of lake C cycling by better defining the link between metabolism and GHG emissions in northern lakes (Fi.g 0.1). This goal is addressed through 4 sequential sub-objectives (Fig. 0.1) representing the focus of each research chapter:

1. Adapt and calibrate a technique to accurately estimate boreal lake ecosystem GPP and R.
2. Determine landscape-level controls of boreal lake GPP, R, and ultimately NEP.
3. Determine the strength and drivers of NEP-CO_2 coupling among boreal lakes.
4. Assess the role of metabolism in the oxic water-column in supporting CH_4 emissions.

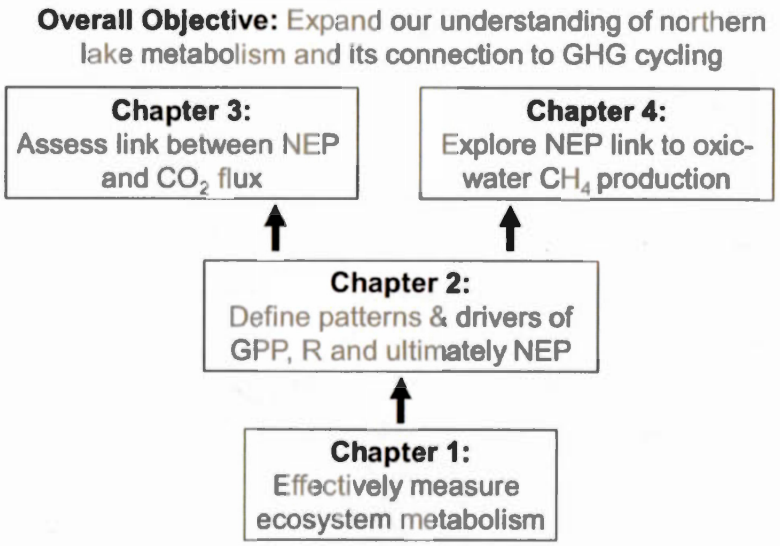

Figure 0.1. Overall thesis objective, and chapter specific themes.

0.3 General Approach

I have used a combination of approaches to address my goal and sub-objectives outlined above. To better define the drivers of lake metabolism and to tease apart biotic and abiotic effects on lake GHG fluxes, I necessarily combine methods across multiple scales: My work exploits published and new datasets, combines *in-vitro* incubations, an *in-situ* mesocosm experiment, habitat-specific and whole lake ambient sampling, as well as the broad scale characterization of catchment and inter-regional environmental characteristics.

0.3.1 Measuring gas dynamics and lake metabolism

A central feature to each of my research chapters is the direct estimation of rates and patterns of lake metabolism (i.e., GPP, R, NEP and GPP : R). Lake metabolism can be quantified with multiple approaches, each with associated strengths and weaknesses, that each capture specific aspects (spatial and temporal) of whole lake metabolism (as detailed below, and by Staehr et al. [2012b]). The main technique I have used is the estimation of metabolic processes from free water dissolved oxygen (DO) patterns (both concentration and isotopic composition), which integrates processes across horizontal and vertical habitats, as well and through time, depending on the lake reaeration rate. In order to effectively use the oxygen isotopic approach, I first tested it alongside *in-vitro* metabolic measurements and another free-water technique based on diel patterns in DO. In subsequent applications, I use both

free-water and *in-vitro* DO approaches to relate different aspects of lake metabolism to environmental characteristics and GHG fluxes.

0.3.2 Mesocosm experiment

Chapters one and four both use a mesocosm experiment conducted in a temperate lake (Lac Cromwell, at the research station of the Université de Montreal), in the summer of 2012. The *in-situ* mesocosms isolated pelagic- from benthic and littoral habitats, allowing me to both test the oxygen isotopic approach in a semi-controlled environment, and then link patterns of metabolism to methanogenesis in oxygenated pelagic waters. The use of mesocosms also enabled the comparison of rates of pelagic CH_4 emissions to rates of littoral diffusive and ebullitive flux.

0.3.3 Lake sampling

My thesis uses data from a combination of low- and high frequency sampling approaches. In chapters two to four I have used different combinations of low-frequency (i.e., typically a single sample) lake data from the Carbon Biogeochemistry in Boreal Aquatic Systems (CarBBAS) research chair program. Lakes in this dataset (and their associated catchment and regional climate characteristics) have been previously documented in detail (Berggren et al. 2012; Lapierre and del Giorgio 2012; Rasilo et al. 2015; Lapierre et al. 2015), and this dataset provides an ideal opportunity to explore the broad scale landscape drivers of lake metabolism and its link to GHG fluxes. I have also taken advantage of detailed, high-frequency (i.e.,

hourly to monthly) datasets generated for two Quebec lakes (Lacs Croche and Simoncouche, at the research stations of the Université de Montreal and the Universite du Quebec a Chcoutimi, respectively). These sites provide an ideal setting to test the oxygen isotopic approach alongside previously published (Carignan et al. 2000; Vachon and del Giorgio 2014; Vachon et al. 2016) metabolic estimates based on *in-vitro* and diel-DO modelling approaches.

CHAPTER I

USING OXYGEN STABLE ISOTOPES TO QUANTIFY ECOSYSTEM METABOLISM IN NORTHERN LAKES

Matthew J. Bogard[1,2], Dominic Vachon[1,3], Nicolas F. St-Gelais[1], Paul A. del Giorgio[1]

[1] Groupe de recherche interuniversitaire en limnologie, Département des sciences biologiques, Université du Québec à Montréal, Montréal, QC.

[2] Now at the School of Environmental and Forest Sciences, College of the Environment, University of Washington, Seattle, WA, U.S.A.

[3] Now at Institute F.-A. Forel, Department of Sciences, University of Geneva, Geneva, Switzerland.

Accepted for publication at *Biogeochemistry*

Keywords: metabolism, oxygen, stable isotope, primary production, respiration, lake, net ecosystem production

N.B. References cited in this chapter are presented at the end of the thesis

1.1 ABSTRACT

In remote regions of the world, whole lake metabolic estimates are scarce, largely because long incubations, intensive sampling and deployment of monitoring equipment are impractical. The oxygen isotope ($\delta^{18}O$) mass balance approach represents a simple and efficient alternative to estimate whole-lake gross primary production (GPP) and respiration (R) from a single point sample, yet this option has not been extensively explored in habitats such as remote northern lakes. Here, we explored the applicability of the method using a sensitivity analysis on simulated data, showing that in large, heterotrophic (i.e., R > GPP) lakes, model outputs are sensitive to input terms for isotopic fractionation and air-water gas exchange. Despite these sensitivities, field applications of the $\delta^{18}O$ method generated promising results that were generally consistent with parallel, free-water diel DO metabolic modelling, but greater than *in-vitro* incubation measurements. The isotopic approach captured both wide-ranging metabolic conditions in *in-situ* experimental mesocosms, and the seasonal trends in GPP and R in a shallow, dystrophic lake. In a clearer, deeper heterotrophic lake, the isotope approach integrated a fraction of metalimnetic metabolism missed by diel DO metabolic estimates. Overall, metalimnetic contributions to surface $\delta^{18}O$-DO dynamics had the greatest potential impact on model outputs, but with accurate information on air-water gas exchange, mixing depth, and the vertical DO and light regime of a given system, these effects can be accounted for and the isotopic approach can yield well constrained, spatio-temporally integrated rates of GPP and R. The approach is clearly suitable for use in oligo- and mesotrophic lakes, especially in remote regions where sampling is logistically difficult.

1.2 INTRODUCTION

Our ability to effectively quantify gross primary production (GPP), respiration (R), and net ecosystem production (NEP = GPP-R) is fundamental to understanding the basic functioning of any ecosystem. These measurements inform us as to how materials and energy move through the system, and how systems integrate with other environments at regional to global scales to broadly support life and drive biogeochemical cycles. For scientists focusing on lakes and rivers in particular, the capacity to quantify ecosystem metabolism has improved with the availability of new approaches, such as advanced sensor technology that allows for the continuous monitoring of gases and environmental variables (Hanson et al. 2008; Staehr et al. 2010) and geochemical techniques (Bender 1990; Luz and Barkan 2000; Parker et al. 2005; McCallister and del Giorgio 2008). In parallel, major advances have been made in the modelling and interpretation of patterns in environmental data (e.g., Tobias et al. 2007; Holtgrieve et al. 2010; Staehr et al. 2010; Solomon et al. 2013; Hotchkiss and Hall 2014), and upscaling patterns of ecosystem metabolism to the global scale (Allen et al. 2005; Pace and Prairie 2005; del Giorgio and Williams 2005; Lewis 2011).

Our capacity to apply these approaches across a large number of ecosystems, however, is still very limited, and this problem represents a major bottleneck in our understanding of the rates, regulation, and spatio-temporal patterns of aquatic ecosystem metabolism for a major fraction of the planet's inland waters. This is particularly the case in the vast boreal biome, which contains the highest density of

lakes in the world (Downing et al. 2006), but which has been vastly under-sampled, due to the remoteness and inaccessibility of most boreal lakes. Approaches requiring intensive *in-situ* and lab-based sampling efforts, including long *in-vitro* incubations (e.g., Bender et al. 1999; McCallister and del Giorgio 2008; Ask et al. 2012), or the deployment and maintenance of equipment to enable extensive temporal coverage (Cole et al. 2000; Solomon et al. 2013) are difficult to implement in remote landscapes, and inevitably come at the cost of reduced spatial coverage. The latter is essential, since the extremely high spatial variability of aquatic ecosystems that exists across northern landscapes (e.g., Lapierre et al. 2015) is impossible to capture and understand on the basis of a few selected sites. Consequently, a much greater sampling effort of ecosystem GPP and R is required to gain a better understanding of the potentially large variability in, and underlying drivers of whole-lake metabolism in remote environments.

An approach that could potentially help address this problem is the combined use of ambient oxygen concentration and isotopic composition to derive metabolic rates (Fig. 1.1). Differences in isotopic composition between atmospheric O_2 ($\delta^{18}O$ = 23.5 to 23.9 ‰; Kroopnick and Craig 1972; Barkan and Luz 2005) and H_2O in aquatic ecosystems ($\delta^{18}O$ = 0 to ~ - 12 ‰; Gat 1996), in combination with the ambient oxygen concentration, provide a basis to distinguish metabolic effects on the DO pool from that of air-water exchanges (Fig. 1.1; Quay et al. 1995). The isotopic

composition of the DO pool is differentially influenced by GPP and R (detailed below), and, when these effects are defined, measurements of DO concentration, δ^{18}O-DO and δ^{18}O-H_2O can ultimately yield estimates of ecosystem metabolic balance (i.e., GPP : R; Quay et al. 1993, 1995, Ostrom et al. 2005; Wang et al. 2008). This approach necessarily assumes that shifts in the ambient balance between GPP and R are reflected in both the magnitude (and sign) of the O_2 exchange with the atmosphere, and in the resulting isotopic equilibrium of dissolved O_2 in surface waters. In cases where air-water gas exchange rates (*F*; Fig. 1.1) can actually be measured or calculated, the above approach can be used to further derive the individual rates of GPP and R (Bocaniov et al. 2012). The free-water nature of the approach integrates across broad horizontal and vertical spatial scales, the extent of which depends on physical mixing characteristics and size of a given system (Van de Bogert et al. 2007; Staehr et al. 2012b). Therefore, depending on the re-aeration rate of the DO pool, measurements of δ^{18}O-DO yield metabolic estimates that are both spatially (across broad horizontal and vertical scales) and temporally (from sub-daily to multi-day time windows) integrative (Bocaniov et al. 2015 and references therein). Overall, the spatio-temporally integrative nature of the δ^{18}O isotopic approach makes it a potentially very effective way to quickly and efficiently assess ecosystem metabolic properties across a wide range of lake ecosystem types (Quay et al. 1995).

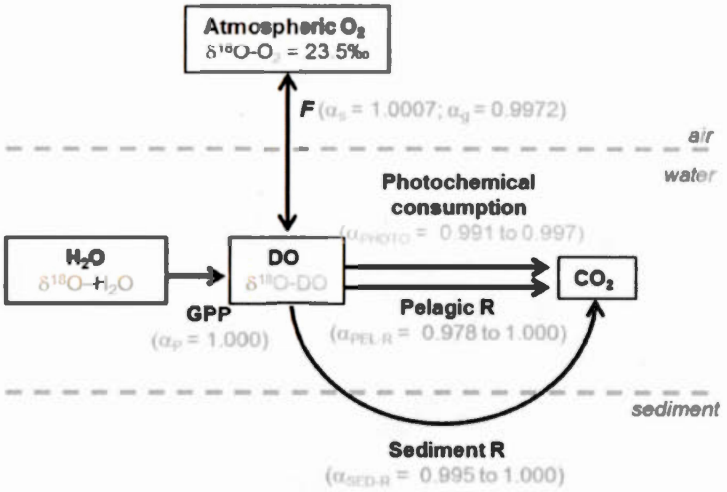

Figure 1.1. Schematic representation of lake oxygen and $\delta^{18}O$ dynamics involved in the oxygen isotope metabolic approach.

Boxes and arrows denote oxygen pools and flux pathways, respectively. Fluxes (in black) include; air water gas exchange (*F*), gross primary production (GPP), pelagic and sediment respiration (R), and DO consumption during photo-oxidation of organic material (OM). Isotopic compositions of each pool and fractionation effects associated with fluxes are shown in grey. Isotopic composition of atmospheric O_2 is assumed constant (23.5‰), while that of H_2O and DO are measured directly. Fractionation effects (shown in parentheses) are shown for air-water gas exchange (α_g), gas solubility (α_s), GPP (α_p), OM photo-oxidation (α_{PHOTO}), and pelagic and sediment R ($\alpha_{PEL\text{-}R}$, $\alpha_{SED\text{-}R}$, respectively). Values are literature derived with references listed in the text (estimates of α_{PHOTO} were both literature derived and measured here [Table 1.1; Supplement 1.1]). The figure is a modified version of those from Holtgrieve et al. (2010) and Quiñones-Rivera et al. (2007).

Despite its great potential, to our knowledge this approach has not been widely used for broad surveys of lake metabolism. The use of $\delta^{18}O$ dynamics to quantify ecosystem metabolism has largely been restricted to surveys of large lakes (Russ et al. 2004; Ostrom et al. 2005; Wang et al. 2008; Bocaniov et al. 2012, 2015; Wassenaar 2012) and open marine environments (Quay et al. 1993; Quiñones-Rivera et al. 2007; Bender and Grande 1987) where longer-term voyages aboard sampling vessels present logistical restrictions similar to those met when sampling lakes in other remote environments. Select applications of this approach in other lentic systems include a series of Amazonian lakes (Quay et al. 1995), and a few lakes and reservoirs in human-dominated environments (Luz et al. 2002; Quiñones-Rivera et al. 2015). For lotic systems as well, few studies have used measurements of $\delta^{18}O$. A few applications have used a point sampling approach at multiple sites (Quay et al. 1995; Wassenaar and Koehler 1999), but rather most applications have used higher frequency (i.e., multiple samples per day) diel sampling at only one or a few sites (e.g., Parker et al. 2005), often in order to employ modelling approaches that simultaneously define GPP, R, and air-water gas exchange (Venkiteswaran et al. 2007; Tobias et al. 2007; Holtgrieve et al. 2010; Hotchkiss and Hall 2014). The need for such approaches stems from the fact that in highly productive flowing waters, extreme diurnal shifts in DO concentration and $\delta^{18}O$-DO, plus large uncertainty in the estimation of air-water gas flux, make the estimation of GPP and R at hourly to daily scales nearly impossible using only point-sampling approaches (Tobias et al. 2007;

Venkiteswaran et al. 2007). For lentic systems, however, patterns of GPP and R (Bocaniov et al. 2012) and the overall net metabolic balance (Dubois et al. 2009) inferred from the point sampling of $\delta^{18}O$ seem to agree with results from bottle incubations that capture patterns at a daily scale. This agreement is promising, but further investigation is needed in a variety of lake environments to more rigorously assess the effectiveness of this approach.

1.2.1 Description of the oxygen isotopic approach

Here we model mixed layer metabolism from $\delta^{18}O$ dynamics (depicted in Fig. 1.1) following Bocaniov et al. (2012, 2015), who adapted an earlier form of the isotope model (Quay et al. 1995; Bender and Grande 1987) to independently estimate GPP and R (Fig. 1.1; in mg O_2 m^{-3} d^{-1}) by accounting for the effects of air-lake gas exchange on the DO pool (*F*; Fig. 1.1). As the isotopic approach is a free water technique, we cannot directly distinguish abiotic from biotic DO fluxes, and as a result the overall rate of R derived here represents the ecosystem-level interaction of individual pathways including pelagic R, OM photo-oxidation (both partial oxidation of OM and complete mineralization to CO_2), and benthic metabolism for the portion of sediments that are in contact with the mixed layer (Fig. 1.1).

Isotope compositions are reported in delta notation following equation 1.1:

$$\delta^{18}O = ((R_{sample} / R_{standard}) - 1) \times 1000 \qquad (1.1)$$

where $\delta^{18}O$ is the isotopic signature of DO, atmospheric O_2, or H_2O, R_{sample} is the

ratio of heavy to light isotope in samples ($^{18:16}O_{DO}$, $^{18:16}O_{atm}$, and $^{18:16}O_{H2O}$, respectively) and $R_{standard}$ is the $^{18:16}O$ value of Vienna standard mean ocean water (VSMOW). Atomic fractions (AF) of ^{18}O in individual oxygen pools (defined as ^{18}O / (^{16}O + ^{18}O)) are summarized following Hotchkiss and Hall (2014) as:

$$AF = R_{sample} / (1 + R_{sample}) \qquad (1.2)$$

with AF_{DO}, AF_{H2O}, and AF_{atm} representing atomic fraction of ^{18}O in dissolved O_2, water, and atmospheric O_2 respectively.

Multiple processes consume DO, each with different associated fractionation effects: Isotopic fractionation during sedimentary DO consumption ($\alpha_{SED\text{-}R}$ = ~0.997; Bender 1990; Brandes and Devol 1997) is small compared to pelagic R ($\alpha_{PEL\text{-}R}$). For $\alpha_{PEL\text{-}R}$, incubation-derived estimates from a large number of studies center around 0.980, but can range by ~ $\pm$10 ‰ beyond this value (Kiddon et al. 1993; Quay et al. 1993, 1995; Luz et al. 2002; Quiñones-Rivera et al. 2007; Bocaniov et al. 2012). Less is known about the fractionation effect of OM photo-oxidation (α_{PHOTO}; Fig. 1.1), which, to our knowledge, has only been measured once (Chomicki and Schiff 2008). To address this knowledge gap, we conducted an experiment (detailed in Supplement 1.1), to help constrain α_{PHOTO}. Our values of α_{PHOTO} were comparable to Chomicki and Schiff (2008), and together averaged 0.993, ranging from 0.991 to 0.997 (Table 1.1).

Table 1.1. Experimentally derived isotopic fractionation factors (α_{photo}) associated with dissolved O_2 uptake and changes in isotopic signature ($\delta^{18}O$-O_2) during the photo-oxidation of dissolved organic matter.

Observations are based on laboratory incubations of filtered water from two boreal lakes (see methods in Supplement 1.1) and in two boreal streams (Chomicki and Schiff 2008). Averages ± 1 standard deviation are reported for all results.

Site	System	Incubation Time (hr)	DO ($mg\ L^{-1}$)	$\delta^{18}O$-O_2 (‰)	α_{PHOTO}	Source
Simoncouche	Lake	0	12.3	24.9	0.991	This study
		24.0	9.2	27.5		
Clarence-Gagnon	Lake	0	9.3	26.2	0.997	This study
		45.0	6.5	27.5		
Dickie	Stream				0.991	Chomicki and Schiff (2008)
Harp 4	Stream				0.992	Chomicki and Schiff (2008)
Average (± 1 S.D.)					**0.993 ± 0.003**	

To estimate GPP and R, DO fluxes and isotopic effects are combined in a series of mass balance equations originally presented by Quay et al. (1995) and Bender and Grande (1987). Assuming no vertical exchange with the deeper layers, temporal changes in surface waters concentrations of DO (dDO/dt) depend on rates of GPP, R, (here in mg O_2 m^{-3} d^{-1}) and rates of F relative to mixed layer depth (Z_{mix}):

$$d\mathrm{DO} / d\mathrm{t} = F / Z_{mix} + \mathrm{GPP} - \mathrm{R} \qquad (1.3)$$

Temporal changes in the concentration of ^{18}O in DO (d^{18}O-DO/dt) depend on the same processes as DO concentration, but additionally depend on the isotopic ratios ($^{18:16}O$) of each oxygen pool, and fractionation factors associated with each process:

$$d^{18}\mathrm{O\text{-}DO} / d\mathrm{t} = k_{O2} \times \alpha_g \times (\mathrm{DO_{sat}} \times \mathrm{AF_{atm}} \times \alpha_s - \mathrm{DO} \times \mathrm{AF_{DO}}) / Z_{mix} +$$

$$(GPP \times \mathrm{AF_{H2O}} \times \alpha_p) - (R \times \mathrm{AF_{DO}} \times \alpha_C) \qquad (1.4)$$

Here DO and DO_{sat} are ambient and saturation DO concentrations, respectively, AF terms represent the atomic fraction of ^{18}O as detailed above. Terms α_g, α_s and α_p represent fractionation effects during kinetic gas exchange at the air-water interface, gas solubility effects, and photosynthesis, respectively.

We used a new term in equation 1.4 (α_C), the combined, ecosystem-level isotopic fractionation during DO uptake, which integrates the individual effects of pelagic R ($\alpha_{PEL\text{-}R}$), sedimentary R ($\alpha_{SED\text{-}R}$), and photochemical DO consumption (α_{PHOTO}) on ^{18}O-O_2 (Fig. 1.1). Though sediment R has been considered in metabolic models for bottom waters (Quiñones-Rivera et al. 2007), most studies have estimated surface water metabolic rates or GPP:R assuming pelagic R (with associated $\alpha_{PEL\text{-}R}$

~0.982 – 0.970) is the only process consuming DO in the water column (Quay et al. 1995; Luz et al. 2002; Russ et al. 2004; Quiñones-Rivera et al. 2007, 2015; Bocaniov et al. 2012, 2015). This assumption can yield reasonable model outputs consistent with *in-vitro* results in large, open aquatic systems that are dominated by pelagic R (Bocaniov et al. 2012). Yet this may not be suitable in other lakes (e.g., small, dystrophic northern systems; Chomicki and Schiff 2008), since sedimentary R and photo-oxidation of OM often contribute significantly to DO uptake (Granelli et al. 1996; den Heyer and Kalff 1998; Kortelainen et al. 2006; Vachon and del Giorgio 2014). Evidence from marine and lotic habitats dominated by sediment R have shown that $\alpha_{SED\text{-}R}$ can importantly affect ecosystem-level fractionation effects, estimated to be ~0.994 in coastal bottom waters (Quiñones-Rivera et al. 2007; Lehmann et al. 2009). Consequently, values of α_C may be larger (i.e., a smaller fractionation effect) than $\alpha_{PEL\text{-}R}$, and the implications for this difference are discussed below.

Assuming no net change in either DO concentration or $^{18}O\text{-}O_2$ over a diel cycle, equations 1.3 and 1.4 can be combined, rearranged, and solved for *GPP* and *R* individually (Bocaniov et al. 2012, 2015), generating equations 1.5 and 1.6:

$$GPP = (k_{O2} / Zmix) \times [\ DO \times (b - c) - DO_{sat} \times (a - c)\ ] / d - c \qquad (1.5)$$

$$R = (k_{O2} / Zmix) \times [\ DO \times (b - d) - DO_{sat} \times (a - d)\ ] / d - c \qquad (1.6)$$

Where, following the notation of Bocaniov et al. (2012) with a modification to include the atomic fraction terms presented by Hotchkiss and Hall (2014), $a = AF_{atm} \times$

$\alpha_s \times \alpha_g$, $b = AF_{DO} \times \alpha_g$, $c = AF_{DO} \times \alpha_C$, and $d = AF_{H2O} \times \alpha_p$.

1.2.2 Uncertainties linked to the isotopic approach

Like any technique used to quantify aquatic metabolism, the oxygen isotope approach has limitations, particularly in its sensitivity to physical exchanges of water masses that alter temperature and gas solubility (Staehr et al. 2012b; Bocaniov et al. 2015; Goldman et al. 2015). As the approach generally assumes an absence of physically driven changes in DO dynamics (concentration, solubility, or isotopic composition) due to vertical and lateral exchange of water masses, equations 4 and 5 do not explain the interaction of, for instance, epi- and hypolimnetic waters, or intense reaeration and temperature change that might occur during sudden events. If gas solubility suddenly changes with mixing of water masses and a sharp change in ambient temperature (Bocaniov et al. 2015), isotopic results often generate unrealistic, negative values (Bocaniov et al. 2015; Goldman et al. 2015). This effect is likely to be minimized in most northern lake habitats: Unlike for extremely wind-exposed systems like the open ocean, the Great Lakes, or large prairie lakes and reservoirs found in catchments with reduced tree cover (Wassenar 2012; Quiñones–Rivera et al. 2015), most boreal and north-temperate lakes are small, have short fetches, and are often sheltered in low-wind environments. These lakes have comparatively small associated values of k_{O2} (Vachon et al. 2010; Vachon and Prairie 2013), and little physically-driven atmospheric O_2 injection (Yang et al. 2015).

Therefore, although physical effects can potentially impede the use of the isotopic approach, it remains unclear how common these effects might be in northern lakes of varying limnological characteristics.

Estimates of GPP and R may also be sensitive to the poorly constrained fractionation values of α_C. A poorly defined fractionation term has been shown to dramatically affect metabolic estimates in lotic (e.g., Holtgrieve et al. 2010; Hotchkiss and Hall 2014) and marine studies (Quiñones-Rivera et al. 2009). As we point out above, there is little information as to how individual processes integrate to yield α_C. By not accounting for the role of OM photo-oxidation (Chomicki and Schiff 2008) or sediment R (Quiñones-Rivera et al. 2007; Tobias et al. 2007; Lehmann et al. 2009) on the ambient δ^{18}O-DO pool (Fig. 1.1), model outputs may be inaccurate, or at the least could have large uncertainties. Values of α_C should be larger than $\alpha_{PEL\text{-}R}$ alone, since α_{PHOTO} and $\alpha_{SED\text{-}R}$ have a comparatively minor fractionation effect on the ^{18}O-DO pool (Fig. 1.1), however relative effects of sediment R, pelagic R, and photochemical processes on the DO pool vary, both across systems and through time (Cory et al. 2014; Vachon and del Giorgio 2014; Vachon et al. 2016 and references therein). Therefore it is unrealistic to attempt to pinpoint exact, system- and time-specific values of α_C, especially in the context of using the isotopic approach to sample lakes in remote environments. This problem may limit the wider use of the δ^{18}O approach, and we therefore need a better understanding of the consequences linked to uncertainty in α_C values.

There is much insight to be gained from the broader application of the $\delta^{18}O$-DO approach throughout the boreal landscape and other remote environments, yet we still have a weak understanding of the actual applicability of this approach, both in terms of the sensitivity of modelled GPP and R to important model terms like reaeration (specifically, k_{O2} and Z_{mix}), α_C, or the diurnal variability in DO concentrations. At a more basic level, this method has seldom been applied alongside other techniques to evaluate its performance. Here, our objective was to first apply an existing form of the isotopic approach (equations 1.5 and 1.6) in an exploratory manner, across a range of simulated, experimental, and ambient lake-based limnological conditions. We used a controlled mesocosm experiment (Bogard et al. 2014) and two lakes that have been studied in detail (Vachon and del Giorgio 2014; Vachon et al. 2016) to validate the approach *in-situ*, and we guide our interpretation of results using a comparison with GPP and R from both in vitro and diel-DO based methods.

1.3 MATERIALS AND METHODS

1.3.1 Sensitivity analyses

Given the potentially large uncertainties linked to estimates of physical (i.e., k_{O2} and Z_{mix}) and fractionation (α_C) variables in equations 1.5 and 1.6, we conducted a series of sensitivity analyses to gain a better understanding of how outputs of GPP and R might vary in response to unaccounted-for changes in key model terms. Simulations were conducted using a range of input values characteristic of Lac Croche (see below for lake details). For α_C, we used a range of values spanning most estimates of ($\alpha_{PEL\text{-}R}$, $\alpha_{SED\text{-}R}$, and α_{PHOTO}; Fig. 1.1). In the first sensitivity analyses, we examined how model outputs varied along gradients in k_{O2} (0.5 – 2.5 m d^{-1}), α_C (0.975 – 0.995), and Z_{mix} (1.5 – 2.5m) by changing these variables one at a time, while holding other model inputs constant. Constants included DO_{sat} = 8.5 mg L^{-1}, α_C = 0.990, α_g = 0.9972, α_s = 1.007, α_p = 1.000, Z_{mix} = 2m, $^{18:16}O_{atmosphere}$ = 0.0020987, $^{18:16}O_{DO}$ = 0.002093, and $^{18:16}O_{H2O}$ = 0.002033. These terms were chosen to roughly reflect seasonal averages for Lac Croche (detailed below). To quantify model sensitivity to changes in DO, for both over-and undersaturated conditions, all calculations were made at multiple DO concentrations (7.5, 8.0, 8.5, 9.0, and 9.5 mg L^{-1}). The DO residence time (Z_{mix} / k_{O2}) in these calculations ranged between 0.8 – 5 days, covering the majority of residence times observed in the study lakes. These results are presented in Supplement 1.2.

In order to assess the interactive effect that model input terms could have on

outputs, we conducted a second set of sensitivity analyses using the same fixed parameters as before, but with simultaneous manipulation of gas exchange and isotopic fractionation. We assessed how changes in k_{O2} values from 0.5 – 2.5 m d^{-1} affected model outputs at different levels of α_C (ranging between 0.970 – 0.995). All simulations were run twice, for a scenario of oversaturation and undersaturation (DO = 9.5 and 7.5, respectively, with DO_{sat} = 8.5 mg L^{-1} in all analyses). All analyses were performed using R version 3.0.3 (R development core team 2014).

1.3.2 Field validation

The performance of the isotopic approach was explored in two northern lakes over the 2011 open water season. These lakes have been the focus of intensive research in the past, and have been described in detail in Vachon and del Giorgio (2014). Briefly, Lac Croche is a small (area = 0.063 km^2), deep (mean depth [Z_{mean}] = 6.0m) oligotrophic (total phosphorus [TP $\pm$ 1 S.D.] concentration = 3.6 $\pm$ 0.9 µg P L^{-1}) headwater lake, with a drainage area of 0.88 km^2, situated at the biological research station (SBL) of the Université de Montréal. Lac Croche has been the subject of intense limnological studies for the past 2 decades, and there is ample background information available, including alternative estimates of planktonic primary production and sediment and water column R (den Heyer and Kalff 1998; Carignan et al. 2000; Forget et al. 2009; Dubois et al. 2009; Vachon and del Giorgio 2014). Lac Simoncouche is larger (area = 0.861 km^2), shallower (Z_{mean} = 2.1m),

mesotrophic (TP = 9.7 $\pm$ 2.6 μg P L^{-1}), and is situated downstream in its respective catchment, with a drainage area of 26.3 km^2. Lac Simoncouche is located in the research forest of the Université du Québec à Chicoutimi. Both lakes have been instrumented with autonomous sampling platforms, which provide high-frequency, continuous measurements of surface water O_2 and CO_2 concentrations, light, water column temperature profiles, and air temperature and wind speed, as described in detail by Vachon and del Giorgio (2014). The latter allowed us to compare our isotope-based estimates with published estimates of GPP and R based on free water diel patterns in DO. For both lakes, Vachon and del Giorgio (2014) applied the 'lakeanalyzer' package in R (Read et al. 2011) to evaluate the changes in physical conditions in the study lakes at the hourly scale. Here we use the 2-day moving average estimates of either Z_{mix} or the depth of the bottom of the metalimnion ($Z_{meta-bot}$) in our mass balance calculations (Equations 1.5 and 1.6).

We used a large-scale mesocosm experiment to also test the isotopic approach across a range of metabolic states, but in a simplified setting under well-defined physical conditions. The mesocosm experiments were carried out in Lac Cromwell, which is a small (0.11 km^2), moderately deep (Z_{mean} = 3.5m) oligotrophic boreal lake situated next to Lac Croche, also within the confines of the Biological Station of the Université de Montréal. The experiment (Bogard et al. 2014) and the lake (Downing and Rath 1988; den Heyer and Kalff 1998) have previously been described in detail. In brief, epilimnetic water was pumped into 1-m diameter, 6-m deep, 4712-L

polyethylene enclosures anchored in the middle of the lake. Treatments included nutrients alone, DOC alone, a combination of both, and a control enclosure free of chemical additions. Mesocosms received KH_2PO_4 and $NaNO_3$ (nutrient treatment) additions to target concentrations of 50 and 700 μg P and N L^{-1}, respectively. Superhume brand humic slurry was added (DOC treatment) to reach a target concentration of 15 mg DOC L^{-1} (Robidoux et al. 2015). For a full review of Superhume properties and applicability to freshwater experimentation, see Lennon et al. (2013).

1.3.3 Field and laboratory methods

For Lacs Croche and Simoncouche, we paired autonomous, high-frequency sampling with point sampling conducted in 2011, at weekly to monthly intervals from July to November,, as detailed by Vachon and del Giorgio (2014). Briefly, low frequency sampling of Lacs Croche and Simoncouche include water column profiles of DO and temperature made using a combination probe (Yellow Springs Instruments, USA). All samples for isotopic analysis were taken at ~25-50 cm depth. Samples for $\delta^{18}O\text{-}O_2$ were stored in 12-ml precombusted borosilicate vials, preserved with $HgCl_2$, and air-free samples capped with a gastight rubber lined plastic cap. Samples for $\delta^{18}O\text{-}O_2$ were analyzed at the University of Ottawa Stable Isotopes Laboratory using standard methods (Barth et al. 2004). Samples for $\delta^{18}O\text{-}H_2O$ were collected in 125ml plastic bottles, filled to full capacity free of air, and stored in the dark until analysis using a Los Gatos water vapour analyzer.

For the mesocosm experiment, sampling was done during the second and fifth weeks of the experiment (initiated on June 18th and July 9th, respectively). We collected one sample of water for $\delta^{18}O$-H_2O analysis prior to filling mesocosms, and assumed it represented all treatments throughout the experiment. We tracked diel DO dynamics in one enclosure per treatment, beginning at mid-day and ending ~24hrs later each on June 18th and July 9th. Samples for DO were collected at roughly 3-hr intervals in acid-washed, airtight glass vials, preserved with $HgCl_2$, and stored in the dark at 4°C until analysis via membrane inlet mass spectrometry (Bouvier and del Giorgio 2002). At the end of the 24-hr period, we collected samples for $\delta^{18}O$-DO following the approach used in both lake surveys, and measured water column temperatures in each enclosure at 0.5m depth intervals using the YSI combination probe. We calculated the enclosure mixed layer depth (Z_{mix}) from temperature profiles (Bogard et al. 2014).

1.3.4 Quantification of air/water gas exchange and fluxes

Air-water O_2 fluxes were calculated using Fick's law of gas diffusion:

$$F = k_{O2} \times (DO_{sat} - DO) \qquad (1.7)$$

where F (Fig. 1) is flux of O_2 across the air-water interface (mg O_2 m^{-2} d^{-1}), and k_{O2} is the oxygen exchange coefficient (m d^{-1}) scaled as a function of temperature (see below). As the isotopic model integrates ecosystem processes over a longer time period (i.e., daily to multi-day; Bocaniov et al. 2015), we averaged the sub-daily k_{O2}

estimates in both field applications of the isotopic model (equations 1.5 and 1.6): For the mesocosms we estimated k_{O2} using 2 independent methods (floating chambers and the wind based empirical model of Cole and Caraco [1998]). The 24-hr average k_{O2} value (0.76 m d^{-1}; used in all calculations here) was estimated from mean wind speeds and the mean of diel surface temperature measurements, and was almost identical to mean flux chamber estimates conducted over complete diel cycles prior to isotopic point sampling (Bogard et al. 2014). Methods and results are fully described in the text and supplementary information of Bogard et al. (2014).

For the two study lakes, we used hourly estimates of k_{O2} originally calculated by Vachon and del Giorgio (2014) using equation 1.8 following Vachon and Prairie (2013):

$$k_{600} = 2.51 + 1.58 \times U_{10} + 0.39 \times U_{10} \times \log_{10}(LA) \qquad (1.8)$$

Here, k_{600} is estimated in cm h^{-1}, U_{10} is wind speed at 10m height above the lake (m s^{-1}), and LA is lake area (km^2). Values of k_{600} were converted to k_{O2} following Jahne et al. (1987):

$$k_{O2} = k_{600} \times (Sc_{O2} / 600)^{-2/3} \qquad (1.9)$$

where Sc is the temperature-specific Schmidt number for O_2 (Wanninkof 1992). We applied a 2-day moving average to the hourly k_{O2} values leading up to the time of point sampling events.

1.3.5 Estimating mesocosm and lake α_C values

For the two study lakes, we approximated the summer and fall mixed layer α_C value using the following steps: We first converted the relative surface water photochemical CO_2 production (7-10% of combined pelagic R and photo-mineralization, Vachon et al. [2016]) to ~15% relative photochemical DO consumption using a photochemical quotient (moles CO_2 produced : moles DO consumed) of 0.75 (Cory et al. 2014). Next, we included the sediment contribution to DO uptake, which we assumed was ~25% following results of Jonsson et al. (2001). Overall, this gave fractional contributions of 60 : 15 : 25 (pelagic/photo/sediment) to DO uptake. Assuming the respective fractionation values are ~0.980, 0.993, and 1.000 (Fig. 1.1), this gives a weighted α_C value of ~ 0.987. For the mesocosms, we used a value of 0.983, assuming the same fractional contributions of pelagic R and photo-oxidation respectively accounted for all DO consumption in the absence of sediment R.

1.3.6 Error analyses

For applications of the isotopic approach in the two study lakes, we used Monte Carlo simulations to help characterize the uncertainty in our estimates of GPP and R by accounting for the potential errors in our estimates of k_{O2} and α_C. In our simulations, we used the same fixed parameters as defined above for equations 1.5 and 1.6, but we applied a uniform range of potential α_C values (0.975 to 0.990) that fully encompassed the potential range of fractionation effects that might have

occurred in our study lakes. For k_{O2}, we derived a normally distributed range of uncertainty ($\pm$ 1 S.D.) from the ordinary least squares regression model describing the relationship between hourly estimates of k_{O2} and the corresponding moving averages ($r^2 = 0.32$). A total of 1000 simulations were run for each observation, generating a normally distributed error range for each GPP and R estimate.

1.4 RESULTS AND DISCUSSION

1.4.1 Results and implications of sensitivity analyses

Our sensitivity analyses were meant to yield a clearer understanding of the main sources of uncertainty and bias in isotopically-derived GPP and R estimates across a range of realistic limnological conditions. Of particular interest in this study was the potential effect on estimates of GPP and R caused by changes in physical conditions (Z_{mix}, k_{O2}) and α_C, since these input values can have large uncertainty (detailed above). We tested how the range of GPP and R outputs responded to manipulation of either α_C, k_{O2} or Z_{mix} alone (Fig. S1.2). Changing k_{O2} (Fig. S1.2a,d) or Z_{mix} (Fig. S1.2c,f) affected model outputs in a linear manner, but the rate of change of model outputs was much steeper for k_{O2} than Z_{mix}, suggesting that when applied to real data, inaccuracies in model inputs of k_{O2} can cause potentially large inaccuracies in model outputs of GPP and R, while incremental inaccuracies in Z_{mix} may be far less consequential.

For α_C on the other hand, the sensitivity of model outputs was not uniform across the tested range of 0.995 to 0.975; rates of change in GPP and R output increased dramatically beyond α_C values < 0.985 (as fractionation effects became larger). The rate of change of GPP and R as a function of model inputs was also heavily dependent on DO deviations from saturation: As DO deviated below saturation (increasingly net heterotrophic conditions) the changing of model inputs had an increasingly large impact on outputs of GPP and R, though this effect was of

much less importance for changes in Z_{mix} (Fig. S1.2). Overall, these results suggest that model outputs were most sensitive to changes in both k_{O2} and to changes in α_C at values < 0.985, and that these effects were exacerbated with the under-saturation of the ambient DO pool.

We were particularly interested in how model outputs responded to simultaneous changes in k_{O2} and α_C, since these two terms change independently both across lakes, and within systems through time. We explored this using the same fixed model inputs as before, once each in an auto- and heterotrophic setting (Fig. 1.2). Across the range of k_{O2} values, rates of change of GPP and R were greater with larger fractionation effects (i.e., decreasing α_C values). Heterotrophic lake outputs (Fig. 1.2a,b) were far more sensitive to changes in k_{O2} and α_C than the autotrophic lake (Fig. 1.2c,d). The use of extreme α_C fractionation values < 0.980 always returned unrealistic, negative metabolic rates (data not shown).

Together, the results from the sensitivity analyses suggest that accurate knowledge of k_{O2} and α_C are needed to apply this model, especially in systems that are net heterotrophic (Fig. 1.2a,b). Since most northern lakes are net heterotrophic to varying degrees (Hanson et al. 2003; Kortelainen et al. 2006; Ask et al. 2012), this should enhance the sensitivity of the isotopic approach in most lake applications. This exercise also shed light on the way in which k_{O2}, α_C, and the net metabolic balance interact to shape model sensitivity. In heterotrophic systems with values < 0.985, model outputs of GPP and R change much more rapidly with changes in k_{O2}

(Fig. 1.2). Therefore, large, net heterotrophic lakes may be the most challenging systems to apply the isotopic approach, since α_C may be dominated by pelagic R and therefore < 0.985 (Quay et al. 1993; Kiddon et al. 1993; Quiñones-Rivera et al. 2007; Bocaniov et al. 2012). Wind speed, fetch, and k_{O2} typically increase in larger systems as well (Wanninkhof 1992; Borges et al. 2004; Vachon and Prairie 2013). Therefore, inaccurate model parameterization in these settings likely has far greater consequences for output of GPP and R than in small lakes in forested and sheltered catchments. The latter tend to have lower k_{O2} values (Cole and Caraco 1998; Vachon and Prairie 2013), and larger α_C values (smaller fractionation effect) as we point out above. Clearly, context matters when assessing the sensitivity and potential errors linked to the isotopic approach.

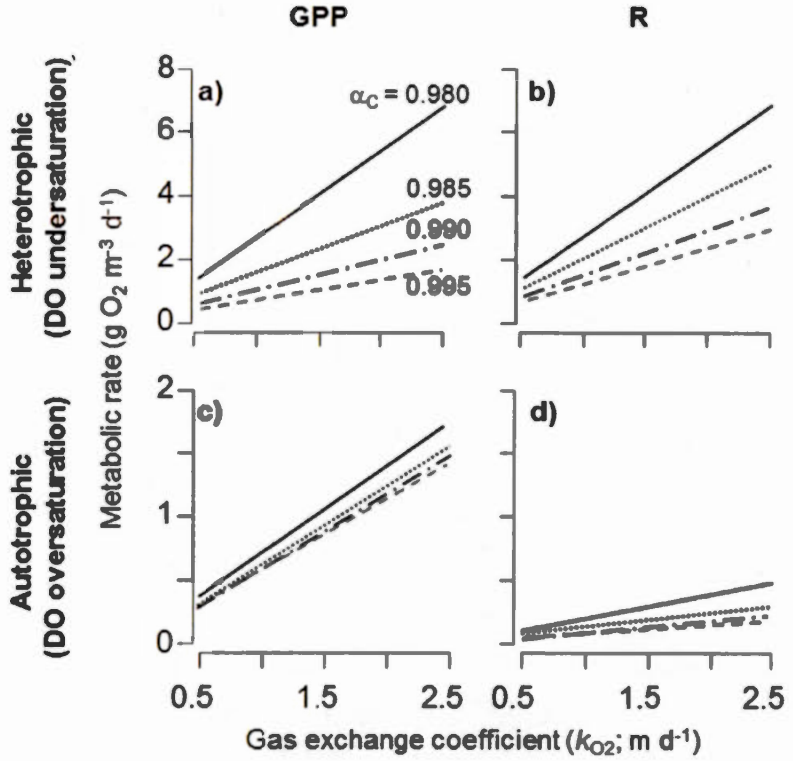

Figure 1.2. Sensitivity analyses investigating how the simultaneous manipulation of model input terms alters estimates of respiration (R) and gross primary production (GPP) in the $\delta^{18}O$ isotopic mass balance model.

The isotopic fractionation factors linked to DO consumption (α_C) and changes in the gas exchange coefficient (k_{O2}) were manipulated. The model was applied to a hypothetical lake ecosystem (see methods section for details) with DO_{sat} = 8.5 mg L^{-1}, and either DO = 7.5 mg l^{-1} (heterotrophic; a,b) or DO = 9.5 mg L^{-1} (autotrophic, c,d).

1.4.2 Model performance and comparisons in mesocosm experiments

At the end of both diel cycles, six of the eight mesocosms were supersaturated in DO concentrations, and seven were isotopically depleted in δ^{18}O-DO relative to atmospheric equilibrium (Fig. 1.3a). This suggests all but the week 2-DOC and control enclosures were autotrophic (GPP > R). As expected, the nutrient (both weeks) and nutrient+DOC treatments (week 5 only) resulted in the most extreme O_2 concentrations and isotopic signatures, indicating GPP >> R at the time of sampling in these treatments. During weeks 2 and 5 of the mesocosm experiment, changes in DO on diel timescales (Fig. 1.3b) were small in control and DOC treatments, compared to mesocosms fertilized with nutrients alone or with nutrients plus DOC, for which the largest changes in DO occurred in week 2. Throughout the diel sampling periods, wind speeds ranged from 0-3 m s^{-1}, and were typically lower during week 5 sampling (Fig. S1.3.1). Estimates of k_{O2} derived from wind speed ranged between ~0.6 – 1.0 m d^{-1}, and were slightly larger in week 2 than 5 at corresponding time points (Fig. S1.3.1). Mean values of wind-based estimates of k_{O2} (0.76 m d^{-1}) were almost identical to averages derived from diel floating chamber measurements (Bogard et al. 2014). Vertical profiles of physico-chemical conditions were also taken in weeks 2 and 5 of the experiment, which showed that water column stratification patterns were consistent across treatments (Fig. S1.3.2), and that the enclosures remained oxic from top to bottom.

We used the diel-DO metabolic modelling approach to help guide the

interpretation of isotopic model results. Our estimates of mesocosm GPP and R were often consistent between both methods (Fig. 1.3c). Metabolic rate estimates from both models loosely followed the 1:1 line along the productivity gradient generated by the experimental manipulations, and were usually on the same order of magnitude for each respective treatment and sampling day. The two approaches significantly diverged on only two occasions (see box in Fig. 1.3c): First, in the DOC treatment in week 2, when, though R values were closer to the 1:1 line, the isotopic model GPP rate was lower than for the diel DO model. Here, it is possible that a transient spike in GPP occurred but was not reflected in the more temporally-integrated isotopic composition of the DO pool, or that isotopic samples were incorrectly stored or capped, and the sample shifted toward to atmospheric equilibration while in storage. However, it was also possible that the isotope model accurately reflected low GPP in the enclosure over the course of the entire day and possibly the day leading up to sampling: Without the addition of nutrients, we had no reason to expect such a large increase in GPP or R, and algal biomass remained low in this treatment relative to those receiving nutrients (difference in chlorophyll *a* of ~ 6 $\mu g\ L^{-1}$; Bogard et al. 2014), signaling no positive shift in NEP. Unfortunately, we cannot confirm the reason for this discrepancy in the week 2 DOC treatment sampling. Second, there was also a discrepancy between approaches in the DOC + nutrient treatment during week 2: Model outputs from the $\delta^{18}O$ approach were much smaller than for the diel DO model for both GPP and R (Fig. 1.3c). On this day, point estimates of $\delta^{18}O$-DO

and ΔDO were both near saturation when we sampled (dashed lines in Fig. 1.3a), and therefore the isotopic approach did not capture the large diel shift in DO that occurred in the 24-hr period leading up to sampling (Fig. 1.3b), which was caused by a peak of metabolism. Both models were, however, in better agreement as point estimates deviated further from atmospheric saturation (Fig. 1.3a): The isotope and diel DO agreed well in the DOC+NP enclosure in week 5 when diel changes in DO were less pronounced (Fig. 1.3b), as well as in the nutrient treatment in weeks 2 and 5 (Fig. 1.3c). Although the diel-DO model approach has its own set of limitations, and there were two occasions where the two approaches clearly disagreed, the general consistencies in GPP and R between it and the isotopic approach suggested that the latter often captured the wide range in metabolic patterns among mesocosm treatments.

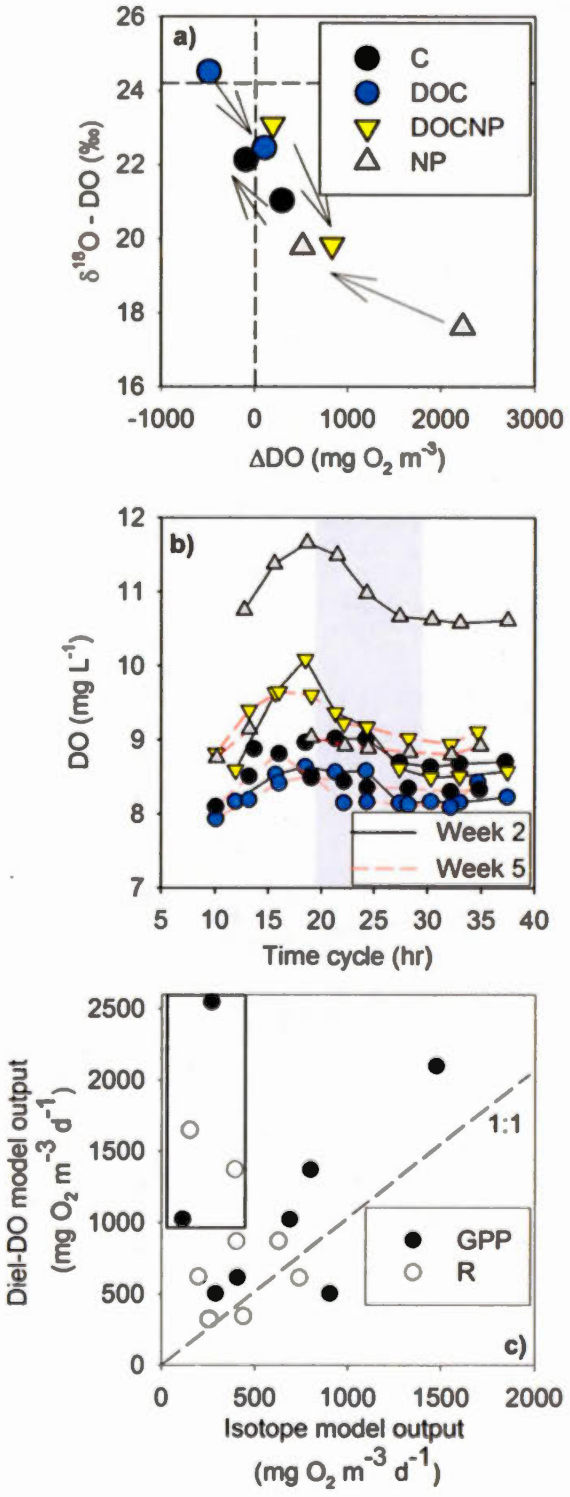
a)
C
DOC
DOCNP
NP
δ18O - DO (‰)
ΔDO (mg O2 m-3)
b)
DO (mg L-1)
Week 2
Week 5
Time cycle (hr)
c)
1:1
GPP
R
Diel-DO model output (mg O2 m-3 d-1)
Isotope model output (mg O2 m-3 d-1)

Figure 1.3. Oxygen and metabolic patterns in the experimental enclosures. a) Biplot of departure from equilibrium with the atmosphere versus DO isotopic signature ($\delta^{18}O$) during experimental weeks 2 and 5 for each treatment. Ambient controls, DOC additions, nutrient additions, and DOC + nutrient additions shown as C, DOC, NP, and DOCNP in the legend, respectively). Dashed lines represent values at equilibrium with the atmosphere. Grey arrows show the change in conditions from week 2 to 5 for each treatment. b) Diel patterns of dissolved O_2 in mesocosms, with treatment symbols as in panel a, and time series defined by black and dashed red lines, for weeks 2 and 5 respectively. The x-axis denotes the course of two sampling days; hour zero is midnight on day 1, hour 40 is 16:00 on day 2. Shaded area shows nighttime periods. c) Comparison of model outputs for gross primary production (GPP) and respiration (R) between the isotopic approach and high frequency diel-DO model approach during weeks 2 and 5 of the experiment. Dashed line denotes 1:1 relationship. Box around four data points denotes outliers that are discussed in text.

1.4.3 Model performance and comparison in lakes

Lacs Croche and Simoncouche differed in physico-chemical dynamics during the 2011 ice-free season: In Lac Croche, low frequency point samples of surface layer DO concentrations were systematically under-saturated and δ^{18}O-DO values ranged between ~ 19.5 to 21.5 ‰ (circles, Fig. 1.4). In contrast, DO in Lac Simoncouche ranged from under- to supersaturated, and δ^{18}O-DO values spanned from ~19.5 to 22.5‰; squares in Fig. 1.4). Corresponding values of δ^{18}O-H_2O ranged from -8.5 to -8.0 ‰ in Croche, and from -13.3 to -11.3 ‰ in Simoncouche (data not shown).

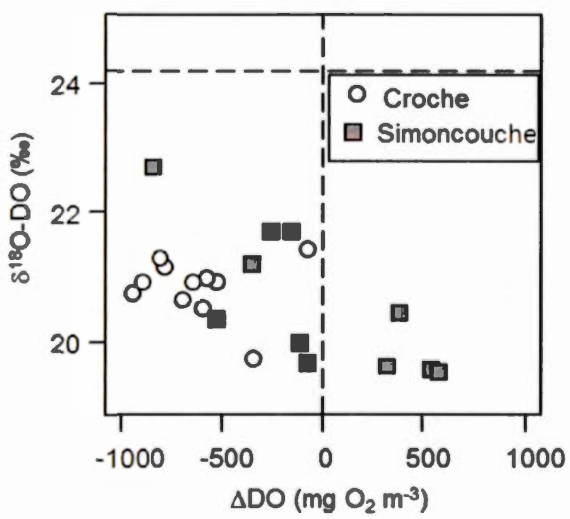

Figure 1.4. Biplot of surface water dissolved oxygen departure from equilibrium with the atmosphere (ΔDO) versus DO isotopic signature ($\delta^{18}O$) for the two study lakes.

Dashed lines represent values at equilibrium with the atmosphere. Values reflect point samples taken for both lakes throughout the July to November ice free period.

High frequency sampling carried out during this period also recorded clear inter-lake differences (Vachon and del Giorgio 2014): The diel change in the degree of DO under- or oversaturation was typically very small in both lakes, usually < 0.5 mg m^{-3} d^{-1} in Simoncouche and < 0.3 mg m^{-3} d^{-1} in Croche (Fig. 1.5a). Lac Croche was consistently undersaturated in DO, while Simoncouche surface waters shifted between under- and oversaturation (Fig. 1.5a). Estimates of k_{O2} were generally larger and more variable in Simoncouche than Croche (Fig. 1.5b). The re-aeration time for DO in Lac Simoncouche was ~1 day longer (mean $\pm$ 1 S.D. = 2.6 $\pm$ 1.9 days) than in Croche (1.4 $\pm$ 1.9 days) for most of the ice-free season (data not shown). High frequency temperature profiles showed Lac Croche (Fig. 1.6d) was strongly stratified and Z_{mix} was ~ 2m closer to the surface of the lake than Simoncouche (Fig. 1.6a), and Z_{mix} increased by ~ 2m from July to November in both lakes. The bottom of the metalimnion ($Z_{meta\text{-}bot}$) ranged from 4m down to the lake bottom, disappearing by October in Simoncouche (Fig. 1.6a), while in Croche it ranged from ~ 2.5m to 6m (Fig. 1.6d). In Croche, the euphotic zone (Z_{eu}) spanned from ~ 6-9.5m, extending far below Z_{mix} and $Z_{meta\text{-}bot}$ (Fig. 1.6d). In Simoncouche, the euphotic zone only reached a maximum of ~5m, reaching below Z_{mix} and $Z_{meta\text{-}bot}$ in the first half of the sampling duration (Fig. 1.6a).

Physical differences in light penetration and water column stability among the lakes influenced vertical DO patterns. In Lac Simoncouche, since the water column was well mixed for most of the lake, the DO profile was relatively uniform, declining from ~ 8 – 2 mg L^{-1} from surface to bottom waters throughout the sampling period

(Fig. 1.6b), and surface DO ranged from under- to supersaturated (~ 80 to 100%; Fig. 1.6c), showing little evidence of a metalimnetic peak in metabolism. Here, DO concentrations increased from ~ 8 mg L^{-1} in surface waters to 12 mg L^{-1} at the base of the metalimnion (Fig. 1.6e) and although DO was undersaturated in surface waters and most of the metalimnion, at the base of the metalimnion it was oversaturated by ~ 110% (Fig. 1.6f). Taken together, DO profiles suggested a potentially intense summertime (until ~ DOY 225) contribution of deep-layer GPP and R that persisted in Lac Croche but not in Simoncouche.

Indirect assessments of the role of deep-layer metabolism suggested that its relative contribution to whole-system GPP and R (and its potential influence on the surface layer δ^{18}O-DO pool) differed markedly between lakes (Fig. 1.7): Models generated for three Danish lakes using vertically-distributed free water measurements of GPP and R have shown contributions of epilimnetic GPP and R to total lake areal rates declines rapidly as Z_{eu} increasingly exceeds Z_{mix} (Obrador et al. 2014). In our study lakes, the mean ($\pm$ 1 S.D.) of daily estimates of Z_{mix} : Z_{eu} in Lac Simoncouche was 0.90 $\pm$ 0.20, but in Croche was only 0.32 $\pm$ 0.19 (Fig. 1.7). Comparing these values to the models of Obrador et al. (2014) suggests that roughly two thirds and one fifth of total areal GPP and R should respectively be generated in the epilimnion of Lac Croche (Fig. 1.7). In Simoncouche we would expect the vast majority of GPP (~ 90%) and R (~70%) to occur in surface waters, based on the corresponding mean Z_{mix} : Z_{eu} value.

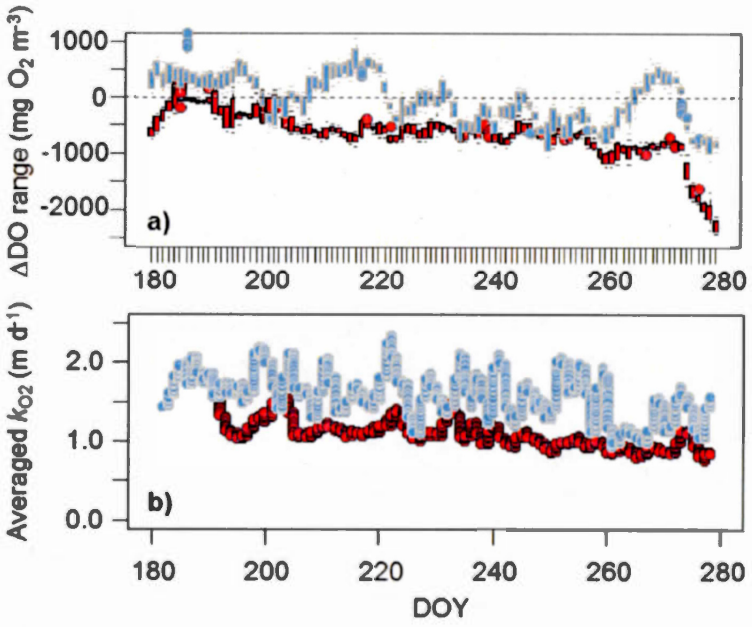

Figure 1.5. High frequency (hourly) mixed layer measurements for Lac Croche (red) and Simoncouche (blue).

a) Boxplots summarize the daily range in dissolved oxygen departure from saturation (ΔDO), with the dashed line denoting atmospheric equilibrium of the DO pool. b) Two-day moving averages of hourly k_{O2} estimates.

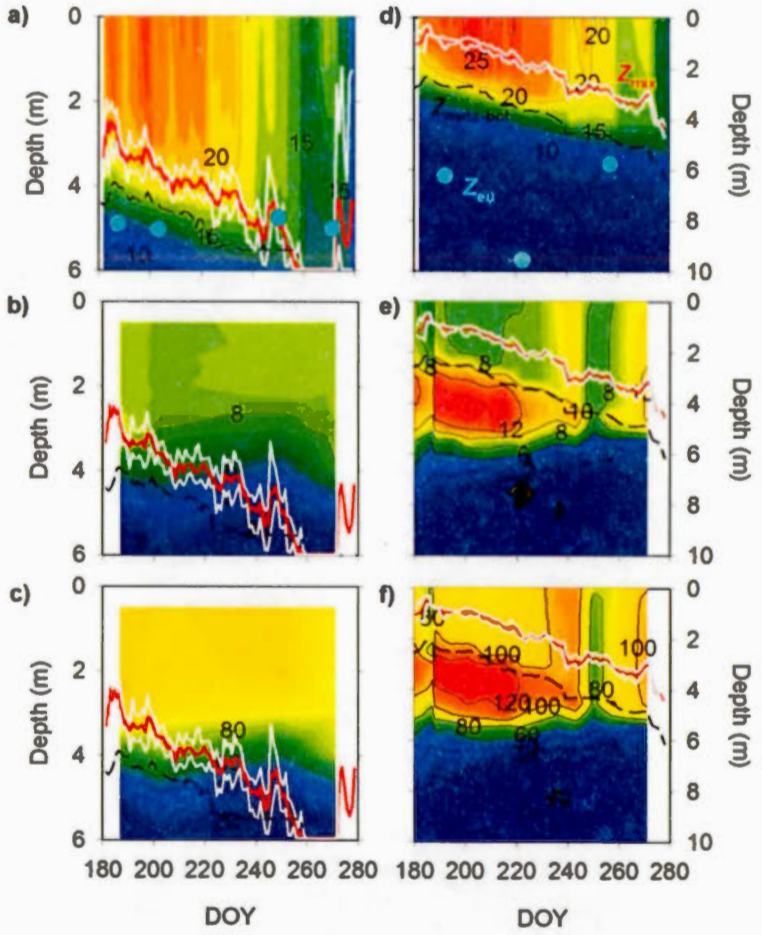

Figure 1.6. Physico-chemical conditions in Lac Simoncouche (a, b, c) and Lac Croche (d, e, f) during the 2011 ice-free season.

Contours depict lake temperature (°C; panels a, d), DO (mg L^{-1}; panels b, f), and DO saturation (%; panels c,g). Daily mean mixed layer depth (Z_{mix}; red line with max. and min. values as white lines) and the bottom of the metalimnion ($Z_{meta\text{-}bot}$; dashed black line) are shown in all panels. Point estimates of euphotic zone depth shown as turquoise circles (Z_{eu}; panels a and d). Data originally presented by Vachon and del Giorgio (2014).

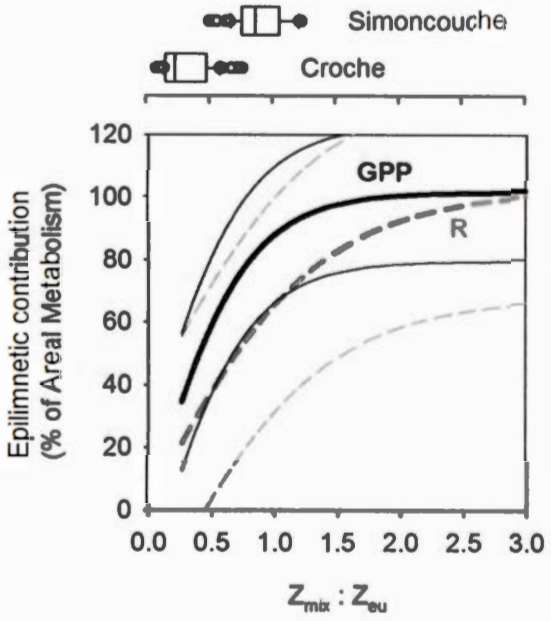

Figure 1.7. Relative contribution of epilimnetic metabolism as a function of the ratio of mixed layer depth (Z_{mix}) to euphotic zone depth (Z_{eu}).

Black solid and grey dashed lines are modelled GPP and R results from Obrador et al. (2014). Thin lines are 95% confidence intervals of each model. Boxplots show the distribution of the ratio of Z_{mix} : Z_{eu} (interpolated daily values) for the measurement periods in Lac Croche and Simoncouche.

Unfortunately, we were unable to assess how deep water GPP and R potentially impacted the surface δ^{18}O-DO pool because we did not have corresponding vertical profiles of δ^{18}-DO for this sampling period. Previous work, however, has shown an intense metalimnetic algal peak in Lac Croche (see control basin in Cantin et al. 2011; Ouellet Jobin and Beinsner, 2014) that is consistent with our expectation of increased deep-layer metabolic activity. Entrainment of metalimnetic water of differing isotopic composition would be expected to affect our calculations of isotopically derived GPP and R. On the other hand, DO concentrations above and below the mixed-layer boundary were typically very close (Fig. 1.6b,e), so incorporation of metalimnetic water into the mixed layer usually would not change diel patterns in DO concentration, and therefore not affect the diel-DO model outputs.

Knowing that the isotopic approach was likely integrating some or all of the deep-layer GPP and R in Lac Croche, we attempted to constrain this effect using two different mass balance approaches either including or excluding metalimnetic waters: First, we assumed no exchange occurred between epi- and metalimnetic water masses, and used the 2-day moving average Z_{mix} value in equations 1.4 and 1.5 (black circles, Fig. 1.8). In Lac Croche (Fig. 1.8a), values of GPP and R ranged from summertime highs of > 3000 to < 1000 mg O_2 m^{-3} d^{-1} by November. These rates were considerably larger than corresponding, published estimates of GPP and R based on diel-DO dynamics, which declined from ~ 1000 to 100 mg O_2 m^{-3} d^{-1} over the same

time period (grey squares and grey line, Fig. 1.8a). In Simoncouche, summertime rates of GPP and R were > ~ 1300 and 900 mg O_2 m^{-3} d^{-1}, respectively, each declining to ~ 500 mg O_2 m^{-3} d^{-1} by fall (Fig. 1.8b). Diel-DO derived rates of GPP and R did not systematically decline through time, but both fluctuated around 500 mg O_2 m^{-3} d^{-1} (Fig. 1.8b). In Lac Simoncouche, the differences in GPP and R derived from each of the free water approaches were also greatest in summer. Overall, the Monte-Carlo derived uncertainty associated with isotopic estimates was greatest in the summer in Lac Croche, but declined through time.

To provide a conservative, lower estimate of GPP and R, we recalculated the rates using the depth of $Z_{meta\text{-}bot}$ in equations 1.4 and 1.5, instead of Z_{mix} (thereby assuming that the metalimnetic δ^{18}O-DO pool completely integrated with the mixed layer DO pool). In Lac Croche, these rates of GPP and R (red circles, Fig. 1.8a) were typically smaller than those calculated using Z_{mix}, especially in the summertime when Z_{eu} penetrated the deepest relative to Z_{mix} (Fig. 1.6d). Overall, these more conservative estimates of GPP and R were closer to the rates derived from the diel DO model (Fig. 1.8a). For Lac Simoncouche, the first two summertime estimates of GPP and R also declined by ~ 30% when $Z_{meta\text{-}bot}$ was used in place of Z_{mix} (Fig. 1.8b). This period was also when Z_{mix} was shallowest and metalimnetic waters were fully lit (Fig. 1.6a). The potential uncertainty in estimates (assessed from the range of associated error) was typically reduced when we used $Z_{meta\text{-}bot}$ instead of Z_{mix} in our estimates of GPP and R. Taken together, though small, incremental changes in the

mass balance depth term have little effect on model outputs (see sensitivity analyses above), our results indicate that where metalimnetic metabolism plays an important role in total areal GPP and R, the isotopic mass balance model outputs depend heavily on an accurate depth estimates. In these instances it is necessary to include metalimnetic waters in the depth term of equations 1.4 and 1.5.

In both lakes, existing rates of pelagic community R (CR) estimated from *in-vitro* incubations (blue circles, Figs. 1.8a,b) were all < ~ 200 mg O_2 m^{-3} d^{-1}, and tended to be lower than the corresponding free water R values. This difference was most pronounced in the summer in Lac Croche. Although we did not have simultaneous estimates of community primary production (CPP), we used July-September average mixed layer incubation results from Carignan et al. (2000) for Lac Croche (dashed blue line = 180 mg O_2 m^{-3} d^{-1}, Fig. 1.8a). Rates of CPP were also much lower than isotopic GPP and moving-averages of diel-DO derived GPP. The large discrepancy we observed between isotopic and incubation results differs from comparisons made in large, pelagic-dominated eutrophic and hypereutrophic lakes (Luz and Barkan 2000; Bocaniov et al. 2012), where methods tend to agree well. In our case, discrepancies between bottle and oxygen isotopic free-water estimates are not surprising: Our study lakes are relatively small, and the isotopic approach integrates metabolic patterns horizontally and vertically to capture metabolic effects from other regions of the system, and may also integrate through time to capture ephemeral contributions often missed by bottle incubations (Quay et al. 2010 and references therein; Staehr et al. 2012b). Additionally, isotopic and diel DO

approaches may have captured respiration of the most labile OC that is consumed within minutes to hours, often before the initiation of incubations (Pollard 2013; Guillemette et al. 2013). Differences between R and CR are also caused by the inclusion of OM photo-oxidation in free-water R values, but not in the light-free CR, however, as calculated in the methods section, this effect only represents < 20% of surface water DO uptake).

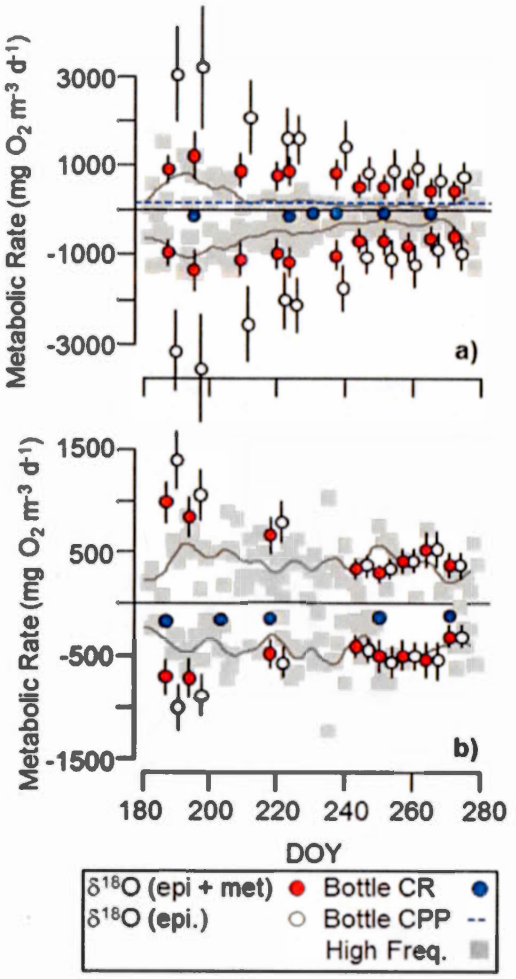

Figure 1.8. Temporal patterns in ecosystem metabolism in (a) Lac Croche and (b) Simoncouche.

Volumetric rates of metabolism in Lac Croche and Simoncouche for the 2011 ice free season. Gross primary production and respiration (GPP and R; positive and negative values, respectively) were estimated using the free water isotopic approach. We estimated GPP and R both including and excluding the metalimnetic layer in mass balance calculations (red and white circles respectively). Inclusion of the

metalimnion increases Z_{mix}, thereby lowering the volumetric metabolic rate that is otherwise attributed entirely to the epilimnetic layer. All estimates used a fractionation value (α_C) = 0.985, and bars represent $\pm$ 1 S.D. error range from Monte Carlo simulations. We compared results from the isotopic approach to a suite of published results, including daily GPP and R derived from high frequency, diel DO measurements (Vachon and del Giorgio 2014: grey square with grey lines showing 7d moving averages). Pelagic community respiration was also estimated using surface dark bottle incubations (CR; Vachon and del Giorgio 2014: blue circles). For Croche, we included an average of pelagic community primary production previously measured from July – September, converted from units of C to O assuming a photosynthetic quotient of 1.25 (CPP; Carignan et al. 2000: dashed blue line).

1.4.4 Assessing uncertainties in model parameters

We typically cannot quantify α_C or k_{O2} for individual lakes, and we are limited to applying generic values or existing empirical models to both, yet despite these limitations, our findings suggest that the isotopic approach can be broadly applied in northern lake environments with relative confidence. Not all of the steps we have taken to assess and account for the uncertainty in model outputs (adjustment of α_C values, comparison with other techniques, and both simulation and error analyses) can always be used in future applications, but there are steps that can and should be taken to improve the quality of GPP and R estimates: First, we have used an approach to estimate k_{O2} that includes both site specific, averaged wind speeds plus individual lake areas (Vachon and Prairie 2013). As major biases in k_{O2} can have important consequences for estimates of GPP and R (Fig. 1.2; Supplement 1.2), our approach likely represents a major improvement over the use of an arbitrary fixed k_{O2} value applied across all systems, especially considering how well constrained our estimates of GPP and R were (see Monte Carlo derived error estimates in Fig. 1.8).

Perhaps the largest potential source of error we encountered in this study was the effect of unaccounted metalimnetic metabolism in our mass balance model calculations, which complicates the application of the isotopic approach; particularly in deeper, clear lakes. In order to accurately determine the mixed layer depth and the presence of deep-layer metabolic peaks, the model should therefore be used in parallel with depth profiles of temperature, light penetration and DO concentration.

To deal with this we have included the entire metalimnetic depth in mass balance calculations, an approach that is supported by the consistency between isotopic and diel-DO derived rates of GPP and R, but there is no explicit rule as to the extent of metalimnion to be included. Rather, exploring a range of calculation depths is likely necessary. There is also no obvious rule as to when the metalimnetic depths must be included in future isotopic applications to lake surface waters. No correction should be necessary when $Z_{mix} = Z_{eu}$, and authors should generally be safe in using the Z_{mix} depth where $Z_{mix} : Z_{eu}$ is above ~ 0.75 (the point roughly between our two sample lakes [Fig. 1.7]), when most of the lake's metabolism occurs in the mixed layer (Fig. 1.7; Obrador et al. [2014]).

Estimates of GPP and R can also be further improved by adjusting α_C values among lakes to more accurately reflect the balance of DO-consuming processes (Fig. 1.1). In our study lakes, our error analyses suggested that even had we miscalculated α_C by plus or minus ~ 5‰, we still would have obtained reasonable measurements of GPP and R (assuming we accounted for metalimnetic influences when present). For future applications, we suggest that α_C values could be adjusted on a case by case basis, potentially along a lake size gradient, with large open lakes using a value reflecting dominance of pelagic R ($\alpha_{PEL\text{-}R}$ ~0.980 to 0.988; Fig. 1.1) up to ~0.987 in small boreal lakes where sediment R and photochemistry may have a larger influence (see methods for calculations).

1.4.5 Summary and Conclusions

We have shown here that the isotope-based estimates of lake GPP and R resulting from a point sample are in overall excellent agreement with estimates based on the more labor intensive diel-DO approach. Although each technique has their own issues and limitations, the agreement between methods is promising. This isotopic approach is simple, extremely versatile and lends itself to large-scale comparative studies of lake metabolism, yet it still has challenges that must be overcome or at least considered when interpreting the results: First, point sampling of DO and δ^{18}O-DO was restricted here to mid-day windows, and further sampling and exploration is needed to confirm if sampling at other times (early morning or evening, for instance) would importantly change model outputs in low productivity northern lakes. Second, our simulations showed that the potential for a lack of accuracy in GPP and R is greatest in heterotrophic lakes undergoing intense air-water gas exchange and intense isotopic fractionation (Fig. 1.2). Additionally, our lake applications showed that metalimnetic influences on surface δ^{18}O-DO can dramatically affect model outputs if not accounted for. Despite both of these potential limitations, the isotopic approach effectively captured patterns of GPP and R in heterotrophic Lac Croche, and Monte Carlo simulations suggested that error linked to these estimates was relatively small. Third, the mesocosm experiment may have identified a situation where the isotopic approach did not capture a transient spike in rates of GPP and R (in the nutrient + DOC treatment, week 2; Fig. 1.3c).

However, most boreal lakes are oligo- to mesotrophic (Karlsson et al. 2009; Lapierre et al. 2015), and are unlikely to undergo these large transient shifts in metabolism that are typical of more eutrophic systems. Therefore, estimates based on point samples of DO concentration and $\delta^{18}O$ should effectively capture the order of magnitude of most of these lakes. Although the diel-DO approach has its own limitations and issues, the consistency of isotopic results with the diel DO method in two such lakes (Fig. 1.8) supports this conclusion.

The isotopic approach thus offers a more integrative perspective of lake metabolism than bottle incubations that have routinely been used to estimate GPP and R (which represent a snapshot point in time for an extremely small parcel of water), because they integrate metabolic processes over the re-aeration time of surface waters in lakes and also integrate the pelagic and sediment components. In this regard, we have shown that the isotope-based estimates of GPP and R agree with those based on high-frequency, diel changes in O_2 concentration, but unlike the latter, they do not require continuous, long-term monitoring of O_2 concentrations, which are logistically difficult to implement across many lakes, especially in remote areas. Overall, our findings suggest that wider application of this method could advance our understanding of the rates and controls of ecosystem metabolism in northern lakes and likely other lake habitats of comparable, low to moderate productivity. Given the fundamental importance of metabolic measurements to our understanding of ecosystem functioning (Staehr et al. 2012), future use of the isotopic approach could

provide new ecological and biogeochemical insights for lakes that have thus far proven difficult to study.

1.5 ACKNOWLEDGEMENTS

We thank Carolina Garcia Chaves, Simon Gauthier-Fautaux, Juan Pablo Nino Garcia, Cynthia Soued, Marilyne Robidoux, and Anthony Merante for field and laboratory assistance, and Alison Derry for use of the mesocosms. Annick St. Pierre, Alice Parks and the employees of the Station de biologie des Laurentides de l'Université de Montréal provided logistical support. We thank Amber Ulseth, Erin Hotchkiss, and Yves Prairie for helpful discussions on lake metabolism and the use of DO stable isotopes, and Biel Obrador for providing published data. M.J.B. was supported by doctoral grants from the National Science and Engineering Research Council of Canada (NSERC) and the Université du Québec a Montréal. This project is part of the program of the NSERC / HQ Industrial Research Chair in Carbon Biogeochemistry in Boreal Aquatic Systems (CarBBAS), co-funded by grants from NSERC and Hydro-Québec (to P.A.d.G.).

1.6 SUPPLEMENTARY INFORMATION

1.6.1 Supplement 1.1: Photomineralization experiment

To better define the isotopic fractionation effect on DO during the photo-oxidation of DOC (α_{PHOTO}), we collected 1L of water at 0.5m depth, each from Lac Simoncouche a neighbouring lake (Lac Clarence-Gagnon) in the spring of 2012. We filtered it across a 0.2 μm membrane filter on site, and transported the water to the lab, on ice, in light-free plastic containers that were triple-rinsed with filtrate prior to filling. Samples were stored in the dark at 4°C until the beginning of the experiment. Measured DOC concentrations at the onset of the experiment were 5.9 and 5.1 mg L^{-1} in samples from Simoncouche and Clarence-Gagnon, respectively.

The photo-oxidation experiment followed standard lab protocol presented by Lapierre and del Giorgio (2014), with few changes. Samples were incubated in 24mm diameter, 40-ml glass tubes, filled to the top to remove ambient air, and capped with gas-tight, Teflon- and rubber lined caps. Samples were warmed to room temperature, then exposed to a standard light dose (0.68W m^{-2} at 340 nm) that replicated exposure to natural sunlight, inside a Q-sun XE1-BC solar simulator (Q-lab, USA). Incubation temperatures were held constant at 24 °C. As shown by Lapierre and del Giorgio (2014), colored DOC has little effect on the effective light dose in the incubation tubes. Separate incubations were conducted for each lake, and we incubated the tubes with Lac Simoncouche water for 24 hr, but extended the incubation time to 45hr for those from Lac Clarence-Gagnon to ensure sufficient

oxidation of DOC and consumption of dissolved oxygen. Calculations of α_{PHOTO} were independent of time, so differences in incubation length for each lake had no effect on results. Samples were collected at time = 0 and at the end of each experiment, with separate tubes collected for DO concentration and isotopic ($\delta^{18}O$-DO) measurements. Samples for dissolved oxygen were immediately stored at 4°C until analysis. Those for isotopic analysis were first transferred to the same 12 ml vials with gastight caps used in field sampling. To minimize contact with the atmosphere, only water from the bottom of the incubation tubes was collected using a peristaltic pump, immediately after uncapping the incubation tubes, and the water was allowed to overflow by roughly one full volume prior to being capped. To prevent any biological activity, $HgCl_2$ was added to samples, and the vials were stored in the dark at 4°C until analysis. Measurements of DO isotopic composition were the same as for field samples.

Calculation of α_{PHOTO} followed Chomicki and Schiff (2008), assuming Rayleigh fractionation effects:

$$R_f / R_i = (DO_f / DO_i)^{(\alpha PHOTO - 1)} \qquad \text{(S1.2)}$$

which was solved for α_{PHOTO} as:

$$\alpha_{PHOTO} = 1 + [\ \ln(R_f / R_i) / \ln(DO_f / DO_i)\ ] \qquad \text{(S1.3)}$$

where R_f and R_i are the ratios of heavy to light isotope in samples from the end and beginning of the experiment, respectively, and DO_f and DO_i are DO concentrations at the end and beginning, respectively.

1.6.2 Supplement 1.2: Sensitivity Analyses

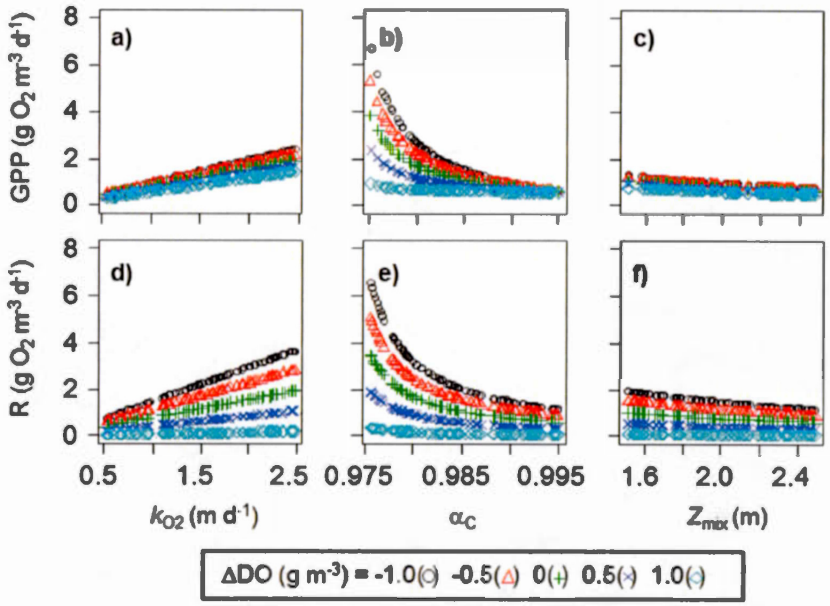

Figure S1.2 Sensitivity analysis investigating how the independent manipulation of model input terms alters estimates of respiration (R) and gross primary production (GPP) in the $\delta^{18}O$ isotopic mass balance model.

The model was applied to a hypothetical lake ecosystem similar to Lac Croche (see methods section for details). Three key parameters were manipulated, including (a,d) the air-water gas exchange coefficient (k_{O2}), (b,e) the isotopic fractionation factor associated with overall dissolved oxygen consumption during R plus abiotic DO consumption (α_C), and (c,f) the mixed-layer depth (Z_{mix}). Parameters of interest were individually manipulated at multiple oxygen saturation levels (ΔDO; see legend) assuming DO saturation was 8.5 mg L^{-1}.

1.6.3 Supplement 1.3: Mesocosm experiment

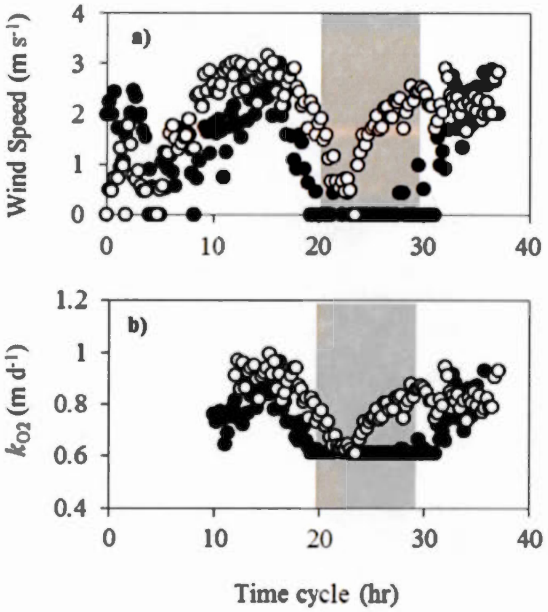

Figure S1.3.1. Diel wind speeds (a) were used to estimate (b) the air water gas exchange coefficient (k_{O2}) for weeks 2 and 5 (white and black circles respectively).

Shaded areas show nighttime periods. The x-axis denotes the course of two sampling days; hour zero is midnight on day 1, hour 40 is 16:00 on day 2.

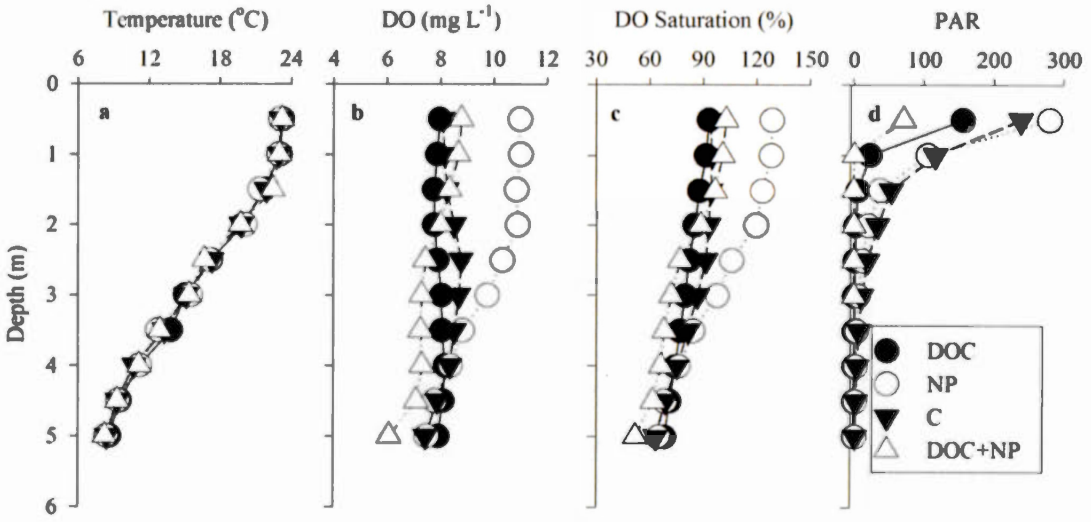

Figure S1.3.2. Vertical profiles of physico-chemical conditions during week 2 of the mesocosm experiment.

Treatments defined in legend. a) Temperature (°C), b) dissolved oxygen concentration (DO; mg L^{-1}), c) dissolved oxygen relative to saturation concentration (%), and d) photosynthetically active radiation (PAR; μE s^{-1} m^{-2}).

CHAPTER II

EMERGENT PATTERNS IN ECOSYSTEM METABOLISM ACROSS BOREAL LAKES

Matthew J. Bogard[1,2,4], Nicolas F. St.-Gelais[1], Dominic Vachon[1,3], Paul A. del Giorgio[1]

[1]Groupe de recherche interuniversitaire en limnologie, Département des sciences biologiques, Université du Québec à Montréal, Montréal, QC, Canada.

[2] Now at the School of Environmental and Forest Sciences, University of Washington, Seattle, WA, U.S.A.

[3] Now at the Institute F.A. Forel, University of Geneva, Geneva, Switzerland.

N.B. References cited in this chapter are presented at the end of the thesis.

2.1 ABSTRACT

Estimating rates of ecosystem metabolism (i.e. gross primary production, GPP; respiration, R; net ecosystem production, NEP = GPP - R) is critical to our understanding of the functioning of aquatic ecosystems, defining material and energy flows through aquatic food webs, providing key insight into connectivity to surrounding watersheds, and ecosystem roles in broader biogeochemical cycles. Northern regions host the greatest density of surface waters on the planet, yet we have a fragmented understanding of ecosystem-level metabolic patterns for lakes of this vast yet remote landscape. Here we use an oxygen isotopic approach to quantify patterns of lake metabolism across a vast (~10^6 km^2) and diverse tract of the boreal Canadian landscape. We show that mixed layer GPP and R is most strongly linked to lake total nitrogen (TN) and dissolved organic carbon (DOC) content (modulated by lake morphometry), and not light availability, despite previous work showing important effects of light on metabolism within individual habitats. We show that ecosystem-scale NEP and GPP:R increases with temperature due to increased GPP but not R, thus deviating from expectations. We link these relationships to broad geographic shifts in air temperature and precipitation, plus local variability in catchment structure, highlighting the fact that ecosystem NEP of northern lakes is under multiple, often opposing controls that are not always easy to predict based on first principles or on patterns drawn from other systems. The opposing temperature and DOC effects on NEP highlight this conclusion, suggesting

that simultaneous increases in each may not dramatically change surface water NEP under scenarios of future change.

2.2 INTRODUCTION

Decades of limnological research have linked rates of water-column gross primary production (GPP), respiration (R), and the balance between each to key features of lakes, such as light, organic matter and nutrient availability, lake temperature and morphometry, and hydrologic residence time (Fee et al. 1992; del Giorgio and Peters 1993,1994; Nurnberg and Shaw 1998; Pace and Prairie 2005; Ask et al. 2012; Staehr et al. 2012a; Solomon et al. 2013). Modeling and controlled experimentation have further linked ecosystem warming to elevated metabolic rates (Kraemer et al 2016; Vasconcelos et al. 2016) and shifts in the balance between GPP and R (Allen et al. 2005; Yvon-Durocher et al. 2010; Kritzberg et al. 2014). Our understanding of lake metabolism is still very fragmented, however, and although the number of metabolic studies of continental waters has increased greatly in recent decades (Williams and del Giorgio 2005; del Giorgio and Williams 2005; Staehr et al. 2012b), there remain large tracts of the planet's surface waters that have never been explored, and for which we lack a basic understanding of ecosystem metabolism (Staehr et al. 2012b). This is particularly true for the vast boreal biome, which harbors the highest densities of freshwaters in the world, and where these surface waters are likely to contribute the most to regional processes.

Most studies that have assessed metabolism in boreal and other northern lakes are largely based on habitat-specific, *in-vitro* incubations of water samples (Schindler 1990; Fee et al. 1992; del Giorgio and Peters 1993; Nurnberg and Shaw 1998; Dubois

et al. 2009; Ask et al. 2012; Seekel et al. 2015), and are typically limited to plankton communities in surface layers. These approaches do not necessarily capture ecosystem-level metabolism, since they exclude metabolic contributions from key aquatic habitats, such as littoral areas, sediments and deep water-column layers during periods of stratification (Vadeboncoeur et al. 2002; Lauster et al. 2006; Staehr et al. 2012a; Vesterinen 2016; Brothers et al. 2016). Further, *in vitro* estimates tend to underestimate R linked to consumption of transient but highly labile organic matter (Pollard 2013), overlook enhanced daytime rates of R (Bender et al. 1987a; Lewitus and Kana 1995; Hotchkiss and Hall 2014), and for GPP, the most commonly used ^{14}C-labelling technique often underestimates gross inorganic carbon uptake (Bender et al. 1987a). The few existing estimates of total, ecosystem-level metabolism for northern lakes, based on whole-ecosystem gas balances (i.e. Dubois et al. 2009; Vachon et al. 2016) indeed suggest that pelagic-based information may not be transposable to whole-ecosystem metabolism: Individual habitats within lakes can differ in metabolic balances (Lauster et al. 2006; Vesterinen et al. 2016), can have contrasting sensitivities to changing physico-chemical conditions (Schindler 1990; Vadeboncoeur et al. 2002; Rodriguez et al 2016; Brothers et al. 2016), and cross-habitat feedbacks may generate unexpected ecosystem-level metabolic responses following perturbations to temperature, light, and nutrient availability (Rodriguez et al. 2016; Zwart et al. 2016; Vasconcelos et al. 2016; Brothers et al. 2016). Given that current paradigms concerning the magnitude and regulation of GPP and R of northern lakes have largely been established using pelagic-based approaches, it is likely that

our understanding of ecosystem functioning in these northern systems needs reconsideration; especially in terms of upscaling lake metabolism at the regional level and establishing links between lake metabolism and gradients in environmental, landscape and climatic drivers.

Here we present a large-scale survey of whole-ecosystem (summer) metabolism (GPP, R, GPP:R and NEP) of boreal lakes, involving 124 extremely diverse systems located across 7 distinct regions in a ~10^6 km^2 tract of the boreal region of Québec, Canada, using free water dissolved oxygen (DO) concentrations and isotopic ($\delta^{18}O$) composition (Quay et al. 1995; Bocaniov et al. 2012; Bogard and del Giorgio 2016). To better define how lake and external environmental features structure patterns of ecosystem-level GPP, R, and ultimately NEP and GPP:R in northern lakes, we first explore the patterns in lake metabolism among distinct geographic boreal regions and their underlying climatic (atmospheric temperature, precipitation patterns) characteristics. We then explore the connections between metabolism and key lake features (nutrient and organic carbon content, light and temperature regimes). We then place these connections into a broader landscape context by linking metabolism to climatic (temperature and precipitation) and catchment-level (topography, plus vegetative, standing water, and wetland coverage) variability via both multiple regression (MR) and structural equation modelling (SEM) approaches. Finally, we compare our results to published, ecosystem- and

pelagic-level lake metabolic patterns to re-evaluate our understanding of whole-lake metabolic rates and balances in northern lakes.

2.3 METHODS

2.3.1 Study area and sampling approach

The lakes sampled in our study are located in north-eastern Canada, in the boreal region of the province of Québec (Fig. 2.1a). Regional and lake characteristics have previously been detailed (Rasilo et al. 2015; Lapierre et al. 2015; Bogard and del Giorgio 2016). Lakes were sampled once each from 2010 – 2013 (late June to mid-August). Samples were collected from the deepest measured site. Depth profiles of temperature, pH, and DO were made with a combination probe (Yellow Springs Instruments, USA), and Secchi depth measurements were made at each site. In lakes where thermal stratification was present, mixed layer depth (Z_{mix}) was estimated visually from temperature-depth curves as the depth of maximal thermal gradient. Estimates of percent DO saturation were corrected for site-specific atmospheric pressure. DO probes were calibrated at each site in vapour-saturated air, at ambient pressure and surface water temperature. Samples for $\delta^{18}O$ analysis were taken at ~25-50 cm depth, using 12-ml precombusted borosilicate vials, preserved with $HgCl_2$, capped free of air with a gastight rubber lined plastic cap, then stored in the dark at 4°C until analysis. Samples for δO^{18}-H_2O were collected in 125ml plastic bottles, filled to full capacity free of air, and stored in the dark until analysis.

2.3.2 Climate and catchment characteristics

As previously described (Bogard and del Giorgio 2016), hourly wind data for the period of sampling from one central location in each region were taken from the Environment Canada website (https://weather.gc.ca/canada_e.html), and from the weather station of the Université de Montréal Biological research station (http://www.sbl.umontreal.ca/territoire-cartes/meteorologie/index.html) for the Laurentians region (Fig. 2.1a). Individual catchment characteristics and regional long-term climatic conditions were estimated and described by Lapierre et al. (2015).

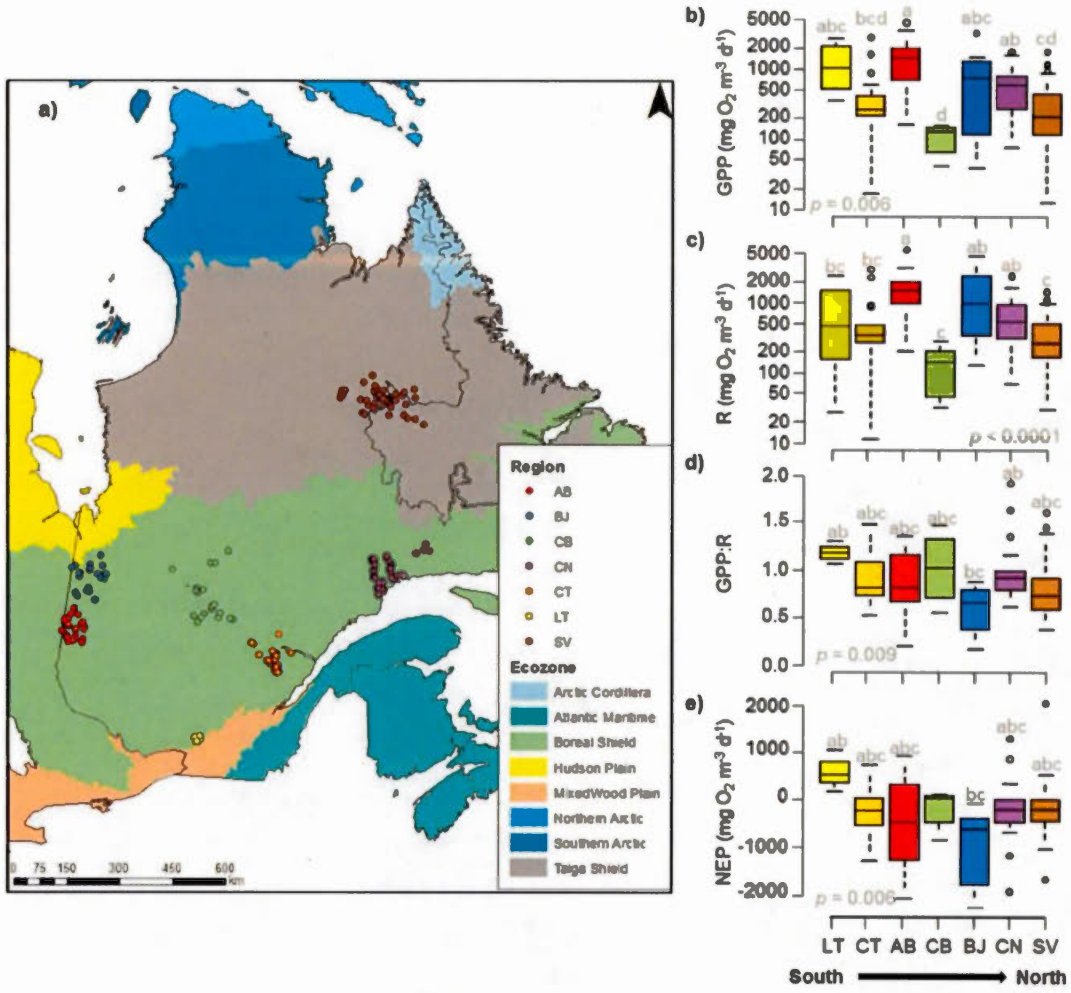

Figure 2.1. Landscape-level shifts in lake ecosystem metabolism throughout north-eastern Canada.

Map of sampled lakes in northern Quebec, Canada (**a**). Boxplots denote GPP (**b**), R (**c**), GPP:R (**d**), and NEP (**e**), grouped and colored by sampling region, and coarsely arranged from south to north. Statistical differences among regions assessed using one way ANOVA and Tukey's HSD post hoc tests (results shown in grey text).

2.3.3 Lake physical and morphometric characteristics

Lake morphometry, including volume, mean and maximum depths (Z_{mean} and Z_{max}, respectively) were modelled from lake area and catchment topography following Heathcote et al. (2015). Water residence times (WRT) were calculated by dividing lake volume (m^3) by catchment specific rates of average annual runoff (i.e., precipitation [m yr^{-1}] multiplied by catchment area [m^2]). We calculated the light extinction coefficient (k_d; the) as 1.7 / Z_{secchi}, and the euphotic zone depth (Z_{eu}; the depth at which only 1% of light from the lake surface penetrates) as 4.605 / k_d following Wetzel (2001).

2.3.4 Laboratory analyses

Samples of epilimnetic water from each lake were brought to the lab, and stored in the dark at 4°C until further analysis. Concentrations of total P (TP), total nitrogen (TN), dissolved organic carbon (DOC), and water absorbances at 440nm, an indication of the presence of colored dissolved organic matter (cDOM). We collected particulate organic matter (POM) in epilimnetic water on filters (GF/F, Whatman, Kent, UK) to then estimate algal biomass as chlorophyll *a* (chl *a*). Each of these analyses is fully detailed in our previous work (Bogard and del Giorgio 2016) and related papers by Rasilo et al. (2015) and Lapierre et al. (2015). In all cases,

duplicate samples were separately collected, stored, and analyzed, and average values are reported here.

2.3.5 NEP and gas flux

In a previous study (Bogard and del Giorgio 2016) we had presented estimates of steady-state, free water NEP for these lakes, where we estimated volumetric rates of NEP as

$$\Delta_{O2} = \text{NEP} - (F_{O2} / Z_{mix}) \qquad (2.1)$$

Where we assume the deviation of DO from saturation (Δ_{O2}; mg O_2 m^{-3}) at steady state results from the balance between NEP and gas exchange with the atmosphere. This assumption has been previously validated for use at the daily- to multi-day scale, and is discussed in detail in Bogard and del Giorgio (2016). Air-water fluxes of O_2 (F_{O2}) were calculated for each lake from Fick's law of diffusion using equation 2.2:

$$F_{O2} = k_{O2} \times \Delta_{O2} \qquad (2.2)$$

where F_{O2} is flux of O_2 across the air-water interface (mg O_2 m^{-2} d^{-1}), k_{O2} is the gas exchange coefficient at a given temperature (m d^{-1}). We estimated k_{O2} for each lake from calculated k_{600} values (following Jahne et al. 1987) in equation 2.3:

$$k_{O2} = k_{600} \times (Sc / 600)^{-2/3} \qquad (2.3)$$

where *Sc* is the temperature-specific Schmidt number for O_2 (Wanninkof 1992). Estimates of k_{600} were based on the model presented by Vachon and Prairie (2013) as a function of wind speed and lake area, using equation 2.4:

$$k_{600} = 2.51 + 1.58 \times U_{10} + 0.39 \times U_{10} \times \log_{10}(LA) \qquad (2.4)$$

where k_{600} is estimated in cm h^{-1}, U_{10} is wind speed at 10m height above the lake (m s^{-1}), and *LA* is lake area (km^2). For each lake, wind speed was estimated as the moving average of the 7 previous days' mean wind speed recorded at the nearest weather station (Bogard and del Giorgio 2016). Of all the lakes for which NEP was estimated, we discarded 5 extreme outliers (> 3 or < -3 g O_2 m^{-3} d^{-1}) that were well beyond any reasonable estimate.

2.3.6 Stable isotopic estimates of GPP, R, and GPP:R

Isotopic compositions are reported in delta (δ) notation following equation 2.5;

$$\delta^{18}O = ((R_{sample} / R_{standard}) - 1) \times 1000 \qquad (2.5)$$

where *R* and $R_{standard}$ is the ratio of heavy to light isotopes (^{18}O : ^{16}O) in lake water samples (R_{sample}) and in Vienna standard mean ocean water (VSMOW; $R_{standard}$), respectively. The isotopic mass balance approaches used here assume an absence of physically driven changes in DO via vertical or lateral exchange of water masses,

such that GPP, R, and atmospheric gas exchange are the only processes driving temporal DO and δ^{18}O-DO dynamics , as expressed by equations 2.6 and 2.7;

$$dDO / dt = k_{O2} \times (DO_{sat} - DO) / Z_{mix} + GPP - R \quad (2.6)$$

$$d^{18:16}DO / dt = k_{O2} \times \alpha_g \times (DO_{sat} \times {}^{18:16}air \times \alpha_s - DO \times {}^{18:16}DO) / Z_{mix} +$$

$$(GPP \times {}^{18:16}H_2O \times \alpha_p) - (R \times {}^{18:16}DO \times \alpha_r) \quad (2.7)$$

where isotopic ratios of DO, atmospheric O_2 and H_2O are summarized as $^{18:16}$DO, $^{18:16}$air, and $^{18:16}H_2O$, respectively, and DO_{sat} represents concentrations of DO at equilibrium with the atmosphere.

In all applications, we assume the δ^{18}O signature of air to be 23.5‰ (Bocaniov et al. 2012). The terms α_g, α_s, and α_p are the respective isotopic fractionation factors related to kinetic gas exchange (0.9972; Knox et al. 1992), gas solubility effects (1.0007; Benson and Krause 1984), and photosynthetic DO production (1.000; Guy et al. 1993). In boreal lakes, the fractionation effect during DO uptake linked to ecosystem R (α_r) reflects the balance of all DO-consuming processes in the mixed layer (pelagic R, sedimentary R and photochemical DO consumption). We have previously discussed these effects in detail (Chapter I), where we have justified the use of an integrated, ecosystem level fractionation factor of roughly 0.985, and have shown (Bogard and del Giorgio 2016) that metabolic calculations and the interpretation of metabolic patterns over the large scale

environmental and metabolic gradients in this dataset are likely insensitive to small inaccuracies in this term. As with all free-water metabolic estimates, we cannot directly tease apart biotic and abiotic DO consumption processes, but suggest that photochemical effects should not greatly affect our calculations since rates of metabolism have been shown to greatly exceed rates of photo-oxidative DO consumption in surface mixed layers of northern lakes (Granéli et al. 1996; Jonsson et al. 2001; Vachon et al. 2016).

Estimation of GPP:R followed Quay et al. (1995), assuming steady state conditions for values of DO and $^{18:16}$DO (i.e., net metabolic effects on the DO pool and $^{18:16}$DO are balanced by net effects of air-water gas flux), by combining equations 2.6 and 2.7 and rearranging to solve for the value of GPP:R (equation 2.8);

$$GPP : R = (^{18:16}H_2O \times \alpha_p - {}^{18:16}O_g) / (^{18:16}DO \times \alpha_p - {}^{18:16}O_g) \qquad (2.8)$$

where $^{18:16}O_g$ summarizes the net flux of O_2 across the air-water interface (equation 2.9):

$$^{18:16}O_g = \alpha_g \times (^{18:16}air \times \alpha_s - {}^{18:16}DO \times DO / DO_{sat}) \; / \; (1 - DO / DO_{sat}) \qquad (2.9)$$

This approach, and the validity of associated assumptions have been previously tested and shown to hold in our earlier work (Bogard and del Giorgio 2016).

Next, we quantified rates of GPP and R for each lake, following Bocaniov et al. (2012, 2015), by incorporating estimates of F_{O2} (equations 2.2 to 2.4) into

equations 2.6 and 2.7, and then rearranging and solving for GPP and R individually. This approach also assumes no net change in DO concentrations or ^{18}O-O_2 over daily- to multi-day periods (i.e., steady-state conditions), an assumption that is suitable for oligo- to mesotrophic boreal lakes (Bogard et al. manuscript under review). We solved for GPP and R using equations 2.10 and 2.11;

$$GPP = (k_{O2} / Zmix) \times [DO \times (b - c) - DO_{sat} \times (a - c)] / d - c \quad (2.10)$$

$$R = (k_{O2} / Zmix) \times [DO \times (b - d) - DO_{sat} \times (a - d)] / d - c \quad (2.11)$$

where, following Bocaniov et al. (2012), $a = {}^{18:16}O_{air} \times \alpha_s \times \alpha_g$, $b = {}^{18:16}O_{DO} \times \alpha_g$, $c = {}^{18:16}O_{DO} \times \alpha_C$, and $d = {}^{18:16}O_{H2O} \times \alpha_p$.

We visually inspected the estimates of GPP, R, and GPP:R, and discarded any extreme outliers or impossibly negative values that likely arose due to physical effects on gas temperature and solubility (Bocaniov et al. 2015) or other errors associated with sample collection and preservation. Further, deep layer metabolic processes may have influenced the isotopic composition of surface DO in some cases where light penetration greatly exceeded mixed layer depth, but the actual mixing depth is difficult to constrain. This effect represents a potentially source of error in the isotopic approach (as detailed in Chapter 1; Bogard et al. under review). In most cases this effect was likely minimized by using a Z_{mix} value (i.e., the depth of maximal vertical temperature change) that would have incorporated a large fraction of metalimnetic metabolism. Further, we closely inspected lakes where light

penetration greatly exceeded Z_{mix} (i.e., Zmix : Zeu < 0.5), and removed 5 outliers that had metabolic rates greatly exceeding any reasonable estimate.

2.3.7 Statistical methods

Analyses were performed using R version 3.0.3 (R development core team 2014). In all analyses, data distributions and distributions of regression residuals were assessed visually, and where necessary, transformed using a $\log_{10}$ approach (or logit approach percentage estimates of relative catchment cover) to meet assumptions of normality. We used a combination of simple regression and Pearson correlation analyses ('Hmisc' package; [Harrell 2014]) to assess bivariate relationships. We used multiple linear regression analyses to both assess the key predictors and relative importance at each level of lake predictors (catchment features, lake structure, and lake physico-chemical conditions), and then to combine parameters to generate the best predictive model for each of GPP, R, GPP:R, and NEP. We assessed the grouped, inter-regional differences in metabolic measurements using one way analysis of variance (ANOVA) and Tukey HSD *post-hoc* comparisons.

We used a structural equation modelling (SEM) approach ('lavaan' package; Rosseel 2012) to assess the drivers of GPP, R, and NEP in a hierarchical manner that incorporated both direct and indirect drivers of lake metabolism, and allowed us to assess the relative strength of individual, direct and indirect factors that shaped

patterns of metabolism. To summarize catchment structure variables in the SEM, we conducted a principal components analysis (PCA; 'vegan' package [Oksanen et al. 2013]). Data were scaled and centered prior to analysis. Scores from the first axis of the PCA were then used in the SEM.

To identify whether other inter-regional features not accounted for in the models could have been important predictors, we took the top combined models for each metabolic parameter, and compared the predictive strength (based on AIC scores) among our standard linear models in tables S2.1 and S2.2, versus models that included either a random intercept, or both random intercept and slope term. In every case, models were not improved with the inclusion of these random effects terms (data not shown), and we did not explore these relationships further.

2.4 RESULTS

2.4.1 Cross-lake and inter-regional patterns in lake metabolism

Metabolism ranged widely across the study lakes, both in terms of GPP (median = 335, interquartile range = 172 to 788 mg O_2 m^{-3} d^{-1}; Fig. S2.1) and R (391, 228 to 895 mg O_2 m^{-3} d^{-1}; Fig. S2.1). Average lake GPP varied among regions (ANOVA: $p < 0.0001$; Fig. 2.1b) and declined weakly with latitude, showing a positive correlation with regional mean annual air temperatures and terrestrial productivity, but no link to precipitation (r = 0.42, 0.44, and 0.11, respectively; Table 2.1). On the other hand, although averaged regional lake R differed among regions (ANOVA: $p < 0.0001$; Fig. 2.1c), there was no clear latitudinal pattern, and values were weakly linked to average regional climate and terrestrial productivity (r = 0.32 to -0.02; Table 2.1).

Most lakes were net heterotrophic during the sampling period (GPP < R), but a major subset (~30%) were net autotrophic (as observed by Bogard and del Giorgio 2016). Despite the wide range in GPP:R (median = 0.84, interquartile range = 0.66 to 1.01; Fig. S2.1), it differed less among regions (ANOVA: $p = 0.009$; Fig. 2.1d) than either GPP or R, and generally declined moving northward, with a comparatively strong correlation to cross-regional gradients in air temperature, total precipitation, and terrestrial productivity (r = 0.57 to 0.63; Table 2.1). Rates of NEP ranged widely across all lakes (median = -202, interquartile range = -512 to 25 mg O_2 m^{-3} d^{-1}; Fig. S2.1), but varied less across regions than did GPP or R (ANOVA: $p = 0.006$; Fig. 1e),

and was only weakly correlated to mean annual air temperature, total annual precipitation, and catchment productivity (r = 0.26 to 0.35; Table 2.1).

Table 2.1. Regional correlations between metabolism and environmental characteristics.

Correlation of averaged, region-specific metabolic parameters (GPP, R, GPP : R, and NEP) and long-term regional mean annual air temperature (MAT; °C), mean of total annual precipitation (Precip; mm yr^{-1}), and net catchment productivity (NPP; g C m^{-2} yr^{-1}).

Regional Characteristics	GPP	R	GPP : R	NEP
	Pearson correlation (*r*)			
MAT	0.42	0.3	0.63	0.35
Precip	0.11	-0.02	0.62	0.35
NPP	0.44	0.34	0.57	0.26

2.4.2 Limnological predictors of lake metabolism

We explored the underlying drivers of lake metabolism more closely by comparing metabolic variables to individual lake physico-chemical characteristics (Figure 2.2). The strongest direct positive predictor of both GPP and R was TN (Fig. 2.2a; GPP: $r^2 = 0.32$, $p < 0.0001$, $\log_{10}GPP = 1.31 + 3.41[\log_{10}TN]$; R: $r^2 = 0.30$, $p < 0.0001$, $\log_{10}R = 1.27 + 3.42[\log_{10}TN]$), followed by DOC (Fig. 2b; GPP: $r^2 = 0.24$, $p < 0.0001$, $\log_{10}GPP = 0.94 + 1.75[\log_{10}DOC]$; R: $r^2 = 0.25$, $p < 0.0001$, $\log_{10}R = 0.98 + 1.77[\log_{10}DOC]$). We also found a positive relationship between the light attenuation coefficient and both GPP and R, such that more colored waters with limited vertical light penetration had overall elevated metabolic rates (Fig. 2c; GPP: $r^2 = 0.25$, $p < 0.0001$, $\log_{10}GPP = 0.77 + 2.63[\log_{10}k_d]$; R: $r^2 = 0.29$, $p < 0.0001$, $\log_{10}R = 0.85 + 2.67[\log_{10}k_d]$). Because the effects on both GPP and R were similar, there was little connection between TN and either NEP or GPP:R (Fig. 2a; $r^2 \leq 0.03$). We found no relationship ($r^2 = 0.00$) between GPP:R and k_d, and a weak relationship between NEP and k_d (fig. 2c; $r^2 = 0.06$, $p = 0.002$; $NEP = -292 - 500[\log_{10}k_d]$). We found a weak, negative relationship between NEP and DOC concentrations (Fig. 2b; $r^2 = 0.04$, $p = 0.01$; $NEP = 176 - 509[\log_{10}DOC]$) but no connection between DOC and GPP:R ($r^2 = 0.00$). Water temperature was a weak direct predictor of GPP:R and NEP in individual lakes (Fig. 2d; $r^2 \leq 0.02$), despite correlations between the patterns in mean regional lake metabolism and regional air temperatures (Table 2.1) discussed above.

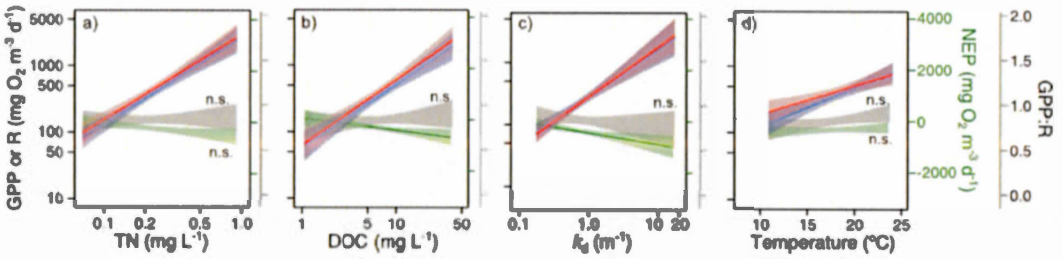

Figure 2.2. Direct drivers of lake ecosystem metabolism.

Simple linear regression models depicting the relationship between rates of GPP (blue), R (red), NEP (green), and GPP:R (grey) as a function of total nitrogen (TN; panel **a**), dissolved organic carbon concentrations (DOC; panel **b**), the light extinction coefficient (k_d; panel **c**), and surface water temperatures (panel **d**). Significant ($r^2 \geq 0.04$) models are presented as solid lines. Non-significant relationships denoted by 'n.s.'.

2.4.3 Combined catchment and lake predictors of metabolism

We used multiple linear regressions on a subset of the lakes (n = 125 after removing lakes with missing data) to assess the key predictors and relative importance among catchment features, lake structure, and lake physico-chemical conditions, with the top models (based on AICc scores and adjusted r^2 values) presented in table 2.2 (the full suite of models given in Supplementary Tables S2.1 and S2.2). Lake physico-chemical features were the strongest predictors of both GPP and R (r^2 adj. = $\geq$ 0.27; Table 2.2). Concentrations of DOC and TN, plus water temperature were always significant and positive, while k_d (the light extinction coefficient) was not significant in either case (Table S2.1) and removed from subsequent models. Lake morphometric (area, perimeter length, and dynamic ratio) and hydrologic (WRT) variables accounted for little of the variability in GPP and R (r^2 adj. $\leq$ 0.06; Table S2.1), while catchment features alone accounted for an intermediate amount of variability in GPP and R (r^2 adj. = 0.14 and 0.17, respectively; Table S2.1). Combinations of predictors from each group generated the best predictive models for both GPP and R (r^2 adj. = 0.36 and 0.41, respectively; Table 2.2): Both the relative water area in catchment and estimates of lake area were negatively related to GPP and R. The relative wetland area in the catchment (% wetlands) was a positive predictor of R, although it was not statistically significant when added (Table S2.1). We retained % wetlands in the model (Table 2.2) as AIC values improved (i.e., lowered) and the adjusted r^2 value improved by 0.03 compared

to models run without it (data not shown). It is clear from these models that both catchment and lake features interact in determining the rates of surface water GPP and R.

For both GPP:R and NEP, the different categories of predictors each accounted for a small fraction of variability and categories were roughly equivalent in adjusted r^2 values (r^2 adj. = 0.04 to 0.09; Table S2.2). Water temperature (positive) and the percentage of catchment wetland cover (negative) were the only significant predictors of GPP:R in individual models (Table S2.2), and were the best combination of predictors, although they only accounted for a small portion of the variability in GPP:R (r^2 adj. = 0.15; Table 2.2). The model results for NEP were generally similar to those for GPP:R. Concentrations of DOC and morphometric variables were marginally significant in the individual models (Table S2.2), although the best combined model included only DOC concentration, temperature, and percent wetland cover (r^2 adj. = 0.11 to 0.15; Table 2.2). Overall, these negative relationships suggested that increased catchment wetland cover and greater lake DOC concentrations favor more heterotrophic conditions, while the positive relationship between net metabolism (as GPP:R and NEP) and water temperature suggests that warming favours net autotrophic ecosystem metabolism.

Table 2.2. Summary of the top multiple regression models predicting lake GPP, R, GPP:R, and NEP from a combination of lake and catchment characteristics. Full results are presented in tables S2.1 and S2.2. Parameters included here are DOC (mg L^{-1}), TN (mg L^{-1}), water temperature (°C), lake area (m^2), and catchment cover as percentage of wetland (%wet) and standing water (%H_2O) in each respective catchment.

Parameter	r^2 adj.	*p*-value	Coefficients	Estimate	S.E.	*t*-value	*p*-value
Log_{10}(GPP)	0.36	< 0.0001	Intercept	1.91	0.47	4.07	<0.00001
			logit(%H_2O)	-0.09	0.05	-1.90	0.060
			log_{10}(lake area)	-0.10	0.03	-3.24	0.002
			log_{10}(TN)	0.69	0.19	3.68	0.000
			log_{10}(DOC)	0.33	0.18	1.87	0.064
			log_{10}(Temp)	1.05	0.31	3.37	0.001
Log_{10}(R)	0.41	< 0.0001	(Intercept)	2.51	0.44	5.70	<0.00001
			logit(%H_2O)	-0.07	0.04	-1.56	0.121
			logit(%wet)	0.02	0.05	0.37	0.714
			log_{10}(lake area)	-0.08	0.03	-2.92	0.004
			log_{10}(DOC)	0.44	0.16	2.68	0.008
			log_{10}(TN)	0.71	0.17	4.28	<0.00001
			log_{10}(Temp)	0.53	0.27	1.93	0.056
GPP:R	0.15	< 0.0001	Intercept	-0.48	0.31	-1.54	0.127
			logit(%wet)	-0.12	0.03	-3.56	0.001
			log_{10}(Temp)	0.76	0.24	3.23	0.002
NEP	0.11	0.0007	Intercept	-1699.91	624.22	-2.72	0.007
			logit(%wet)	-161.89	71.61	-2.26	0.026
			log_{10}(DOC)	-454.01	229.85	-1.98	0.051
			log_{10}(Temp)	1030.97	467.70	2.20	0.029

The interactions between limnological, landscape and climate drivers determining the regional spatial patterns in whole-lake GPP, R, and NEP became more apparent when explored using a structural equation modeling (SEM; Fig. 2.3) approach on the same data subset as was used in MR analyses. Because the catchment metrics tend to strongly co-vary at regionals scales, we summarized these highly collinear catchment structure variables (including total catchment area and slope, relative coverage of wetlands, standing water, forests, and total vegetation) with a principal components analysis (PCA; Fig. S2.2), whose first axis scores co-varied with latitude (standardized effect = -0.56; Fig. 2.3) with a south to north trend towards flatter, more water-rich catchments, and with a parallel shift toward larger lakes. We used the scores of this axis in the SEM as an emergent variable that integrates catchment and lake properties.

The SEM suggests that the influence of the climatic and watershed drivers on lake metabolism (GPP and R) is complex, but mostly meditated by their effect on lake nutrients and DOM: Northward declines in precipitation were associated to increases in lake TN (-0.45; Fig. 2.3), possibly through greater evapo-concentration and less dilution of nutrients (Schindler et al. 1996), which in turn appeared to enhance both GPP and R (0.33, 0.37 respectively; Fig. 2.3). There was a direct negative effect of latitude on TN (-0.48; Fig. 2.3) may indicate northward declines in total bio-available N entering lakes as a function of declining catchment net primary production (NPP *versus* latitude: $r^2 = 0.89$, $p < 0.00001$). Although NPP was

estimated at too coarse a resolution to include at the individual lake level, this potential explanation is supported by the positive relationship that we observed between average regional terrestrial NPP, and both lake GPP and R (r = 0.34 and 0.44; Table 2.1), which were absent for precipitation (0.11 and -0.02; Table 2.1). Interestingly, the positive effect of TN on both GPP and R was roughly of the same magnitude (Fig. 2.3), and therefore the effect of TN on the resulting NEP was weak. Further, lakes tended to increase in size in the more northerly, flatter catchments (-0.31; Fig. 2.3), which also had a near equal, negative effect on GPP and R (-0.26, -0.23 respectively; Fig. 2.3). Taken together, SEM results suggest that combined shifts in trophic status and lake morphometry across the boreal landscape interact to shape GPP and R, but these effects offset each other such that NEP shows little relationship with these drivers.

The large-scale spatial patterns in lake NEP responded most strongly to regional patterns in water temperature and DOC concentrations. Northward cooling of water temperatures (-0.39; Fig. 2.3) negatively affected rates of GPP (0.14; Fig. 2.3) but surprisingly not R, resulting in the unexpected, aforementioned northward shift to negative (heterotrophic) NEP. Shifts toward increased lake net heterotrophy were also favored by increasing lake DOC concentration, although this relationship was complex: Lake DOC concentrations simultaneously increased in flatter, water-rich catchments (0.20; Fig. 2.3), but declined via an opposing connection to latitude (-0.77; Fig. 2.3), possibly reflecting northward declines in catchment soil content and

NPP (as discussed above for TN) and reductions in terrestrial OC delivery to more northerly lakes. Increased DOC concentrations had a positive effect on both R and more surprisingly on GPP (0.31, 0.20 respectively; Fig. 2.3). These patterns collectively point to a complex regulation of lake NEP via the interplay between both lake DOC and nutrient content, and temperature, in ways that cannot necessarily be extracted from exploring the drivers of GPP and R individually.

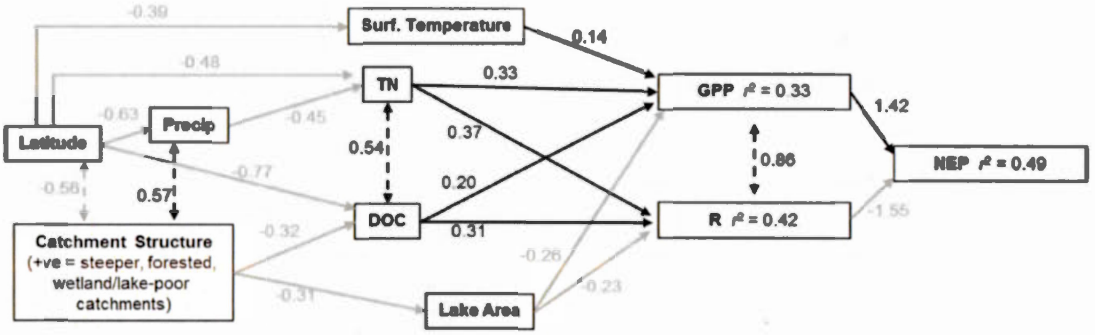

Figure 2.3. Hierarchical control of landscape-level metabolic variability in northern lakes.

A structural equation model (SEM) was used to define the hierarchical regulation of lake GPP, R, and ultimately, NEP. Solid black and grey arrows denote positive and negative effects, respectively. Dashed arrows denote residual covariance between 2 variables. Standardized coefficients summarizing the relative effect sizes are given beside each arrow. $n = 125$; χ^2 test statistic = 26.8; model degrees of freedom = 25; $P = 0.37$.

2.5 DISCUSSION

Global syntheses of ecosystem metabolism in largely sub-boreal lakes indicate that NEP is relatively insensitive to changes in limnological features compared to either GPP or R (Hoellein et al. 2013; Solomon et al. 2013), a conclusion that we confirm here for northern lakes (Fig. 2.2; Table 2.2). It is widely assumed indirect human activities that are warming lake waters and often enhancing lake DOC content may be favouring shifts in the food web toward more negative NEP (Jansson et al. 2003, 2007; Yvon-Durocher et al. 2010; Larsen et al. 2011; Ask et al. 2012). Our results contradict this prediction, and suggest that both effects may actually oppose one another to make lake NEP less sensitive to change than expected, an observation that is consistent with recent experimental work (Kritzberg et al. 2014; Rodriguez et al. 2016). Although we found a very wide range in the rates of NEP and GPP:R among lakes (Figs. 2.1b-e & S2.1), these variables were only weakly (and opposingly) predicted by water temperature and DOC (Fig. 2.3, Table 2.2), despite GPP and R being strongly positively linked to lake TN and DOC content, and negatively to lake size (Figs. 2.2 & 2.3; Table 2.2). These key relationships between GPP, R and lake solute content (TN, DOC), morphometry, and water temperature were ultimately linked to broad geographic shifts in air temperature and precipitation, plus local variability in catchment structure (Figure 2.3). These relationships highlight the underlying complexity of the regulation of ecosystem NEP, with multiple, often opposing environmental controls, which must be simultaneously

considered if we are to understand the underlying mechanisms and accurately predict future trajectories of northern lake metabolism and food web functioning.

2.5.1 Whole-lake versus habitat-specific lake metabolism

The rates of GPP and R that we measured here scale well with existing whole lake estimates (Fig. 2.4a,b; Solomon et al. 2013), but are generally much higher than incubation-based estimates of pelagic community primary production and R (Fig. 2.4a,b; del Giorgio and Peters 1994), or indirect estimates based on adding pelagic and benthic primary production measurements (Fig. 2.4a; Seekel et al. 2015). This discrepancy is not surprising and has been reported in previous comparisons of free-water versus bottle-based approaches (Lauster et al. 2006; Staehr et al. 2012a,b). Ecosystem and community-level rates tend to converge in oligotrophic systems (Fig. 2.4a,b), generally as a function of lake size (Staehr et al. 2012a). The trends shown in Fig. 2.4a and b suggest that rates of material and energy flow have been systematically underestimated in most northern lake food webs; assessments of northern lake metabolism have almost exclusively been generated from *in vitro* measurements of planktonic production and respiration (Kelly et al. 2001; Carignan et al. 2000; Jonsson et al. 2001; Jansson et al. 2003; Ask et al. 2012; Kankaala et al. 2013; Seekell et al. 2015). These estimates have been shown to potentially underestimate pelagic metabolism (Bender et al. 1987a; Quay et al. 2010; Pollard

2013), and exclude key lake habitats (Vadeboncoeur et al. 2002; Lauster et al. 2006; Lewis 2011; Vestereinen et al. 2016; Brothers et al. 2016). Underestimation of metabolic rates, in turn, may limit our understanding of the magnitude at which important processes (e.g., food web interactions, biogeochemical processes, the cycling and transformation of contaminants) are occurring throughout northern aquatic landscapes.

In addition to potential differences in magnitude, our findings indicate that the actual patterns of ecosystem-level net metabolism across lakes deviate from those that have been reported for pelagic metabolism (Fig. 2.4c). Our estimates of NEP span the full range of globally reported ecosystem NEP (Fig. 2.4c; Solomon et al. 2013), even though the global lake dataset spans a much longer nutrient gradient (TN range = 0.13 to 5.84 mg L^{-1}, TP range = 4.3 to 186 μg L^{-1}) than our lakes (TN range = 0.07 to 0.91 mg L^{-1}, TP range = 2.58 to 153.20 μg L^{-1}). The consistency in NEP range between the two datasets is due in part to the fact that we are comparing our summertime estimates to annual averages of global lake data that are constrained by light and temperature restrictions in shoulder seasons, and also because our point sampling approach has a large degree of natural variability linked to methodological limitations (discussed fully in Bogard and del Giorgio 2016). Despite these issues, our estimates of ecosystem NEP and GPP:R (not shown) showed a large range in net metabolism (Fig. 2.4c), with no clear link to shifts in trophic status, a result that is consistent with whole-ecosystem metabolic surveys (Solomon et al. 2013; Hoellein et

al. 2013), but deviates from planktonic community assessments (del Giorgio and Peters 1994; Sand-Jensen and Staehr 2009; Ask et al. 2012; but see Carignan et al. 2000), which show planktonic communities are mostly net heterotrophic, and net metabolism is positively linked to trophic status such that planktonic communities only reach net autotrophy under highly eutrophic conditions (Schindler 1990; del Giorgio and Peters 1994; Sand-Jensen and Staehr 2009). Consistent with recent experimental findings (Rodriguez et al. 2016), our results suggest that cross habitat interactions likely strongly offset changes within individual habitats of northern lakes, to ultimately render whole-lake NEP a less sensitive property than would be expected based on the patterns derived for any individual lake habitat.

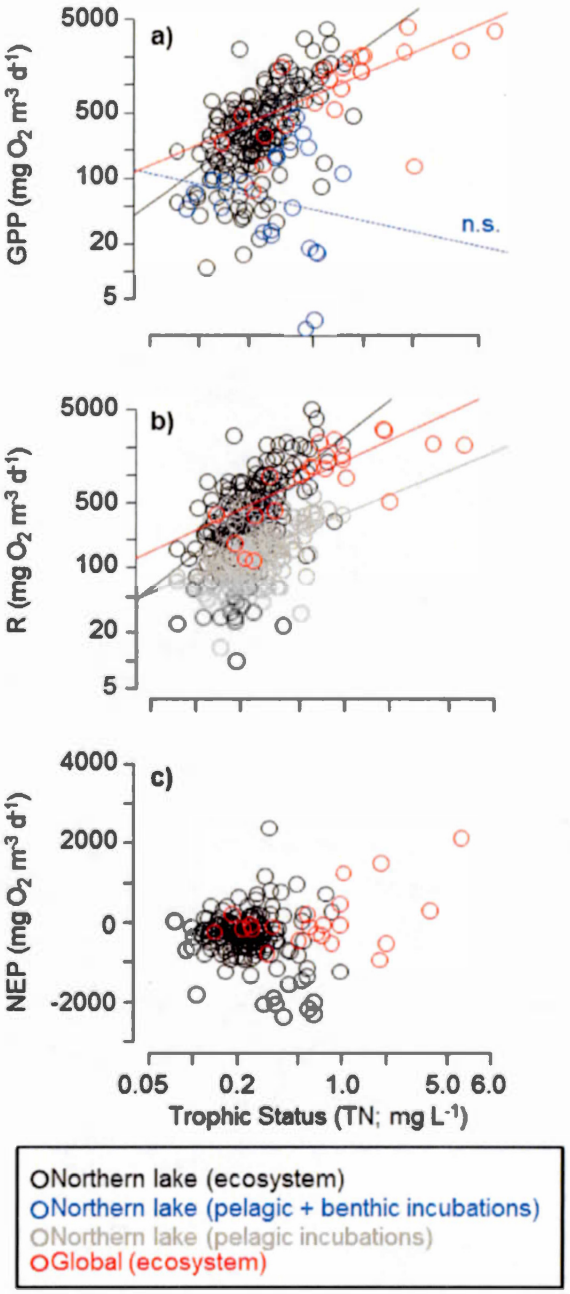

Figure 2.4. Ecosystem-scale metabolic patterns deviate from community assessments in northern lakes.

Rates of GPP (**a**), R (**b**), and NEP (**c**) as a function of trophic status (i.e., total nitrogen). Black points represent free water metabolic data from this study (regression models reported above for figure 2.2), blue points from Seekell et al. (2015; n.s. = non-significant regression model; $r^2 = 0.00$), which were converted from areal to volumetric rates by dividing rates by reported lake depth. Grey points are community respiration data from our northern lakes (previously presented in Lapierre et al. 2015; pelagic R: $r^2 = 0.24$, $\log_{10}\text{pelR} = 61 + 474[\log_{10}\text{TN}]$), and red points are global free-water metabolic data from Solomon et al. (2013; GPP: $r^2 = 0.47$, $\log_{10}\text{GPP} = 807 + 661[\log_{10}\text{TN}]$; R: $r^2 = 0.23$, $\log_{10}\text{GPP} = 1042 + 366[\log_{10}\text{TN}]$).

2.5.2 Trends in lake metabolism along DOC and light gradients

Across the landscape, DOC concentrations were positively linked to rates of mixed layer R slightly more so than GPP, thus favouring a small decline in NEP at elevated DOC levels (Fig. 2.2b; Table 2.2). These effects of DOC agree strongly with results from a survey of DOC versus volumetric rates of pelagic production (Nurnberg and Shaw 1998) and respiration (Pace and Prairie 2005). They also agree with a recent experimental whole lake DOC enrichment that caused rates of both R and GPP to increase, but favouring R > GPP and thus lowering NEP (Zwart et al. 2016). The seemingly contradictory role of DOC, favouring both GPP and R, is nevertheless within the context of what we know concerning the biogeochemical dynamics of these lake ecosystems: Terrestrial DOC acts both as a vector of nutrients that fuel autotrophic growth, and as a source of substrates to the microbial community that fuels heterotrophic respiration (Jones 1992). Although the balance of these two DOC-mediated effects tends to favour R, leading to net heterotrophy in many lakes (del Giorgio and Williams 2005; Solomon et al. 2013; Zwart et al. 2016), volumetric rates of GPP nevertheless increased with increasing DOC and lake color (CDOM), despite concomitant declines in light availability (Fig. 2.2c), a pattern that has been previously shown (Nurnberg and Shaw 1998; Zwart et al. 2016).

These results contrast with previous reports combining in vitro estimates of pelagic and benthic primary production into areal rates of production, which tend to be unrelated to trophic status, and rather appear to track the DOC-mediated light

environment that limits production by the benthic algal community (Ask et al.2012; Seekel et al. 2015). Declines in light availability similarly restrict macrophyte growth and biomass (Duarte et al. 1986), suggesting further restrictions on lake GPP in darker, DOC-rich lake environments. We further explored whether light-mediated restrictions on GPP were apparent in our dataset by converting our volumetric estimates of GPP into area rates for the mixed layer, but like former, these areal rates were also positively related to TN, DOC, and temperature in a multiple regression model, showing no effect of light (data not shown). These contrasts that exist between trends in ecosystem-level GPP rates that we present here, versus those based on habitat-specific production rates (Ask et al. 2012; Seekel et al. 2015) underscore the complexity of regulation of whole lake GPP, and the existence of internal compensation pathways associated to the loss of light (Vestereinen et al. 2016), wherein one food web component or habitat type may offset losses of functioning (in this case, primary production) from another habitat (Schindler 1990; Vasconcelos et al. 2016; Brothers et al. 2016). Such responses, in turn, likely inhibit extreme declines in mixed layer NEP linked to browning of the water column, a conclusion consistent with recent whole-ecosystem manipulations (Rodriguez et al. 2016; Zwart et al. 2016). Overall, our findings indicate that in the absence of other widespread ecosystem changes such as temperature (discussed below), or intensive trophic manipulations (Cole et al. 2000), increases in lake DOC content clearly favour shifts toward net heterotrophy.

2.5.3 Temperature effects on lake metabolism

The positive response of ecosystem-level NEP and GPP:R to ambient temperature that we report here (Fig. 2.2c; Table 2.1) deviates strongly from expectations based on metabolic theory of ecology (Allen et al. 2005), and from results from controlled experimentation and community-level investigations (Yvon Durocher et al. 2010; Regaudie de-Gioux and Duarte 2012). Temperature sensitivity of catabolism and cellular respiration tends to exceed that of photosynthesis (Allen et al. 2005; Yvon-Durocher et al. 2010; but see Demars et al. 2016), yet the response of community or ecosystem-level metabolism is not simply the sum of cellular level processes, and there may potentially be large discrepancies between cellular- and ecosystem-level metabolic temperature sensitivities (reviewed by Cross et al. 2015; delSontro el al. 2016). Although our sampling took place during the summer, there was nevertheless a ~14°C range in surface water temperature across our study lakes that reflected latitudinal gradients. Both NEP and GPP:R were weakly linked to temperature in bivariate comparisons (Fig. 2.2c), however we found a positive relationship between temperature and both NEP and GPP:R after having removed the effect of other co-varying factors, such as nutrients, DOC and geographic position (Table 2.2; Fig. 2.3). This trend strongly suggests that the temperature dependency of the balance between GPP and R at the whole ecosystem level is not a simple reflection of the cellular- or organism-scale responses to warming, an interpretation

that is consistent with northern pond ecosystem experimentation (Rodriguez et al. 2016).

The positive connection between NEP and both water temperature (Fig. 2.2c; Table 2.2) and regional air temperature (Table 2.1) depicted here may represent an underlying connection between shortened ice cover duration (which generally increases with latitude; Weyhenmeyer et al. 2004) and the growth and establishment of the autotrophic community of the lake. For one northern lake, shortening of ice cover duration has been shown to affect the algal community composition and timing of spring blooms, but not overall biomass (Weyhenmeyer 2001). Across lakes, however, the drivers of lake temperature are complex and variable (O'Reilly et al. 2015), rendering a mechanistic interpretation of the temperature-GPP link very speculative for now. Taken together, it appears that the ongoing and widespread warming of surface waters in northern regions (Magnuson et al. 2000; O'Reilly et al. 2015) may, in the absence of opposing effects (discussed below), lead to positive shifts in the metabolic balance of lakes, but this pattern requires further exploration.

2.5.4 Mechanisms underpinning landscape patterns of lake metabolism

NEP is not a metabolic process in itself, but rather a mathematical construct that simply depends on the patterns of its two constituents. The fact that NEP responded far less to environmental variability than either GPP or R (Table 2.2; Fig.

2.4c) suggests that even though these two aspects of lake metabolism show somewhat different cross-lake patterns and relationships to main drivers, they are nevertheless relatively closely coupled at the landscape scale. NEP had weak patterns with environmental variables, and among these, it is interesting to note that water temperature and DOC concentrations had significant, opposing relationships with NEP, despite their positive connections to GPP and R (Table 2.2). The strong collinearity between DOC, wetland cover and other catchment structure variables (i.e., vegetative and standing water cover; Fig. S2.2) makes it difficult to identify any clear mechanistic connection between catchment features and NEP using MR (Table 2.2), but the fact that inclusion of landscape features weakly improved the predictive strength of MR models of NEP and GPP:R (by 4 - 9 %,Tables S2.1, S2.2), points to the need to consider these effects hierarchically, not additively, in a manner consistent with the way in which external forcing mechanisms transmit an effect on the biotic community through changes in the physico-chemical structure of lakes (Leavitt et al. 2009; Lapierre et al. 2015).

Our SEM results (Fig. 2.3) highlight the complex regulation of lake metabolism *via* combinations of internal and external environmental forcing mechanisms; lake NEP in particular appears to follow emergent patterns and regulation at the landscape scale that cannot be deduced or predicted either from metabolic principles, or from existing information of its constituents GPP and R. These patterns in lake NEP are in some cases counterintuitive, and have major

implications for our understanding not just of the functioning of boreal lakes, but also how this functioning might shift under scenarios of future change. Our results strongly imply that to best understand future trajectories of northern lake metabolism, we must simultaneously weigh the effects of multiple environmental changes, particularly the heterogenous patterns of warming (O'Reilly et al. 2015) and terrestrial organic matter loading (Schindler et al. 1997; Monteith et al. 2007; Zhang et al. 2010; Solomon et al. 2015). Taken together, these findings collectively provide much needed, mechanistic information to better understand how whole-lake metabolism is regulated, and how it may respond to intensifying changes in climatic- and catchment characteristics in northern environments (Schindler et al. 1996; Brandt et al. 2013; Gauthier et al. 2015). In these water-rich boreal landscapes, where lakes play a major role in regional C balances, in terms of carbon processing, greenhouse gas emissions and C storage (Algesten et al. 2004; Benoy et al. 2007; Humborg et al. 2010; Ferland et al. 2012), the emergent patterns in lake metabolism have implications for our understanding of the present and future biogeochemical functioning of the whole landscape.

2.6 ACKNOWLEDGEMENTS

This work would not be possible without the field and lab efforts of past and present lab members, especially A. St. Pierre and A. Parkes. We thank R. Vogt, J.F. Lapierre, A. Ulseth and E. Hotchkiss for helpful discussions over the course of this study. J.F. Lapierre, R. Hutchins, and R. Nahas compiled climate and catchment data, R. Nahas provided the map of Quebec. M.J.B. was directly supported by doctoral scholarships from the National Science and Engineering Research Council of Canada (NSERC) and the Université du Québec a Montréal. This project is part of the program of the NSERC / Hydro-Québec Industrial Research Chair in Carbon Biogeochemistry in Boreal Aquatic Systems (CarBBAS), co-funded by grants from NSERC and Hydro-Québec to P.A.d.G.

2.7 SUPPLEMENTARY MATERIAL

2.7.1 Supplementary figures

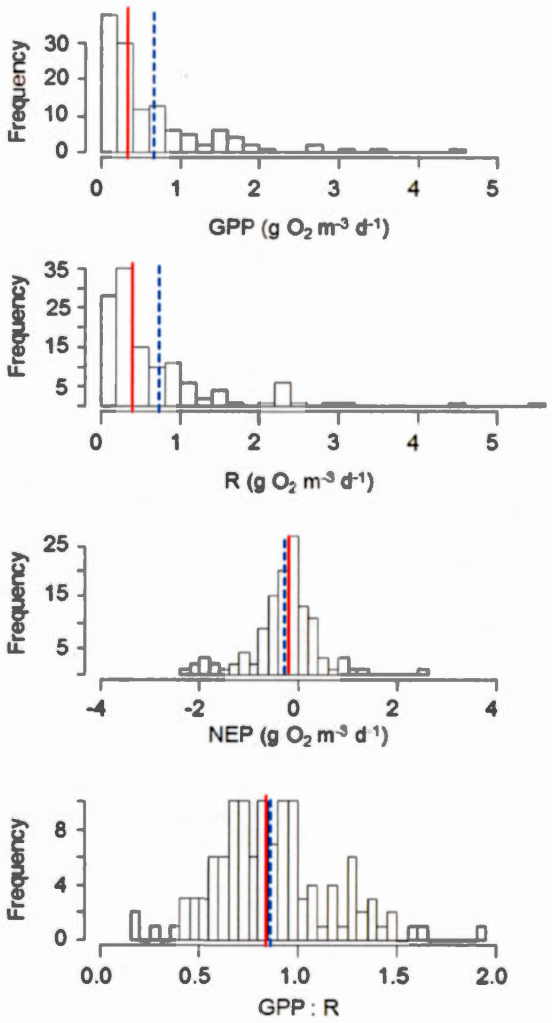

Figure. S2.1. Histograms depicting the distribution of surface-water metabolism in our study lakes.

Dashed blue and solid red lines denote the mean and median, respectively.

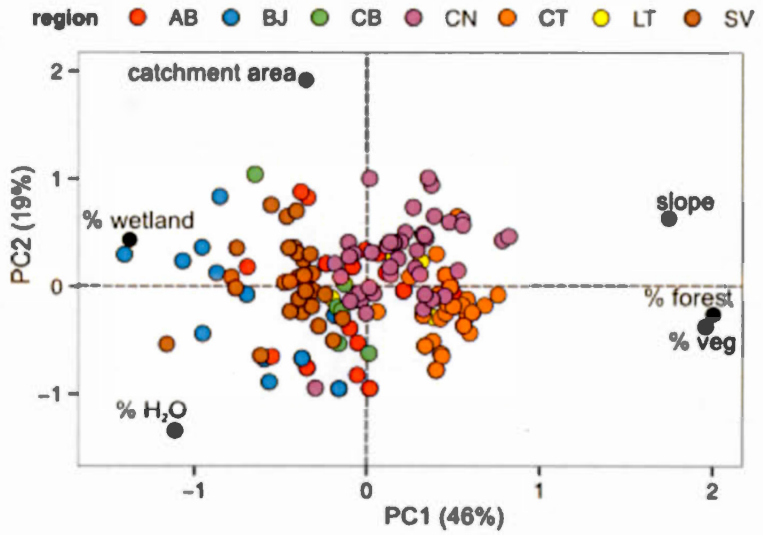

Figure S2.2. Principal components analysis (PCA) summarizing the relationship among landscape characteristics of individual lake catchments.

The first 2 components of the PCA captured 65% of the variance in the dataset, which included as parameters (black circles) catchment slope (slope), catchment area, and the relative proportion of wetland area (% wetland), total standing water area (% H_2O), and total vegetation and forest area (% veg and % forest, respectively). Lakes are color coded by region (see legend in figure 2.1a).

2.7.2 Supplementary tables

Table S2.1. Multiple regression results including models of GPP and R. Parameters include here are DOC (mg L^{-1}), TN (mg L^{-1}), light extinction coefficient (k_d; m^{-1}), water temperature (°C), water residence time (WRT; years), lake area (m^2), perimeter (m), dynamic ratio (d-rat), percentage of wetland (%wet), standing water (%H_2O), total vegetation (%veg), mean catchment slope (°) and area (m^2).

Parameter	Model category	r^2 adj.	*p*-value	AIC	Coefficients	Estimate	S.E.	*p*-value
Log_{10}(GPP)	phys-chem	0.27	< 0.0001	106	Intercept	1.39	0.44	0.002
					log_{10}(DOC)	0.38	0.20	0.054
					log_{10}(TN)	0.63	0.23	0.007
					$log_{10}(k_d)$	0.04	0.15	0.786
					log_{10}(Temp)	1.03	0.33	0.002
	morphometric	0.04	0.05	140	(Intercept)	3.09	0.41	<0.00001
					log_{10}(WRT)	-0.08	0.06	0.220
					log_{10}(lake area)	-0.11	0.19	0.588
					log_{10}(perimeter)	0.03	0.25	0.909
					log_{10}(d-rat)	0.07	0.12	0.560
	catchment	0.14	0.0003	128	Intercept	2.65	0.32	<0.00001
					logit(%wet)	0.06	0.06	0.318
					logit(%H_2O)	-0.23	0.06	0.000
					logit(%Veg)	0.07	0.03	0.024
					slope	-0.02	0.02	0.169
					log_{10}(catch. area)	-0.04	0.03	0.208
	Combined	0.36	< 0.0001	90	Intercept	1.91	0.47	<0.00001
					logit(%H_2O)	-0.09	0.05	0.060
					log_{10}(lake area)	-0.10	0.03	0.002
					log_{10}(TN)	0.69	0.19	0.000

					$\log_{10}$(DOC)	0.33	0.18	0.064
					$\log_{10}$(Temp)	1.05	0.31	0.001
Log_{10}(R)	phys-chem	0.36	< 0.0001	67	Intercept	2.00	0.38	<0.00001
					$\log_{10}$(DOC)	0.44	0.17	0.010
					$\log_{10}$(TN)	0.56	0.20	0.006
					$\log_{10}(k_d)$	0.17	0.12	0.182
					$\log_{10}$(Temp)	0.53	0.28	0.063
	morphometric	0.06	0.02	114	(Intercept)	3.13	0.37	<0.00001
					$\log_{10}$(WRT)	-0.07	0.06	0.191
					$\log_{10}$(lake area)	0.04	0.17	0.822
					$\log_{10}$(perimeter)	-0.17	0.22	0.457
					$\log_{10}$(d-rat)	0.15	0.11	0.171
	catchment	0.17	< 0.0001	100	Intercept	2.89	0.28	<0.00001
					logit(%wet)	0.12	0.05	0.026
					logit(%H_2O)	-0.24	0.05	<0.00001
					logit(%Veg)	0.05	0.03	0.068
					slope	-0.03	0.01	0.078
					$\log_{10}$(catch. area)	-0.03	0.03	0.321
	Combined	0.41	< 0.0001	59	(Intercept)	2.51	0.44	<0.00001
					logit(%H_2O)	-0.07	0.04	0.121
					logit(%wet)	0.02	0.05	0.714
					$\log_{10}$(lake area)	-0.08	0.03	0.004
					$\log_{10}$(DOC)	0.44	0.16	0.008
					$\log_{10}$(TN)	0.71	0.17	<0.00001
					$\log_{10}$(Temp)	0.53	0.27	0.056

Supplementary Table S2.2. Multiple regression results including models of GPP:R and NEP.

Predictors as described in table S2.1.

Parameter	Model category	r^2 adj.	*p*-value	AIC	Coefficients	Est.	S.E.	*p*-value
GPP:R	phys-chem	0.07	0.01	38	Intercept	0.04	0.34	0.897
					$\log_{10}$(DOC)	-0.11	0.15	0.474
					$\log_{10}$(TN)	0.17	0.18	0.340
					$\log_{10}(k_d)$	-0.15	0.11	0.179
					$\log_{10}$(Temp)	0.83	0.25	0.001
	morphometric	0.05	0.04	41	(Intercept)	0.98	0.28	0.001
					$\log_{10}$(WRT)	-0.01	0.04	0.823
					$\log_{10}$(lake area)	-0.24	0.13	0.072
					$\log_{10}$(perim.)	0.32	0.17	0.062
					$\log_{10}$(d-rat)	-0.10	0.08	0.219
	catchment	0.09	0.006	37	Intercept	0.59	0.22	0.008
					logit(%wet)	-0.10	0.04	0.018
					logit(%H_2O)	-0.03	0.04	0.558
					logit(%Veg)	0.04	0.02	0.109
					slope	0.00	0.01	0.734
					$\log_{10}$(catch. area)	-0.02	0.02	0.363
	Combined	0.15	< 0.0001	26	Intercept	-0.48	0.31	0.127
					logit(%wet)	-0.12	0.03	0.001
					$\log_{10}$(Temp)	0.76	0.24	0.002
NEP	phys-chem	0.07	0.01	1924	Intercept	-1305	641.1	0.044
					$\log_{10}$(DOC)	-490	282.8	0.085
					$\log_{10}$(TN)	-154	336.5	0.648
					$\log_{10}(k_d)$	-83.55	210.3	0.692
					$\log_{10}$(Temp)	1089.7	478.9	0.025
	morphometric	0.05	0.04	1927	(Intercept)	-480.0	520.1	0.358
					$\log_{10}$(WRT)	-30.71	79.01	0.698

				$\log_{10}$(lake area)	-371.2	246.3	0.135
				$\log_{10}$(perim.)	569.9	316.1	0.074
				$\log_{10}$(d-rat)	-260.4	150.2	0.086
	catchment	0.06	0.03	1927	Intercept	-820.2	420.1	0.053
					logit(%wet)	-177.1	79.43	0.028
					logit(%H_2O)	96.25	81.75	0.241
					logit(%Veg)	27.64	42.52	0.517
					slope	19.79	21.08	0.350
					$\log_{10}$(catch. area)	-8.98	46.59	0.848
	Combined	0.11	0.0007	1918	Intercept	-1699	624.2	0.007
					logit(%wet)	-161.8	71.61	0.026
					$\log_{10}$(DOC)	-454.0	229.8	0.051
					$\log_{10}$(Temp)	1030.9	467.7	0.029

CHAPTER III

THE ROLE OF METABOLISM IN MODULATING CO_2 FLUXES IN BOREAL LAKES

Matthew J. Bogard[1,2] and Paul A. del Giorgio[1]

Published in *Global Biogeochemical Cycles* (2016) 30: 1509-1525, 10.1002/2016GB005463

[1] Groupe de recherche interuniversitaire en limnologie, Département des sciences biologiques, Université du Québec à Montréal, Montréal, QC, Canada.
[2] Now at the School of Environmental and Forest Sciences, College of the Environment, University of Washington, Seattle, WA, U.S.A.

Key Points:

- CO_2 fluxes were correlated to net ecosystem production (NEP) in most boreal lakes.
- CO_2 fluxes > NEP in over 50% of lakes, linked to external inputs and possibly anaerobic processes.
- Unexpected prevalence of excess CO_2 outgassing in net autotrophic lakes.

N.B. References cited in this chapter are presented at the end of the thesis.

3.1 ABSTRACT

Lake CO_2 emissions are increasingly recognized as an important component of the global CO_2 cycle, yet the origin of these emissions is not clear, as specific contributions from metabolism and in-lake cycling, versus external inputs, are not well defined. To assess the coupling of lake metabolism with CO_2 concentrations and fluxes, we estimated steady-state ratios of gross primary production to respiration (GPP:R) and rates of net ecosystem production (NEP = GPP-R) from surface water O_2 dynamics (concentration and stable isotopes) in 187 boreal lakes spanning long environmental gradients. Our findings suggest internal metabolism plays a dominant role in regulating CO_2 fluxes in most lakes, but this pattern only emerges when examined at a resolution that accounts for the vastly differing relationships between lake metabolism and CO_2 fluxes: Fluxes of CO_2 exceeded those from NEP in over half the lakes, but unexpectedly, these effects were most common and typically largest in a subset (~30% of total) of net autotrophic lakes that nevertheless emitted CO_2. Equally surprising, we found no environmental characteristics that distinguished this category from the more common net heterotrophic, CO_2 outgassing lakes. Excess CO_2 fluxes relative to NEP were best predicted by catchment structure and hydrologic properties, and we infer from a combination of methods that both catchment inputs and internal anaerobic processes may have contributed this excess CO_2. Together, our findings show the link between lake metabolism and CO_2 fluxes is often strong, but can vary widely across the boreal biome, having important implications for catchment-wide C budgets.

3.2 INTRODUCTION

Freshwaters play a major role in global carbon (C) processing and emissions (Cole et al. 2007; Battin et al. 2009), especially in northern environments (Raymond et al. 2013; Benoy et al. 2007). In the boreal biome, the extensive land-water interface facilitates intense terrestrial export of organic C (OC) and dissolved inorganic C (DIC) to boreal aquatic ecosystems. Up to ~80% of terrestrial OC exports are mineralized or buried in freshwaters (Molot and Dillon, 1996; Algesten et al. 2004; Tranvik et al. 2009; Ferland et al. 2012). This, along with soil- and ground water derived CO_2, fuels intense aquatic CO_2 emissions to the atmosphere (Striegl et al. 2001; Rasilo et al. 2015). The relative role of internal- and externally derived CO_2 in supporting lake emissions, however, is difficult to distinguish, varying both through space (Lapierre and del Giorgio, 2012; Weyhenmeyer et al. 2015) and time (Vachon and del Giorgio, 2014; Perga et al. 2016). An understanding of this balance is needed both to better define the controls of aquatic CO_2 flux, and to combine terrestrial and aquatic C cycles into accurate, unified regional and continental C budgets (Humborg et al. 2010; Hotchkiss et al. 2015; Butman et al. 2016).

Whether a given system emits or in-gasses CO_2 depends on the simultaneous net balance of external and internal inputs, and in-lake consumption via gross primary production (GPP). Alongside catchment-derived DIC, terrestrial OC inputs fuel CO_2 supersaturation in lakes via biological and photochemical OC mineralization (Molot and Dillon, 1997; McCallister and del Giorgio, 2008; Cory et al. 2014; Vachon and

del Giorgio, 2014). Other processes, such as calcite precipitation during intense GPP at elevated pH, may further generate CO_2, but this is uncommon in northern soft water lakes. GPP simultaneously removes CO_2 from lakes, and where GPP > R, may offset a fraction of terrestrial or chemical CO_2 input (Finlay et al. 2010; McDonald et al. 2013; Perga et al. 2016). The magnitude of this offset varies greatly across lakes and as a function of nutrient enrichment, light and other factors that control photosynthesis, whereas terrestrial DIC and OC input can be regulated by different factors and may be decoupled from lake metabolism (Dubois et al. 2009; Lapierre and del Giorgio, 2012; Wilkinson et al. 2016). Further decoupling of aerobic lake metabolism and CO_2 flux may occur if anaerobic processes generate or consume significant amounts of CO_2 independent of DO cycling (Gu et al. 2004; Torgerson and Branco, 2007; Dubois et al. 2009; Holgerson, 2015). Consequently, CO_2 outflux from a lake cannot always be interpreted as a sign that the lake has a net heterotrophic metabolic balance, since a lake that is net autotrophic may still emit CO_2 to the atmosphere if CO_2 inputs beyond those from aerobic R exceed the net photosynthetic CO_2 uptake (Dubois et al. 2009; Finlay et al. 2010; McDonald et al. 2013; Wilkinson et al. 2016). Conversely, in lakes that have strong net autotrophic metabolism and act as net sinks of CO_2, the magnitude of the CO_2 sink may be greatly reduced by inputs of terrestrially-derived CO_2, or anaerobic CO_2 production and may thus not be commensurate with net metabolism (Dubois et al. 2009; McDonald et al. 2013). Therefore, although we can determine a lake's net CO_2 source/sink strength with

relative ease, mechanistically interpreting the observed gas exchange is more difficult.

The control of lake CO_2 flux is inherently complex, and the literature abounds with conflicting reports as to the regulation of lake CO_2 flux: Some suggest a major role of internal CO_2 production (Duarte and Prairie, 2005; Jonsson et al. 2003; Ask et al. 2012; Trolle et al. 2012; Yang et al. 2015), while others suggest that emissions are predominantly fueled by catchment CO_2 inputs (Jones et al. 2001; Dubois et al. 2009; Maberly et al. 2013; Weyhenmeyer et al. 2015) and depend on the interaction of net metabolism with shifts in solute load, pH, and DIC equilibrium (Trolle et al. 2012; Finlay et al. 2015). Such widely differing conclusions are not mutually incompatible, but may originate from spatio-temporal variation in the relative contribution of the various CO_2 flux pathways (Lapierre and del Giorgio, 2012; Vachon and del Giorgio, 2014; Weyhenmeyer et al. 2015; Perga et al. 2016). Further, most studies focus on specific components of the CO_2 balance, without comprehensively assessing CO_2 dynamics. For example, studies of boreal lake C gas dynamics (e.g., Algesten et al. 2004; Kortelainen et al. 2006; Lapierre and del Giorgio, 2012; Weyhenmeyer et al. 2015) typically do not include estimates of ecosystem-level metabolism. Where metabolic measurements do exist, GPP (e.g., Kelly et al. 2001; Seekell et al. 2015) and R (e.g., Marchand et al. 2009; Berggren et al. 2009; 2012) have mostly been quantified independently, and few direct measurements of ecosystem-level NEP exist for boreal lakes (but see Ojala et al. 2011; Solomon et al. 2013; Vachon and del Giorgio, 2014). A handful of studies have attempted to reconstruct the entire balance

underlying lake CO_2 emissions by quantifying major pathways and inputs, combined with detailed mass balance and modeling (Jonsson et al. 2001; Wilkinson et al. 2016). Others have experimentally manipulated lake conditions to infer the relative importance of metabolism (Wilkinson et al. 2016). Although these studies have yielded valuable insights, these approaches are extremely labor intensive and impractical when exploring the regulation of CO_2 dynamics across many lakes at the landscape-scale. Thus, it remains difficult to broadly identify how lake metabolism actually modulates CO_2 dynamics and fluxes throughout the boreal landscape.

An alternative approach to assess the drivers of surface water CO_2 flux across lakes is to compare CO_2 dynamics with co-occurring O_2 dynamics (e.g., Prairie et al. 2002; Kortelainen et al. 2006; Roehm et al. 2009). If aerobic lake metabolism were the main driver of lake CO_2 concentrations, then lake CO_2 fluxes would be quantitatively bound by DO-derived NEP. On the other hand, processes such as soil-derived CO_2 loading or anaerobic CO_2 cycling can result in the deviation of observed CO_2 flux relative to aerobic lake metabolism (Torgerson and Branco, 2007; Holgerson, 2015; Wilkinson et al. 2016). Here, we use this approach to investigate the relative importance of aerobic metabolism versus anaerobic and non-metabolic processes in modulating surface water lake CO_2 dynamics across 187 boreal Canadian lakes. We compare mixed layer aerobic NEP and GPP : R (based on free-water DO concentrations and isotopic dynamics, respectively) to measured CO_2 fluxes, and determine the magnitude of deviation of ambient CO_2 flux from NEP among lakes. We examine the processes potentially causing these deviations, and

how they may vary in relative importance along broad environmental gradients.

3.3 METHODS

3.3.1 Study Area and Sampling Approach

The lakes sampled in our study are located in north-eastern Canada, in the boreal region of the province of Québec (see mapped locations in Rasilo et al. 2014; Lapierre et al. 2015). Regional and lake characteristics have been thoroughly described (Rasilo et al. 2014). The lakes sampled span a broad range in geographic position, landscape features, regional climatic conditions, and limnological characteristics (Table 3.1). Lakes were each visited once in the summers of 2010 – 2013, from late June to mid-August, which covers the period of summer stratification (in deeper lakes) in all the regions. For the vast majority of sites, we sampled only during mid-morning to early afternoon periods. This standardization helped to minimize the diel variability in gas dynamics in our dataset that potentially could have obscured the patterns of NEP and CO_2 flux among lakes.

Samples were collected from the deepest measured point in the lake. The full suite of measured parameters and sampling methods has been previously detailed (Berggren et al. 2012; Rasilo et al. 2014; Lapierre et al. 2015). In brief, we estimated lake mixed layer depths from temperature profiles made with a combination probe (Yellow Springs Instruments, USA). Measurements of dissolved gasses were made at ~0.5m depth below the lake surface. Estimates of DO concentration and percent saturation were taken with the combination probe, and percent saturation was later corrected for site-specific atmospheric pressure. DO probes were calibrated at each site in vapour-saturated air, at ambient pressure and surface water temperature. *In-*

situ surface pCO_2 was measured using an EGM-4 infrared gas analyzer (PP-systems, Boston, MA, USA) after water was pumped to the surface, and equilibrated with ambient air using a Liqui-Cell Mini Module membrane (Charlotte, NC, USA). The pCO_2 of ambient air was also measured and subtracted from in-lake values to estimate deviation from atmospheric equilibrium. Samples for the isotopic composition of dissolved inorganic carbon (DIC) were collected at a subset of lakes in 60ml gas-tight plastic syringes, and gently filtered across a 0.45 μm filter into acid-washed, 40ml vials with both Teflon and rubber-lined gas-tight plastic caps. All samples for $\delta^{18}O\text{-}O_2$ isotopic analysis were taken at ~25-50 cm depth. Samples were stored in 12-ml precombusted borosilicate vials, preserved with $HgCl_2$, and capped, free of air, with a gastight rubber lined plastic cap. Samples for $\delta O^{18}\text{-}H_2O$ were collected in 125ml plastic bottles, filled to full capacity free of air, and stored in the dark until analysis.

Table 3.1. Regional, catchment, and lake-specific environmental characteristics associated with eastern Canadian boreal lakes (n = 187) sampled in this study. Abbreviations defined in text.

	min	1st Quartile	median	mean	3rd Quartile	max
Climatic conditions						
runoff (mm y^{-1})	307	405	570	564	676	881
mean annual temperature (°C)	-5.7	-1.8	0.2	-0.7	1	4.5
total annual precipitation (mm y^{-1})	708	845	905	964	1099	1289
Catchment characteristics						
Slope (°)	0.1	2.0	3.9	4.4	6.5	12
Catchment area (km^2)	0.06	1.8	8.6	641.3	53.8	$5.5x10^4$
Wetland cover (%)	0	0	0.3	3.5	1.4	93.6
Vegetative cover (%)	6.4	73.7	92.0	84.5	98.5	100
Aquatic habitat cover (%)	0	8.4	13.9	15.8	21.3	57.5
Limnological characteristics						
Elevation (m asl)	60	270	380	406	559	894
Lake area (km^2)	0.002	0.15	0.81	55	5.6	4345
Volume (km^3)	$4.8x10^{-6}$	$2.57x10^{-3}$	0.024	2.54	0.25	87.1
Z_{max} (m)	2	22	42	62	80	288
Residence time (y)	$8x10^{-4}$	0.8	2.8	7.4	9.7	91.5
Surface temp (°C)	10.9	15.4	17.2	17.8	20.4	24.1
Chl *a* (μg L^{-1})	0.19	0.84	1.47	2.42	2.61	36.05
TN (mg L^{-1})	0.07	0.17	0.23	0.25	0.29	0.91
TP (μg L^{-1})	2.9	6.6	9.9	14.5	15.3	153.2
DOC (mg L^{-1})	1.4	5.6	8.0	8.7	10.9	39.7
abs_{440} (m^{-1})	0.12	1.38	2.76	3.5	4.95	20.04

3.3.2 Climate and Catchment Characteristics

Hourly wind data for the period of sampling from one central location in each region were taken from the Environment Canada website (https://weather.gc.ca/canada_e.html) (Fig. S3.1), and from the weather station of the Université de Montréal Biological research station (http://www.sbl.umontreal.ca/territoire-cartes/meteorologie/index.html) for the Laurentians region. Lake-specific catchment characteristics and regional long-term climatic conditions have been assembled and previously published, along with a justification of their use (Lapierre et al. 2015). Water residence times in the lakes were estimated following Heathcote et al. (2015).

3.3.3 Laboratory Analyses

Samples of epilimnetic water from each lake were brought to the lab, and stored in the dark at 4°C until further analysis. As detailed by Rasilo et al. (2015), concentrations of total P (TP) and nitrogen (TN) in surface waters were estimated by oxidizing samples via persulfate and alkaline persulfate digestions, respectively, then measuring TP as orthophosphate using the spectrophotometric molybdenum blue method ((Wetzel and Likens, 2000); 890 nm, Ultrospec 2100 pro, Biochrom Ltd., Cambridge, UK) and TN as NO_3^- using an Alpkem Flow- Solution IV autoanalyzer (OI Analytical, College Station, TX, USA). Dissolved organic carbon (DOC) concentrations were estimated from filtered samples (0.45 lm PES cartridge, Sarstedt AG & Co., Nümbrecht, Germany) with a TOC analyzer (OI 1010, OI Analytical,

College Station, TX, USA) after sodium persulfate digestion. Estimates of algal biomass as chlorophyll *a* (chl *a*) were made by collecting particulate organic matter (POM) on filters (GF/F, Whatman, Kent, UK), pigments were extracted from filters with hot ethanol (90%) via sonication and analyzed spectrophotometrically with an acidification step to correct for phaeophytin (665 and 750 nm, Ultrospec 2100 pro, Thermo Fisher Scientific Inc., Waltham, MA, USA). Colored dissolved organic matter (cDOM) was measured as absorbance at 440 nm (Cuthbert and del Giorgio 1992) using an Ultrospec 3100 spectrophotometer (Thermo Fisher Scientific Inc.,Waltham, MA, USA). In all cases, duplicate samples were separately collected, stored, and analyzed, and average values are reported here.

3.3.4 Isotopic Analyses

All isotope compositions are reported in delta (δ) notation following equation 3.1,

$$\delta^{18}O,\ \delta^{13}C \text{ or } \delta^{2}H = ((R_{sample} / R_{standard}) - 1) \times 1000 \qquad (3.1)$$

where R and $R_{standard}$ is the ratio of heavy to light isotopes (^{18}O:^{16}O, ^{13}C:^{12}C, or ^{2}H:^{1}H) present in samples and standards, respectively. The standard for $\delta^{18}O$ and $\delta^{2}H$ is Vienna standard mean ocean water (VSMOW), and Vienna Pee-Dee Belemnite (VPDB) for $\delta^{13}C$. We calculated $\delta^{13}C$-CO_2 from $\delta^{13}C$-DIC following Stumm and Morgan (1996) using fractionation factors of Mook et al. (1974).

To approximate the relative effect of evaporation on lake water in a given system, we used the isotopic deviation of lake water from the global meteoric water line (GMWL; Craig 1961) to calculate d-excess (‰) from lake water isotopic samples (Dansgaard 1964; Turner et al. 2014) following equation 3.2,

$$\text{d-excess} = \delta^2H - 8 \times \delta^{18}O \qquad (3.2)$$

Here, we use the extent of evaporation, as inferred from values of d-excess, as a proxy for the relative water residence time in the catchment, in order to strengthen our examination of how hydrologic conditions relate to lake CO_2 dynamics. Values of d-excess spanned a ~25‰ range (Fig. S3.2), reflecting a wide range of evaporative influence on lakes. In line with its use as a proxy for catchment water residence time, d-excess values were positively related to regional precipitation, catchment slope and runoff estimates, but negatively related to the proportional coverage of standing water in the catchment (Table S3.1).

3.3.5 Calculating Gas Flux and NEP

Air-water fluxes of O_2 and CO_2 were calculated for each lake from Fick's law of diffusion using equation 3.3, where negative values of F_{gas} are invasion, and positive values are evasion across the air-water interface:

$$F_{gas} = k_{gas} \times \Delta_{gas} \qquad (3.3)$$

where F_{gas} is flux (mmol m^{-2} d^{-1}) of O_2 (F_{O2}) or CO_2 (F_{CO2}), k_{gas} is the gas exchange coefficient at a given temperature (m d^{-1}), and Δ_{gas} is the departure of DO or CO_2

from concentrations at equilibrium with the atmosphere (Δ_{DO} or Δ_{CO2}; mmol m^{-3}). We converted measurements of pCO_2 to concentrations using Henry's constant corrected for temperature. We estimated k_{O2} and k_{CO2} for each lake from calculated k_{600} values following Jahne et al. (1987) in equation 3.4:

$$k_{gas} = k_{600} \times (Sc_{gas} / 600)^{-2/3} \quad (3.4)$$

where Sc is the temperature-specific Schmidt number for O_2 or CO_2 (Wanninkof 1992). The estimates of k_{600} were calculated with equation 3.5, a wind-based model that accounts for lake area (Vachon and Prairie 2013):

$$k_{600} = 2.51 + 1.58 \times U_{10} + 0.39 \times U_{10} \times \log_{10}(LA) \quad (3.5)$$

where k_{600} is estimated in cm h^{-1}, U_{10} is wind speed at 10m height above the lake (m s^{-1}), and LA is lake area (km^2). For each lake, wind speed was estimated as the moving average of the 7 previous days' mean wind speed recorded at the nearest weather station.

We estimated steady-state, volumetric rates of NEP using equation 3.6, where positive and negative NEP values denote rates of net auto- and heterotrophy, respectively:

$$\Delta_{DO} = NEP - (F_{O2} / Z_{mix}) \quad (3.6)$$

where we necessarily assume that the deviation of DO from saturation (Δ_{DO}) is sustained at steady state by NEP and gas exchange with the atmosphere. We estimated NEP (mmol m^{-3} d^{-1}) and multiplied these values by Z_{mix} (Z_{max} for shallow, fully mixed lakes) to get areal rates. In order to compare NEP to CO_2 flux directly,

we converted oxygen-based NEP to units of C assuming a net metabolic quotient of 1 mole DO consumed for every mole CO_2 produced. This approach does not distinguish between aerobic R and abiotic DO consumption processes such as photo-oxidation of OC, therefore representing total *in-situ* OC mineralization rates. However, these rates are largely driven by biological OC mineralization in summer months in the temperature range of our study lakes (Granéli et al. 1996; Jonsson et al. 2001; Vachon et al. 2016).

3.3.6 Isotopic estimates of GPP : R

We estimated GPP : R from DO, δ^{18}O-DO and δ^{18}O-H_2O using the model developed by Quay et al. (1995) based on the work of Bender and Grande (1987). Assuming an absence of physically driven changes in DO due to vertical and lateral exchange of water masses, GPP, R, and atmospheric gas exchange are the only processes driving temporal DO and δ^{18}O-DO dynamics in the study lakes, as expressed by equations 3.7 and 3.8;

$$dDO / dt = k_{O2} \times (DO_{sat} - DO) / Z_{mix} + GPP - R \qquad (3.7)$$

$$d^{18:16}DO / dt = k_{O2} \times \alpha_g \times (DO_{sat} \times {}^{18:16}air \times \alpha_s - DO \times {}^{18:16}DO) / Zmix +$$

$$(GPP \times {}^{18:16}H_2O \times \alpha_p) - (R \times {}^{18:16}DO \times \alpha_r) \qquad (3.8)$$

including isotopic ratios of DO, atmospheric O_2 and H_2O ($^{18:16}DO$, $^{18:16}air$, and $^{18:16}H_2O$, respectively) and concentrations of DO at 100% saturation with the atmosphere (DO_{sat}). If steady state conditions are assumed for values of DO and

$^{18:16}$DO (i.e., net metabolic effects on the DO pool and $^{18:16}$DO are balanced by net effects of air-water gas flux), then equations 3.7 and 3.8 can be combined to solve for the value of GPP : R (Quay et al. 1995);

$$GPP : R = (^{18:16}H_2O \times \alpha_p - ^{18:16}O_g) / (^{18:16}DO \times \alpha_r - ^{18:16}O_g) \qquad (3.9)$$

where the term $^{18:16}O_g$ summarizes the net flux of atmospheric O_2 and across the air-water interface:

$$^{18:16}O_g = \alpha_g \times (^{18:16}air \times \alpha_s - ^{18:16}DO \times DO / DO_{sat}) / (1 - DO / DO_{sat}) \qquad (3.10)$$

We assume the $\delta^{18}O$ signature of air to be 23.5‰, consistent with previous studies (e.g., Quiñones-Rivera et al. 2007; Bocaniov et al. 2012). The terms α_g, α_s, and α_p are the respective fractionation factors for kinetic gas exchange (0.9972; Knox et al. 1992), gas solubility effects (1.0007; Benson and Krause 1984), and photosynthetic DO production (1.000; Guy et al. 1993). In boreal lakes, the fractionation effect during DO uptake linked to ecosystem R (α_r) reflects the balance of all DO-consuming processes in the mixed layer. This includes pelagic R, for which fractionation typically ranges between ~0.982 – 0.970 (Quay et al. 1995; Luz et al. 2002; Quiñones-Rivera et al. 2007; Bocaniov et al. 2012). This term also includes both sedimentary R and photochemical DO consumption, processes with much smaller associated fractionation effects of ~0.997 (Brandes and Devol 1997) and ~0.991 (Chomicki and Schiff 2008). These processes can account for a significant fraction of ecosystem DO uptake (Granéli et al. 1996; Jonsson et al. 2001; Algesten et al. 2005; Vachon and del Giorgio 2014). With this in mind, we made two

estimates of GPP:R using α_r values of both 0.990 and 0.985 to account for potentially greater effects on δ^{18}O-DO by processes other than pelagic R. However, since the use of different α_r values did not significantly alter the overall patterns derived from the regression analyses, and our interpretation of these models, we only present results calculated using $\alpha_r = 0.985$.

3.3.7 Lake CO_2 Excess Emissions and Mass Balance Calculations

We quantified the deviation of CO_2 fluxes from NEP ($\Delta_{emissions}$), where $\Delta_{emissions}$ represents the absolute difference between CO_2 in- or outgassing and the CO_2 derived from NEP. Negative $\Delta_{emissions}$ values denoted situations where CO_2 derived from NEP > CO_2 flux. Where values of $\Delta_{emissions}$ were positive, an additional source of CO_2 on top of aerobic NEP was required to sustain the observed fluxes. In these cases, we used a mass balance approach to calculate the partial pressure of CO_2 in inflowing water required to sustain the observed excess CO_2 flux. Assuming a condition of hydrologic steady state (lake inflows = outflows), the balance of catchment CO_2 input (CO_{2input}) and lake export ($CO_{2outflow}$) should equal the difference between whole lake air-water flux and NEP, which was estimated as $\Delta_{emissions}$ × lake area ($\Delta_{emissions\text{-}total}$):

$$CO_{2input} - CO_{2outflow} = \Delta_{emissions\text{-}total} \qquad (3.11)$$

We defined loading and export each as the product of flow rate (Q) and CO_2 concentration of the water entering or leaving the lake (CO_{2input} or $CO_{2outflow}$,

respectively). We assumed $CO_{2outflow}$ was equal to the measured lake CO_2 concentration, and then rearranged equation 3.11 to solve for CO_{2input}:

$$CO_{2input} = \Delta_{emissions\text{-}total} / Q - CO_{2outflow} \qquad (3.12)$$

We estimated Q (m^{-3} day^{-1}) by converting average annual runoff (from Lapierre et al. 2015) to daily rates (m d^{-1}) and multiplying by catchment area (m^2). From CO_{2input}, we calculated the hypothetical pCO_2 of incoming water using Henry's constant corrected to an ambient temperature of 10°C. Changing this temperature over a ~10°C range had little effect on the distribution of pCO_2 values and thus was sufficient for the level of analysis in this study. This calculation was meant to serve as a general estimate of the potential for external inputs to support $\Delta_{emissions}$, and was only used at an order of magnitude scale resolution.

3.3.8 Statistical Methods

Analyses were performed using R version 3.0.3 (R development core team 2014). We used a combination of major axis regression ('lmodel2' package (Legendre 2014)) and Pearson correlation analyses ('Hmisc' package (Harrell 2014)) to assess bivariate relationships. To assess how catchment and in-lake characteristics related to $\Delta_{emissions}$, we used a partial least squares (PLS) regression analysis ('pls' package (Mevik et al. 2013)). Data were scaled and centered prior to analysis. We assessed the differences in environmental and limnological characteristics among the lake type categories using one-way analysis of variance (ANOVA) and Tukey HSD

post-hoc comparisons. In all cases, data distributions and distributions of regression residuals were assessed visually, and where necessary, $\log_{10}$ transformations were used to meet assumptions of normality.

3.4 RESULTS

3.4.1 Patterns of CO_2 and metabolic dynamics

Across the surveyed lakes, surface water pCO_2 was most often supersaturated relative to the atmosphere (which was assumed to be ~400 μatm), ranging from 162 to 1637 μatm (mean = 725, median = 625, interquartile range = 520 to 855 μatm; Fig. 3.1a). Consequently, most lakes outgassed CO_2 to the atmosphere, with surface CO_2 fluxes ranging from -187 to 979 mg C m^{-2} d^{-1} (mean = 232, median = 181, interquartile range = 97 to 334 mg C m^{-2} d^{-1}; Fig. 3.1b). NEP also spanned a large range, across these lakes, from net heterotrophic to net autotrophic conditions (-1599 to 1982 mg C m^{-2} d^{-1}) with a predominance of negative (net heterotrophic) values (mean = -172, median = -188, interquartile range = -587 to 197 mg C m^{-2} d^{-1}; Fig. 3.1c). Consistent with patterns of NEP, our $\delta^{18}O$-derived estimates of the GPP:R ratio spanned a large range of net auto- and heterotrophic metabolism (i.e., > and < 1, respectively), but most systems were net heterotrophic (0.13 to 1.91, mean = 0.88, median = 0.88, interquartile range = 0.71 to 1.02; Fig. 3.1d). We found a strong positive relationship between our estimates of NEP and model-derived GPP:R ratio (data not shown; $r^2 = 0.39$, $p = <0.0001$; GPP:R $= -1471 \pm 146 + 1321 \pm 158 \times$ NEP). There was no significant relationship between surface water pCO_2 and either ecosystem GPP:R (Fig. 3.2a) or NEP (Fig. 3.2b) when all lakes were considered together. Despite the lack of a relationship between metabolic indices and pCO_2, we observed a significant shift in the isotopic composition of CO_2 ($\delta^{13}C$-CO_2) with

increasing pCO_2 (Fig. 3.2c; (r^2 = 0.07; p = 0.03; $\delta^{13}C\text{-}CO_2$ = -15.2 $\pm$ 0.7 - 0.002 $\pm$ 0.0009 × pCO_2)). For a subset of the study lakes, $\delta^{13}C\text{-}CO_2$ became more isotopically depleted, shifting from ~ -12 to -21‰, as pCO_2 increased from undersaturation up to ~1,700 μatm.

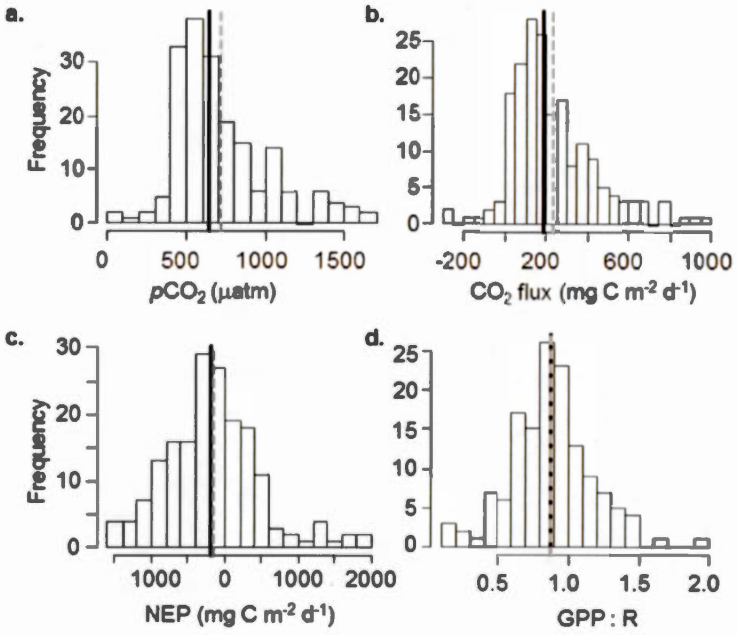

Figure 3.1. Histogram of (a) surface water pCO_2, (b) daily air-water CO_2 flux, (c) rates of net ecosystem production (NEP), and (d) the ratio of GPP : R.

Mean and median values shown by grey dashed and solid black lines, respectively.

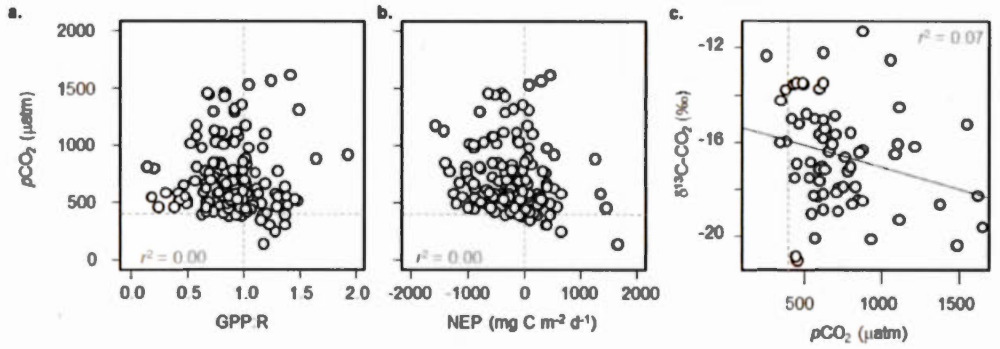

Figure 3.2. How partial pressure of CO_2 (pCO_2) relates to indicies of lake metabolism and C cycling in the surface mixed layer of boreal lakes.

pCO_2 is compared to (a) isotopically-derived ($\delta^{18}O$) ratios of free-water ecosystem GPP:R, and (b) free water estimates of ecosystem NEP (i.e., GPP-R). Horizontal dashed lines denote atmospheric pCO_2 = 400 µatm, and vertical dashed lines denote rates of GPP = R. In both cases regression relationships were non-significant. (c) For a subset of lakes (n = 68) we examined the relationship between $\delta^{13}C$-CO_2 and pCO_2 in surface waters. Here, the vertical dashed grey line denotes atmospheric pCO_2 and the solid black line is the significant regression model.

3.4.2 Categorizing lakes by NEP and CO_2 flux

Although there was no overall relationship between CO_2 flux and NEP (Fig. 3.2a,b), closer inspection revealed three distinct lake groupings based on patterns of CO_2 flux and NEP (shown as log-transformed axes in Fig. 3.3a for visual clarity, but see Fig. S3.3 for the untransformed version of this plot). Most lakes (64%; top left panel, Fig. 3.3a) were net emitters of CO_2 with a mean flux of 253 (interquartile range = 115 to 352) mg C m^{-2} d^{-1}, and also net heterotrophic, with median NEP of -440 (-238 to -823) mg C m^{-2} d^{-1}. A few lakes (5%, bottom right panel, Fig. 3.3a) were net autotrophic, with median rates of NEP = 615 (353 to 1610) mg C m^{-2} d^{-1}. These lakes were undersaturated in CO_2, and in-gassed at mean rates of -77 (-36 to -177) mg C m^{-2} d^{-1}. A surprisingly large subset of lakes (32%, top right panel, Fig. 3.3a), emitted CO_2 despite having NEP > 0. This category had high median CO_2 flux rates of 170 (90 to 333) mg C m^{-2} d^{-1}, despite a median positive NEP of 337 (189 to 588) mg C m^{-2} d^{-1}.

The degree of coupling between NEP and CO_2 flux varied greatly among these three categories of lakes: The lakes in both heterotrophic + outgassing and autotrophic + in-gassing groups aligned roughly along the diagonal that would be expected if CO_2 dynamics were mostly driven by ambient aerobic metabolism, whereas lakes grouped as autotrophic + outgassing departed completely from this metabolic diagonal (Fig. 3.3a). In autotrophic + outgassing lakes, CO_2 flux was completely unrelated to NEP (r = -0.07). In heterotrophic + outgassing lakes, CO_2 outgassing predictably increased as NEP became more negative (r = -0.39), although

there was much scatter around this general pattern. In autotrophic + in-gassing lakes, there was a strong inverse relationship between NEP and CO_2 flux ($r = 0.98$).

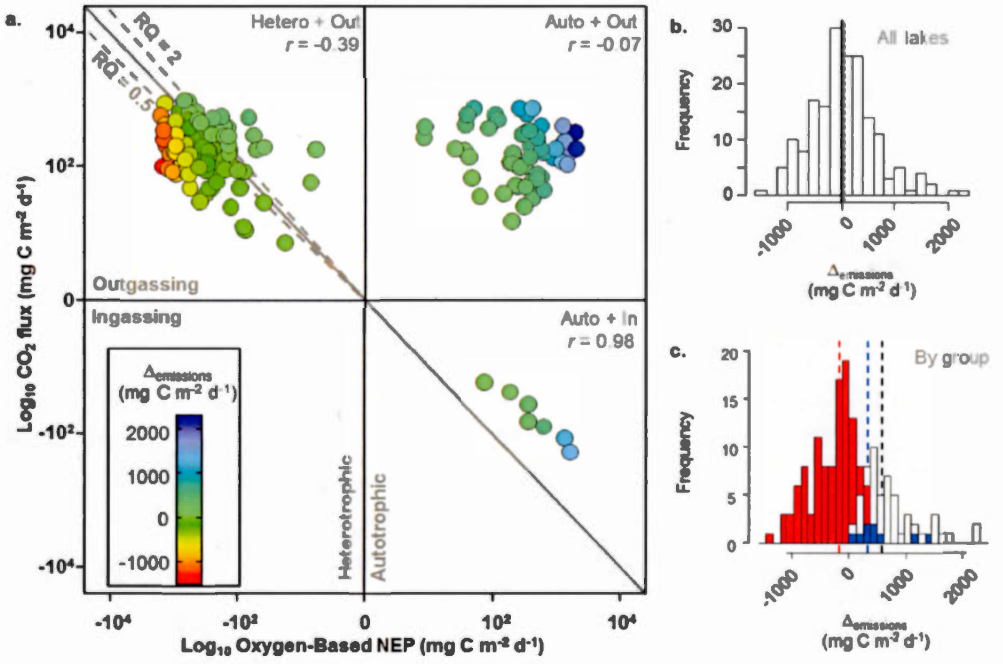

Figure 3.3. Comparing patterns of aerobic metabolism and biotic CO_2 production to surface emissions from boreal lakes.

(a) Both aerobic net ecosystem production (NEP) and CO_2 flux are $\log_{10}$ transformed away from zero, retaining both positive and negative signs on each axis (see methods for calculation details). Solid grey line is the inverse 1:1 line. Dashed grey lines denote the aerobic catabolic bounds under conditions where the ecosystem-level respiratory quotient (RQ) is 0.5, or 2, respectively. The excess or deficit of CO_2 emissions ($\Delta_{emissions}$) relative to NEP is indicated by color (see legend for the untransformed scale), estimated as the vertical departure from the solid grey line. (b) Histogram of $\Delta_{emissions}$ across all lakes, with mean and median as grey dashed and solid black lines, respectively. (c) Histogram of $\Delta_{emissions}$ within each lake group, as

defined by quadrants in panel (a). Dashed lines denote median values by group. White bars (black dashed line) denotes autotrophic + outgassing lakes, red bars and dashed line denotes heterotrophic + outgassing lakes, while blue bars and dashed line represents autotrophic + in-gassing lakes.

3.4.3 Differentiating the 3 categories of lakes

Results of ANOVA revealed no significant differences across the three CO_2 / NEP groups described above, in terms of lake area, ratio of catchment to lake area, modelled lake maximum depths, average regional climatic conditions (mean annual temperature, total precipitation, or catchment runoff), or terrestrial C dynamics (net primary production, soil OC content) (data not shown). Interestingly, there was no systematic difference in ecosystem features between outgassing heterotrophic and autotrophic lakes (Fig. 3.4). On the other hand, autotrophic in-gassing lakes tended to be located in catchments with flatter topography, reduced forest coverage ($p \leq 0.1$; Fig. 3.4a,b), and greater aquatic cover ($p = 0.006$; Fig. 3.4c). Water residence times were weakly distinguishable between the three categories, increasing from heterotrophic, to autotrophic outgassing, to autotrophic in-gassing systems ($p = 0.02$; Fig. 3.4d). We found a corresponding, weak difference in d-excess with median values slightly greater (i.e., less evaporated water masses) in the in-gassing lakes than in the outgassing lakes ($p = 0.07$; Fig. 3.4e), although this relationship was not significant in *post-hoc* comparisons. In-gassing lakes also had higher concentrations of TN ($p = 0.03$; Fig. 3.4f), and marginally higher TN:TP ($p = 0.12$; Fig. 3.4g). We found no clear difference among categories for DOC concentration ($p = 0.27$; data not shown) or chl *a* concentrations ($p = 0.25$; data not shown), although autotrophic in-gassing lakes tended to have less colored DOC concentration, as suggested by the lower absorbance values and greater light penetration in these lakes ($p = 0.001$; Fig. 3.4g).

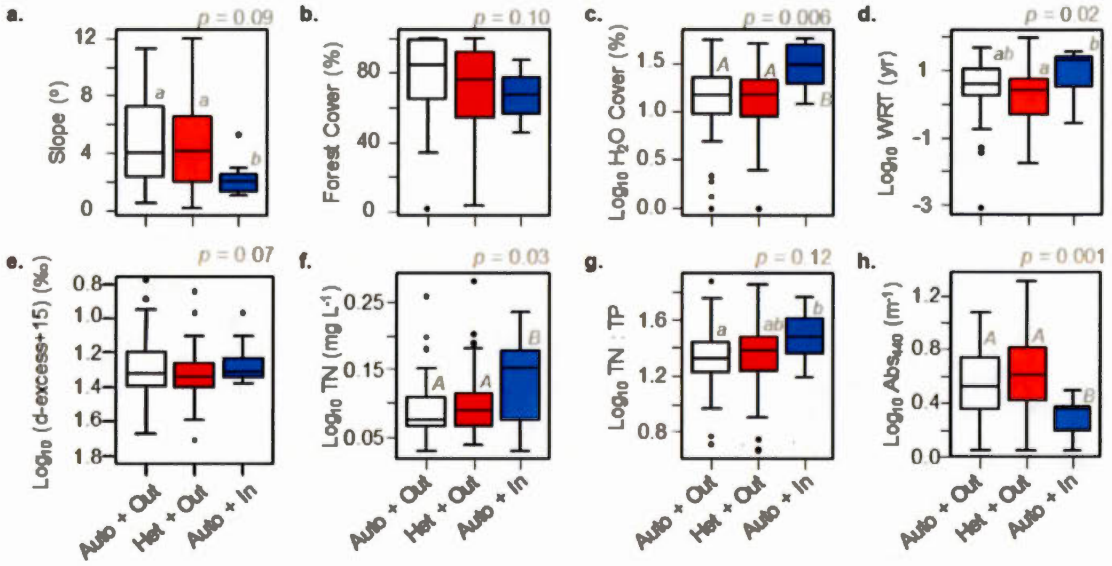

Figure 3.4. Environmental and limnological conditions associated with each lake Group from Fig. 3.3a (Auto + out = net autotrophic and CO_2 out-gassing, Het + Out = net heterotrophic and CO_2 out-gassing, Auto + In = net autotrophic and CO_2 ingassing).

Comparisons include (a) catchment slope, (b) relative catchment forest cover, (c) the logarithms of relative catchment aquatic habitat cover, (d) lake water residence time, (e) d-excess (+15, to make all values positive), (f) total N concentration, (g) ratio of total N:P concentrations by mass, and (h) light absorbance at 440nm,. Statistical significance of one way ANOVAs (*p* values) given above each plot. Tukey HSD *post hoc* groupings denoted by grey italicized letters (capital letters = $p < 0.05$, lower case = *p* of 0.05 – 0.10).

3.4.4 Deviation of CO_2 flux from NEP ($\Delta_{emissions}$)

We quantified the deviation of CO_2 fluxes relative to what would be expected from NEP alone (as the vertical deviation from the metabolic reference line shown as the solid grey 1 : -1 line in Fig. 3.3a), and referred to it as $\Delta_{emissions}$. Values of $\Delta_{emissions}$ spanned from -1,400 to 2,215 mg C m^{-2} d^{-1} (mean = 60; Fig. 3.3b). This scatter around the metabolic line can be partly explained by the variability surrounding the respiratory and photochemical quotients (i.e. molar ratios of CO_2 production to DO consumption) (Berggren et al. 2012; Cory et al. 2014), however the observed magnitude and range of $\Delta_{emissions}$ requires the contribution of processes other than aerobic metabolism. The largest positive values of $\Delta_{emissions}$ were observed in the most autotrophic lakes (Fig. 3.3a), and this category tended to have the largest excess CO_2 flux rates (Fig. 3.3c), while the most negative values (greatest CO_2 deficits) were found in the most heterotrophic systems (Fig. 3.3a), the category with the smallest overall $\Delta_{emissions}$ values (Fig. 3.3c).

3.4.5 Exploring the drivers of $\Delta_{emissions}$

We used PLS regression analysis (Fig. 3.5) and correlation analysis (Table 3.2) to examine the variables explaining the large observed range in $\Delta_{emissions}$ (Fig. 3.3). Combined, the first 2 components of the PLS (Fig. 3.5) accounted for just over 32% of the variance in $\Delta_{emissions}$. The strongest of all in-lake predictors was surface water CH_4 concentration, which was strongly positively associated with axis 1 (Fig.

3.5; $r = 0.54$, Table 3.2). The first component was also linked to variables describing catchment structure, which were then next strongest predictors of $\Delta_{emissions}$. Catchment slope, relative vegetation and forest cover (r = 0.42, 0.31, and 0.34 respectively; Table 3.2) all loaded positively on this axis (Fig. 3.5) while lake area, catchment area, and the presence of wetlands and standing water loaded negatively (Fig. 3.5; r = -0.41 – -0.30, Table 3.2). Axis 2 was associated with both hydrology and limnological characteristics (Fig. 3.5) which accounted for 13.7% of the variance in $\Delta_{emissions}$ but were individually very weak predictors ($p \geq 0.16$; Table 3.2). Both d-excess and variables associated with the regulation of terrestrial OC delivery (catchment area : lake area, DOC concentration, and water color as absorbance) loaded negatively on the second axis, while residence time, lake depth, algal biomass, and nutrient concentrations (N and P) loaded positively on this axis (Fig. 3.5 and Table 3.2).

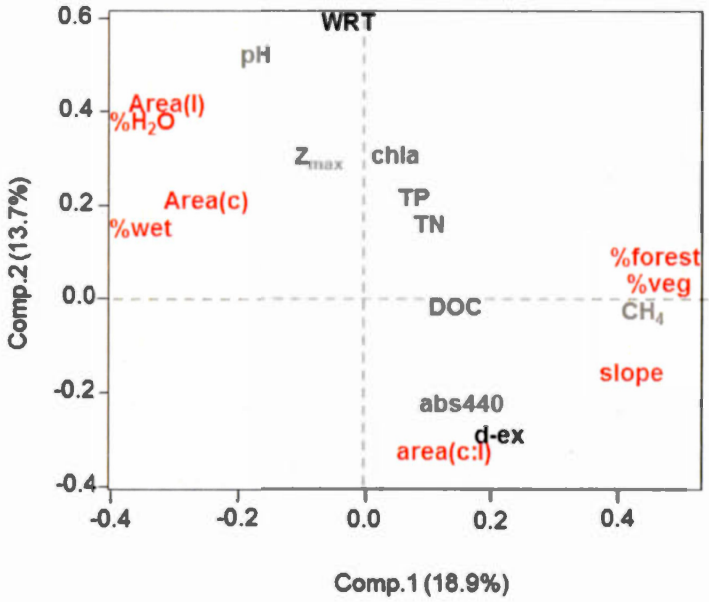

Figure 3.5. Predictors of excess CO_2 emissions ($\Delta_{emissions}$; Fig. 3.3) were assessed using partial least squares regression analysis (PLS) on a subset of boreal lakes (n = 155).

Hydrological variables (black) included lake water residence time (WRT), and lake water isotopic d-excess (d-ex). Catchment characteristics (red) include proportional total water and wetland cover ($\%H_2O$ and %wet, respectively), catchment slope, lake and catchment surface area and their ratio (Area(l), Area(c), and Area(c:l), respectively). Proportional vegetative and forest cover (%veg and % forest, respectively). Lake conditions (grey) include light penetration (abs440), total P (TP) and N (TN), pH, CH_4 concentrations, dissolved organic C (DOC), algal biomass as chlorophyll *a* (chl *a*), and maximum lake depth (Z_{max}).

Table 3.2. Top limnological and environmental predictors of $\Delta_{emissions}$ (mg C m^{-2} d^{-1}) for Canadian boreal lakes (n = 139).

* denotes $\log_{10}$ transformation.

Predictor	Pearson *r*	Pearson *p*
CH_4 (μM)*	0.54	0.01
Slope (°)	0.42	0.05
Catchment area (m^2)*	-0.42	0.05
Lake area (m^2)*	-0.41	0.06
Wetland cover (%)*	-0.40	0.07
Forest cover (%)*	0.34	0.13
Chl *a* (μg L^{-1})*	-0.31	0.16
Vegetative cover (%)*	0.31	0.16
Aquatic habitat cover (%)*	-0.30	0.18
TP (μg L^{-1})*	-0.25	0.27
pH	-0.24	0.28
TN (mg L^{-1})*	-0.19	0.40
DOC (mg L^{-1})*	-0.18	0.41
Catchment area : Lake area*	-0.14	0.52
Abs440 (m^{-1})*	-0.12	0.59
Water residence time (yr)*	-0.10	0.67
Z_{max}(m)*	-0.09	0.70
d-excess (‰)	-0.04	0.88

To distinguish the influence of the different processes shaping the CO_2 pool and $\Delta_{emissions}$, we explored the isotopic composition ($\delta^{13}C\text{-}CO_2$) of dissolved CO_2 (Fig. 3.6). Aerobic respiration of terrestrial OC generates CO_2 with an isotopic signature ~ -27‰, while atmospheric exchange and anaerobic CO_2 inputs generally enrich the isotopic composition of the CO_2 pool (Dubois et al. 2009, and references therein). Across all lakes, $\delta^{13}C\text{-}CO_2$ ranged from ~ -8 to -21‰, but surprisingly, $\delta^{13}C\text{-}CO_2$ exhibited no relationship with $\Delta_{emissions}$ (r^2 = 0), suggesting there was no systematic shift in the processes regulating the flux of CO_2 along the gradient of $\Delta_{emissions}$. As expected due to the strong influence of atmospheric CO_2 inputs (~ -8‰; Venkiteswaran et al. 2014), values of $\delta^{13}C\text{-}CO_2$ in in-gassing lakes spanned a small, and comparatively enriched range (~-12 to -16‰; Fig. 3.6). Although the outgassing lakes spanned the complete (heterotrophic lakes) or near-complete (autotrophic lakes) isotopic gradient, we found no systematic change in $\delta^{13}C\text{-}CO_2$ in each of the outgassing lake categories. This pattern was surprising, since $\delta^{13}C\text{-}CO_2$ decreased as a function of pCO_2 across all lakes (Fig. 3.2c). The lack of a clear relationship between isotopic composition and $\Delta_{emissions}$ in the outgassing lakes suggests that no individual process (terrestrial CO_2 loading, or in-lake anaerobic CO_2 processing) drove the patterns of $\Delta_{emissions}$ across lakes.

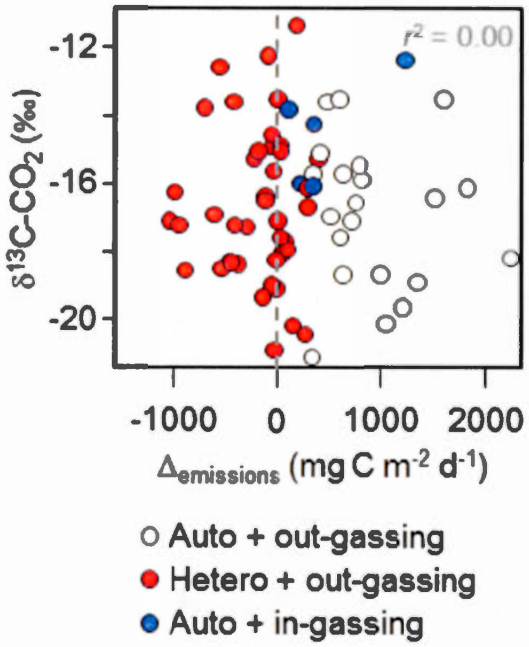

Figure 3.6. For the same subset of lakes examined in Fig. 3.2c (n = 68), we compared $\delta^{13}C\text{-}CO_2$ and the deviation of CO_2 flux rates from the metabolic reference line ($\Delta_{emissions}$; see Fig. 3.3a).

Colors represent the 3 lake groups (see legend). The dashed grey line denotes zero deviation from the metabolic reference line.

3.5 DISCUSSION

Most lakes studied to date are net CO_2 emitters, and our results are in line with this trend, with 95% of sampled lakes outgassing CO_2, in agreement with previous studies in the boreal biome (Algesten et al. 2004; Kortelainen et al. 2006; Roehm et al. 2009). The prevalence of CO_2 emissions in lakes has led to the commonly accepted idea that inputs of terrestrial organic matter support net heterotrophy and net biotic CO_2 production in the vast majority of boreal lakes. Surprisingly, our results contradict this paradigm; when lakes were categorized in three distinct groups based on their joint NEP and CO_2 flux patterns, roughly a third of sampled lakes were concurrently net autotrophic and net CO_2 emitting (upper right panel in Fig. 3.3a). Equally surprising, autotrophic and heterotrophic CO_2 outgassing lakes could not be distinguished based on environmental characteristics (Fig. 3.4). When lakes were pooled together, patterns of excess CO_2 flux ($\Delta_{emissions}$) were best predicted by cross-lake differences in catchment structure (Fig. 3.5), and most strongly, their propensity to harbor anaerobic processes (inferred from relationship to CH_4; Fig. 3.5; Table 3.2). These observations support the idea that factors shaping lake CO_2 flux can vary widely over broad spatial gradients, paralleling similar temporal shifts that have been observed within a system (Vachon and del Giorgio 2014; Wilkinson et al. 2016), ultimately supporting a wide range in relationships between metabolism and CO_2 flux in lakes across the boreal landscape.

3.5.1 CO_2 fluxes track metabolism in most lakes

For most lakes sampled, metabolism explained a large degree of the variability in CO_2 flux. Roughly two thirds of sites were net heterotrophic and outgassed CO_2 (upper left panel; Fig. 3.3a), and a small subset were autotrophic and in-gassed CO_2 (bottom right panel; Fig. 3.3a). The lakes in both categories tended to follow the metabolic reference line, with significant correlations between CO_2 flux and NEP (Fig. 3.3a). Positive deviations in $\Delta_{emissions}$ suggested that lakes in both of these categories received CO_2 independent from NEP-driven inputs (heterotrophic + outgassing lakes) or consumption (autotrophic + ingassing lakes). For the autotrophic + ingassing lakes, CO_2 inputs independent of NEP were sometimes very large, as $\Delta_{emissions}$ reached > 1 g C m^{-2} d^{-1} (Fig. 3.3c). Here, it is likely that this positive offset was also partially supported by shifts in DIC equilibrium linked to the conversion of HCO_3^- to CO_2 On the other hand, NEP exceeded CO_2 flux in many net heterotrophic lakes, and we observed negative $\Delta_{emissions}$ values (Fig. 3.3c). These deficits in CO_2 flux relative to NEP may partly be caused by ecosystem level respiratory (Berggren et al. 2012) or photochemical (Cory et al. 2014) quotients < 1, or effects such as increased photorespiration or the Mehler reaction that enhance ecosystem DO consumption relative to CO_2 production (Luz et al. 2002). These patterns also likely result from methodological artefacts (see section 3.5.2). Although we cannot fully explore this phenomenon in the present study, we importantly point out that for most heterotrophic + outgassing lakes, rates of NEP fully explained rates of CO_2

emissions. Overall, the fact that most lakes tend to align along the aerobic metabolic reference line suggests that internal aerobic processes are the main drivers of the rates and spatial patterns of CO_2 fluxes in many boreal lakes, in agreement with previous studies (Duarte and Prairie 2005; Kortelainen et al. 2006; Yang et al. 2015), although the large range of variation along the line suggests the contribution of other processes as well. Not all lakes followed this pattern, however, and CO_2 dynamics in a subset of our lakes were clearly uncoupled from NEP, in agreement with recent reports suggesting most lake CO_2 emissions are externally derived (Maberly et al. 2013; Weyhenmeyer et al. 2015). It is clear that these different scenarios of CO_2 regulation appear to coexist within the boreal landscape.

3.5.2 Methodological effects on $\Delta_{emissions}$ variability

To some degree, both positive and negative offsets (i.e., $\Delta_{emissions}$; Fig. 3.3a,b) in CO_2 flux relative to the metabolic reference line reflect both methodological limitations and natural variability in our estimates of CO_2 flux and NEP. For instance, as stated above, lakes will deviate from the metabolic reference line in part due to natural variability in respiratory and photochemical quotients and a suite of other processes shaping the molar ratios of CO_2 production to DO consumption. Additionally, spatial and temporal variability in gas dynamics (Hanson et al. 2006; Staehr et al. 2012b) introduces some degree of error in our estimates of both NEP and CO_2 flux since they are computed assuming steady state conditions. Physically driven

gas intrusions at the air-water interface are small in most boreal lakes (Yang et al. 2015), yet a portion of the variability in our estimates may be linked to our calculation of k_{600}, which is based on weather data at a regional resolution, and not site-specific. The aforementioned methodological constraints are expected to account for at least some of the variability in $\Delta_{emissions}$. We explore this in greater detail in Supporting Text S3.1 in the supplementary material, where we confirm (using a detailed seasonal exploration of two of our lakes; Figs. S3.4 to S3.6) that our point sampling approach does yield representative estimates of short term (daily to multiday) NEP and CO_2 fluxes for most lakes. The resulting range in NEP across our study lakes is much larger than the potential short-term variability within any given lake (see Figs. S3.4 to S3.6), and with this in mind, here we have focused on the broader patterns across lakes, and not on the detailed variability in gas dynamics within any individual lake. The resulting categories of lakes are thus robust, as are the relationships within each category; i.e., lakes grouped as either heterotrophic + outgassing or autotrophic + ingassing both exhibit significant correlations between NEP and CO_2 flux while also often exhibiting positive $\Delta_{emissions}$. Further, over a third of the lakes grouped within a category of autotrophic + outgassing, have large CO_2 emissions that are completely decoupled from NEP, beyond what any reasonable methodological bias could explain.

3.5.3 Patterns of excess CO_2 flux – predominance in autotrophic outgassing lakes

The fact that over half of the lakes in the dataset displayed CO_2 fluxes >> NEP (i.e., $\Delta_{emissions} > 0$; Fig. 3.3b) supports the notion that soil-derived CO_2 inputs are a major feature of CO_2 dynamics in boreal lakes, as has been previously suggested (Dubois et al. 2009; Humborg et al. 2010; Lapierre and del Giorgio 2012; Weyhenmeyer et al. 2015). Perhaps the most interesting finding in our study is that positive $\Delta_{emissions}$ values were most common and greatest in magnitude in the autotrophic, CO_2 outgassing lakes (white bars in Fig, 3.3c). This is a very counterintuitive result, both in terms of the co-occurrence of net autotrophy and CO_2 outgassing, but also because the magnitude of outgassing was often very large, sometimes exceeding that of net heterotrophic lakes (Fig. 3.3a). Equally intriguing, we were unable to distinguish between the two categories of CO_2 outgassing lakes based on either environmental conditions (Fig. 3.4) or the isotopic composition of CO_2 (Fig. 3.6). The autotrophic, CO_2 outgassing lakes represented instances where NEP was actually a sink of lake CO_2 that derived from non-atmospheric sources. This effect of NEP is understood to occur in eutrophic lakes with intense primary production that are typically found in human dominated regions (Finlay et al. 2010; McDonald et al. 2013), and can be induced with experimental eutrophication (Wilkinson et al. 2016). Further, summertime pelagic net autotrophy in CO_2 outgassing lakes has been shown for a small number of systems in the Canadian boreal zone (Dubois et al. 2009). Yet the notion that lake NEP also represents an offset to external inputs of CO_2 in comparatively pristine, oligo- and mesotrophic

boreal aquatic systems has seldom been considered. This observation ultimately suggests that in the boreal biome, and likely in other regions as well, the role of lake metabolism in shaping surface water CO_2 dynamics is more diverse than currently recognized under the assumption that the vast majority of systems are net heterotrophic.

3.5.4 Catchment structure shapes the CO_2-NEP relationship

Our findings indicate that catchment slope was important in structuring the relationship between CO_2 flux and NEP among lakes (Fig. 3.5). Previous work suggests that the relative role of catchment CO_2 inputs in sustaining lake pCO_2 increase as a function of catchment elevation, slope and declining lake area (Humborg et al. 2010; Lapierre and del Giorgio 2012). Similar observations in lotic systems show that contributions of in-stream CO_2 production to emissions increases moving downstream with increased river size, decreased river replenishment rates, and declines in terrestrial CO_2 input per unit volume of flowing water (Hotchkiss *et al.*, 2015). Clearly, this connection to the terrestrial environment should be mediated by the movement of water, and we tried to capture the strength of the hydrological connection between lakes and the terrestrial environment using measurements of d-excess (Fig. S3.2). Interestingly, we did not find a direct link between $\Delta_{emissions}$ and d-excess (Table 3.2; $r = -0.04$, $p = 0.9$), despite the strong positive relationship between lake d-excess and catchment slope (Supplementary Table S3.1), and the importance

of d-excess on axis 2 of the PLS regression (Fig. 3.5). This pattern is surprising and requires further study.

3.5.5 Sources of excess CO_2 flux

The most obvious process that could support CO_2 fluxes beyond those generated by NEP is loading of soil-derived CO_2 from river and groundwater, which has been shown to be important in many lakes (Jones et al. 2001; Finlay et al. 2010; Maberly et al. 2013). Previous work (which includes a subset of our lakes) has shown using a different methodology that terrestrially-derived CO_2 inputs may explain the roughly 10-fold range in baseline lake pCO_2 that exists across boreal regions (Lapierre and del Giorgio 2012). If soil respiration were the only source of CO_2 driving excess flux, then $\delta^{13}C\text{-}CO_2$ and $\Delta_{emissions}$ should have been inversely related, decreasing toward the $\delta^{13}C$ signature of soil-derived CO_2 (i.e., ~ -27 ‰, Jones et al. 2001; Venkiteswaran et al. 2014). No such relationship was found here, despite the inverse relationship between $\delta^{13}C\text{-}CO_2$ and pCO_2 (Fig. 3.2c) that is consistent with previous work (Striegl et al. 2001; Dubois et al. 2009). Values of $\delta^{13}C\text{-}CO_2$ deviated from the terrestrial OC isotopic signal and reached up to ~ -12 ‰ (Fig. 3.6), suggesting that other processes heavily influenced the CO_2 pool in many of these lakes. Incoming CO_2 was possibly enriched via re-aeration during stream flow or in the lake (Jones et al. 2001; Striegl et al. 2001; Dubois et al. 2009; Venkiteswaran et al. 2014), which would have introduced scatter in the $\delta^{13}C\text{-}CO_2$

versus $\Delta_{emissions}$ relationship (Fig. 3.6). Yet the fact that no relationship was observed whatsoever strongly suggests that other CO_2 sources, not just catchment derived CO_2, determined the patterns of $\Delta_{emissions}$ across lakes.

To further explore if external inputs of CO_2 could fully sustain the positive deviation of emissions from the metabolic reference line (Fig. 3.3a), we used a mass balance approach (see methods for details) to determine the hypothetical pCO_2 of incoming waters required to account for observed $\Delta_{emissions}$ (Fig. 3.7, n = 92). Estimates of pCO_2 in incoming water ranged from 15 to 1.67 x 10^6 µatm. It is clear that this simple mass balance offers only a very coarse perspective, especially because it does not distinguish between surface versus ground water inputs, and is based on an annual water load and not that expected during summer, but it does provide an idea of whether the excess CO_2 recorded in many of these lakes could be plausibly delivered by groundwater and streams entering the lakes.

This mass balance exercise showed that for 49 of 92 lakes that had excess CO_2, the estimated incoming pCO_2 values fell within a plausible potential range of stream and groundwater pCO_2 (Fig. 3.7; grey shaded area from Macpherson (2009), further constrained by measured boreal ground-, soil-, and stream water pCO_2 to an upper limit of ~40,000 µatm (P. del Giorgio and D. Vachon, personal communication). In the remaining 43 lakes, the observed CO_2 excess required concentrations of CO_2 in incoming water that are well beyond measurements from any boreal watershed. ANOVA showed that lakes where external inputs of CO_2

could not plausibly account for the CO_2 excess were generally found in flatter catchments with smaller catchment to lake ratios, longer water retention times, and higher chl *a* concentrations and NEP (Fig. 3.8a-e). Concentrations of CH_4 were roughly equivalent between the two groups (Fig. 3.8f). Together, these patterns suggest that anaerobic processes may have been relatively more important in supporting $\Delta_{emissions}$ in lakes with weaker hydrologic connectivity and likely smaller soil CO_2 influence. In this regard, the strong positive relationship between CH_4 and $\Delta_{emissions}$ (Table 3.2; Fig. 3.5) suggests that there may be an association between excess CO_2 flux and the occurrence of anaerobic processes that can generate CO_2 (Torgerson and Branco 2007; Holgerson 2015). Previous studies have shown that anaerobic CO_2 inputs can be large enough to significantly alter the isotopic composition of the DIC pool (Striegl et al. 2001; Gu et al. 2004), and may potentially decouple CO_2 flux from NEP (Holgerson 2015; Dubois et al. 2009), but this phenomenon has seldom been explicitly investigated in the context of lake CO_2 dynamics (Torgerson and Branco 2007). Although these anaerobic pathways likely operate in all lakes, our results suggest that they may be relatively more important in lakes that are both hydrologically less connected to land, and also more productive.

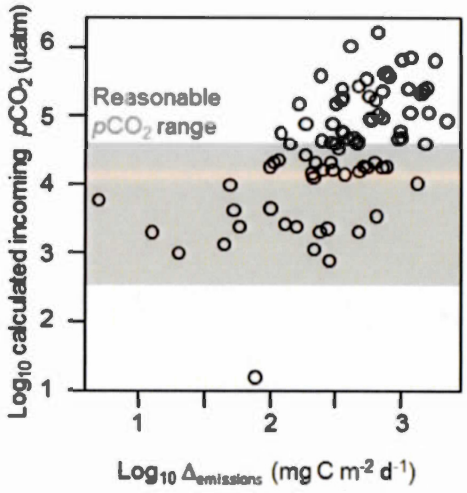

Figure 3.7. Mass balance calculation estimating the hypothetical pCO_2 needed for incoming water in order to sustain the observed $\Delta_{emissions}$ rates (i.e., rates of lake CO_2 emissions exceeding rates of NEP, as presented in Fig. 3.3a).

The shaded plot area denotes a pCO_2 range of ~400 – 40,000 µatm, the approximate range of groundwater and stream water pCO_2.

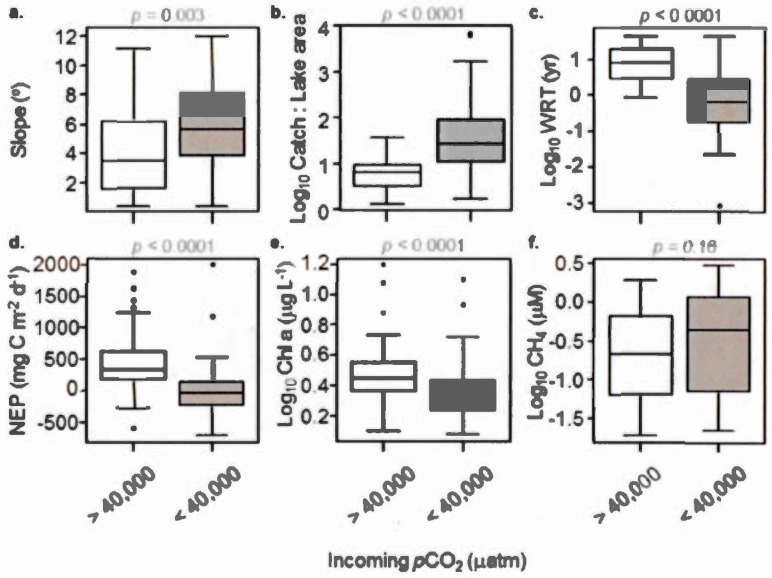

Figure 3.8. Environmental and limnological conditions associated with lakes for which mass-balance derived pCO_2 of incoming water was within, or above a reasonable range based on known ranges of stream- and groundwater pCO_2 (see Fig. 3.7).

Comparisons include (a) catchment slope, (b) the logarithms of the ratio of catchment to lake area and (c) lake water residence time, (d) net ecosystem production, (e) the logarithms of algal biomass as chlorophyll *a*, and (f) surface concentrations of CH_4. Statistical significance of one way ANOVAs (*p* values) given above each plot.

3.5.6 Implications for regional C balances

Most lakes are sources of CO_2 to the atmosphere, but our results suggest that the role of individual lakes in catchment C cycling can shift dramatically throughout the landscape. The degradation of terrestrial OC within these lakes is already accounted for in NEP, and in net heterotrophic lakes, this phenomenon is well understood to reduce the C sink strength of the surrounding catchment (Algesten et al. 2004; Duarte and Prairie 2005; Tranvik et al. 2009; Buffam et al. 2011). On the other hand, lakes that are net autotrophic + CO_2 outgassing (Fig 3.3a) either reduce or enhance catchment C sink strength, depending on the pathway supporting CO_2 emissions: In lakes where excess emissions are potentially all driven by soil-CO_2 input (Fig. 3.7), aerobic NEP acts as a sink of terrestrially derived CO_2 and offsets a fraction of terrestrially-derived emissions. At the catchment scale, these lakes actually enhance the C sink strength of the whole watershed. On the other hand, if a significant portion of excess CO_2 is driven by anaerobic metabolism, then the source of C supporting this metabolism will determine the role of the lake in the catchment-level C budget. Anaerobic production of CO_2 from terrestrial OM reaching lake sediments via sedimentation or flocculation represents a scenario where lakes burn more terrestrial OC than is obvious from aerobic metabolism alone, and therefore reduces the catchment sink strength. Conversely, if this anaerobic metabolism is supported by authochthonous C derived from the positive lake NEP (Fig. 3.7, Fig. 3.8d), this would significantly reduce the magnitude of the lake C sink, and its

capacity to offset the evasion of soil-derived CO_2. Unfortunately, our data do not allow us to define the actual contribution of anaerobic CO_2 production in the study lakes, or the source of C supporting these pathways. The coexistence of net autotrophy and CO_2 outgassing in northern lakes had been identified before (Dubois et al. 2009), but our study has shown that this feature is widespread, comprising roughly a third of all lakes sampled across the vast and heterogeneous boreal biome of Québec. These lakes are often characterized by high average CO_2 emissions, yet none of the common features measured in lakes were able to distinguish them from the more classical category of net heterotrophic, outgassing lakes, which points to major gaps that still exist in our understanding of C dynamics in boreal lakes and their role in the broader catchment C cycle.

3.6 ACKNOWLEDGEMENTS

We thank past and present lab members, especially A. St. Pierre and A. Parkes, for data collection in the field and lab, this work would not have been possible without their collective efforts. We thank D. Vachon, Y. Prairie, and R. Vogt for important discussions, and J.F. Lapierre, R. Hutchins, and R. Nahas for compiling climate and catchment data. C. Soued provided helpful comments on an early version of the paper. All data are freely available upon email request to: del_giorgio.paul@uqam.ca. M.J.B. was directly supported by doctoral scholarships from the National Science and Engineering Research Council of Canada (NSERC) and the Université du Québec a Montréal. This project is part of the program of the NSERC / Hydro-Québec Industrial Research Chair in Carbon Biogeochemistry in Boreal Aquatic Systems (CarBBAS), co-funded by grants from NSERC and Hydro-Québec to P.A.d.G.

3.7 SUPPORTING INFORMATION

3.7.1 Supporting Figures

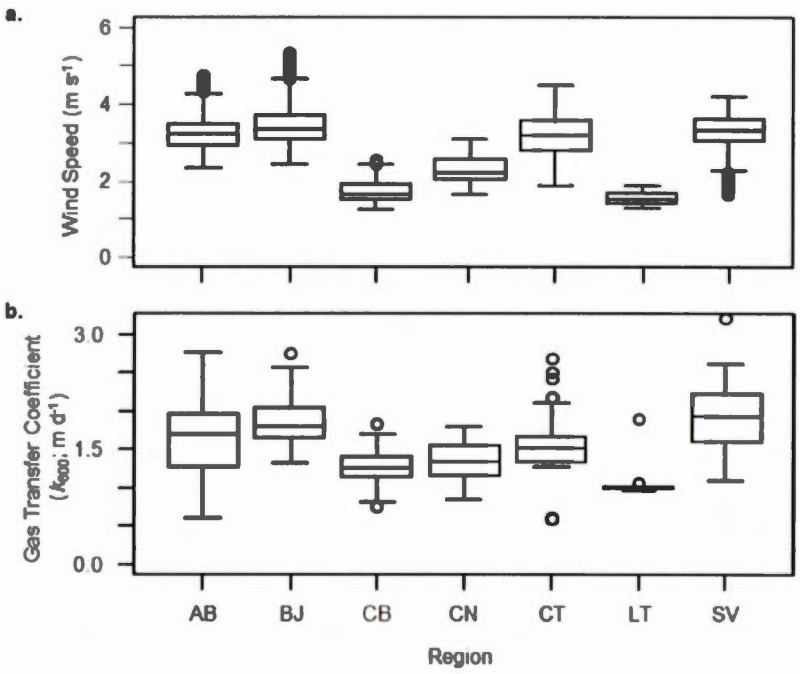

Figure S3.1. Physical conditions in boreal sampling regions.

a) 7-day moving average wind speed estimates from Environment Canada weather stations for each sampling region, for time periods individually covering the regional sampling campaigns. b) boxplot of modelled gas transfer coefficients, by sampling region, estimated from 7-day moving average wind speed and lake area (see methods in text for details).

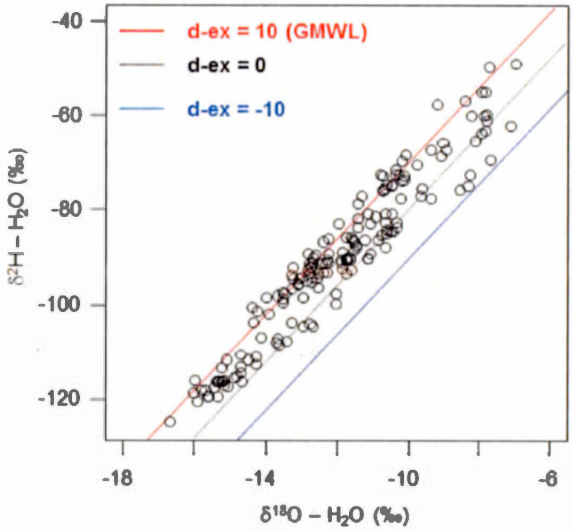

Figure S3.2. Isotopic composition of boreal lake surface water.

The global meteoric water line (GMWL; $\delta^2H = 10 + 8 \times \delta^{18}O$) is shown in red, corresponding to a d-excess value of 10, with d-excess values of 0 (grey line), and -10 (blue line) denoting the relative extent of evaporation in each lake.

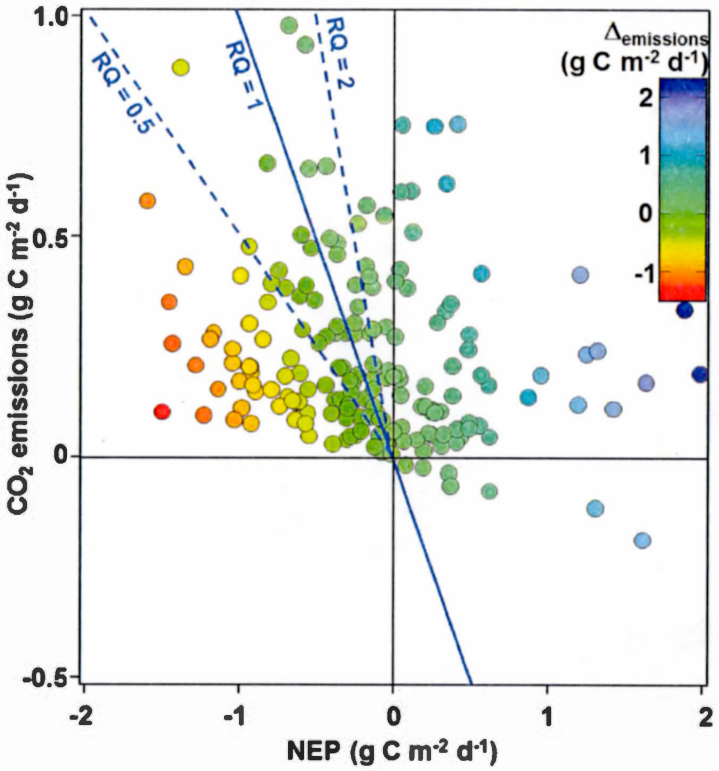

Figure S3.3. Replotting of Fig. 3.3a from main text, but with untransformed axes.

All other features are consistent with and described in the legend of Fig. 3.3a.

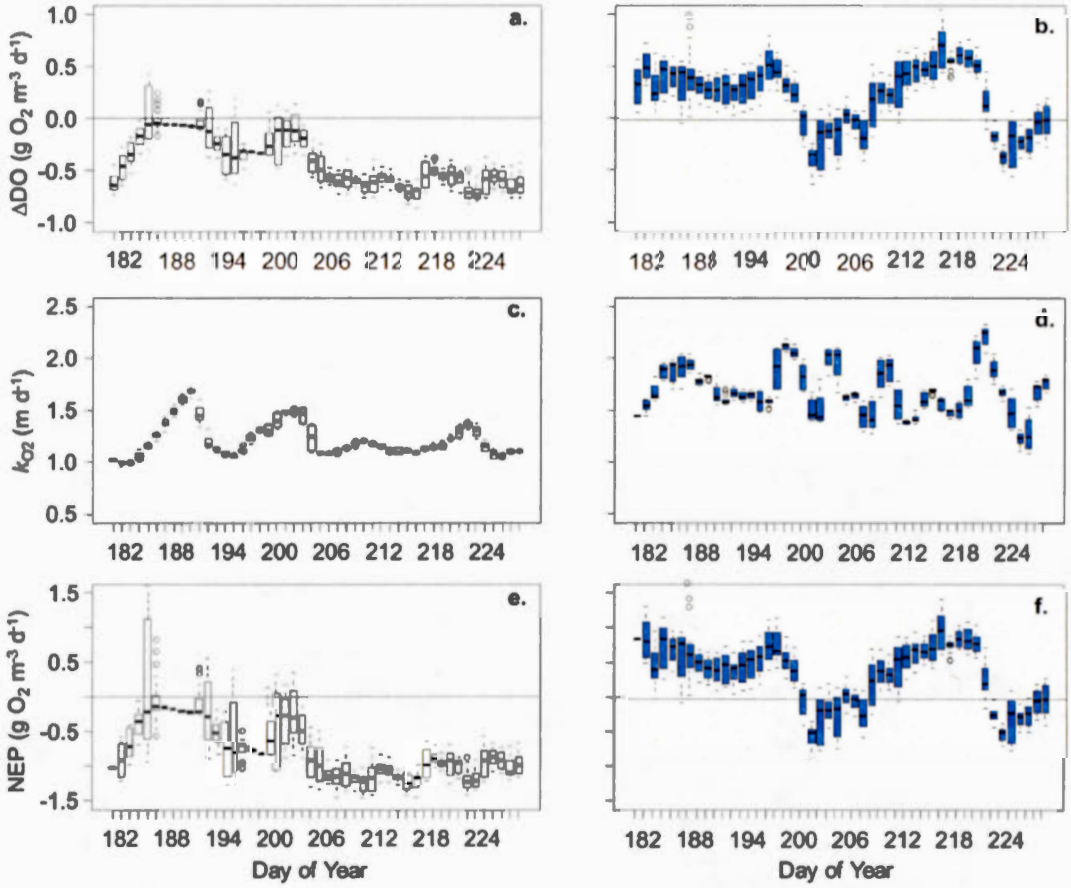

Figure S3.4. Exploring hourly summertime gas dynamics using previously published data (Vachon and del Giorgio 2014) from two of our northern Canadian lakes (Lac Croche, white fill; Lac Simoncouche, blue fill).

Both lakes serve as long term study sites, and provide an ideal setting to explore the consequences of using point dissolved oxygen (DO) sampling methods to assess surface layer net ecosystem production (NEP). The time series reflects the summertime sampling period of the broader lake survey. Boxplots denote hourly estimates, grouped by day, for DO deviation from saturation (ΔDO; panels a, b), estimates of the gas transfer coefficient (k_{O2}; panels c, d) derived from hourly wind

speed and lake area (Vachon and Prairie 2013), then smoothed using 48-hour moving averages, and finally hourly estimates of surface layer volumetric NEP (panels e,f), calculated as detailed in the methods. In all plots, the horizontal solid line denotes ΔDO at atmospheric saturation (panels a, b), or cases where NEP = 0 (panels e, f).

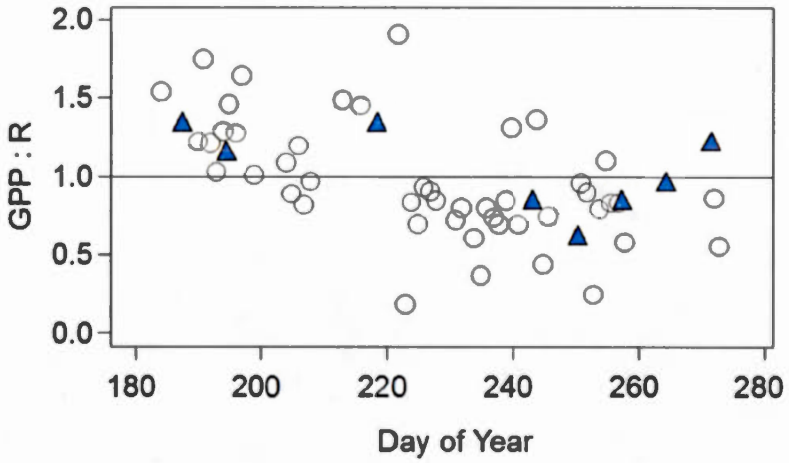

Figure S3.5. Patterns of isotopically-derived metabolic balance estimates (ratio of gross primary production to respiration; GPP : R) for surface waters of Lac Simoncouche, one of two reference lakes described in Fig. S3.3.

Here, we apply the isotopic ($\delta^{18}O$) approach (blue triangles) described in the methods section to previously unpublished data (Bogard et al., manuscript in preparation) gathered throughout the majority of the 2011 ice-free period. Data are shown alongside published GPP : R estimates (open circles) generated from hourly surface layer DO measurements (detailed in Vachon and del Giorgio, 2014).

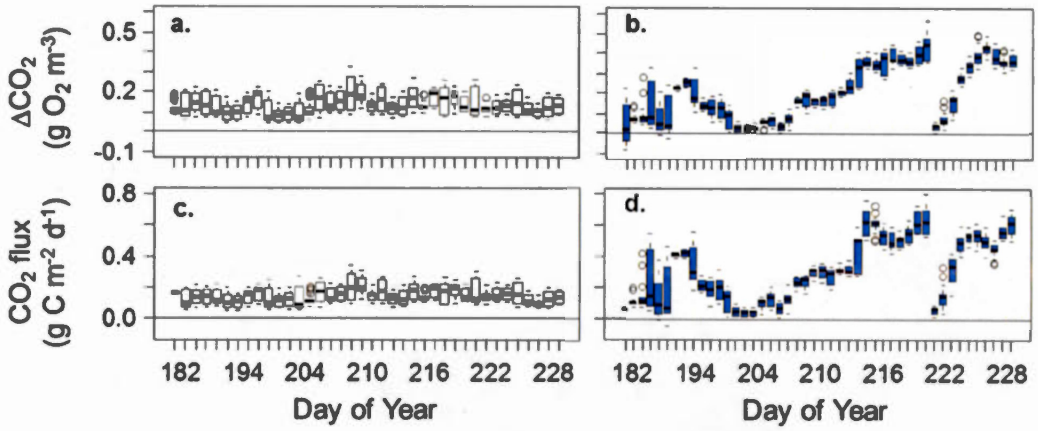

Figure S3.6. Summertime CO_2 dynamics based on previously published data (Vachon and del Giorgio 2014) from two of our northern Canadian lakes (presented in Fig. S3.3; Lac Croche, white fill; Lac Simoncouche, blue fill).

The time series reflects the summertime sampling period of the broader lake survey. Boxplots denote hourly estimates, grouped by day, for CO_2 deviation from saturation (ΔCO_2; panels a, b), and hourly flux estimates calculated, as described in the methods section, using ΔCO_2 and a CO_2-specific gas transfer coefficient (calculated from k_{O2} values of Fig. S3.3c, d). Horizontal solid line denotes ΔCO_2 at atmospheric saturation (panels a, b), or net air-water CO_2 flux = 0 (panels c, d).

3.7.2 Supporting Tables

Table S3.1. Correlation strength of lake water d-excess (‰) to individual environmental variables.

* Predictor $\log_{10}$ transformed.

Predictor	Pearson *r*	Pearson *p*
Slope (°)	0.50	0.00
Aquatic habitat cover (%)*	-0.37	0.00
Vegetative cover (%)*	0.29	0.00
Total annual precip. (mm y^{-1})	0.41	0.00
Total annual runoff (mm y^{-1})	0.44	0.00
Catchment area : Lake area*	0.27	0.00
Mean annual air temp. (°C)	0.13	0.08
Water temp. (°C)	-0.10	0.20
Elevation (m asl)	0.00	1.00

3.7.3 Supporting Text S3.1: Exploring the validity of methodological assumptions

In this study, we rely on a single point sample to infer metabolic and CO_2 flux dynamics in each study lake. Using this approach, we assume that within-lake gas dynamics are stable enough through time, particularly relative to cross-lake variability in CO_2 flux and NEP, that we can derive representative metabolic and gas flux rate estimates from these point samples. We explore these assumptions below.

To some degree, we minimized the effects of diel variation in our approach by limiting sampling of dissolved oxygen (DO) and CO_2 concentrations, as well as $\delta^{18}O$-DO and $\delta^{18}O$-H_2O, to between mid-morning and mid-afternoon, only during Summer months (late June – mid August). Despite this effort, gas dynamics vary both over sub- and multi-day periods, and to assess how such variability might impact our estimates of NEP, we explored different scales of variability (in Fig. S3.4) using two previously published (Vachon and del Giorgio 2014), high frequency datasets from two of our well-studied lakes (Lacs Croche and Simoncouche, both are described in detail by Vachon and del Giorgio [2014]). First, we conclude from these lakes that during the summer, DO deviations from saturation (Fig. S3.4a,b) are actually quite stable over shorter time periods in these two relatively nutrient-poor surface waters: On any given day, it was very uncommon for ΔDO to change in sign, and throughout the survey, this only occurred on a handful of days. Over diel cycles, the range in ΔDO was typically small (i.e., interquartile ranges were usually < 0.25 and < 0.5 g O_2 m^{-3} d^{-1} in Croche and Simoncouche, respectively). Given that daily variability in k_{O2}

was also small (Fig. S3.4c,d), this translated into small changes in NEP on most days (Fig. S3.4e,f), making it quite straightforward to assess the sign, and approximate rate of NEP on most sampling days, from most hourly samples.

Seasonal variability in net departure from saturation (Fig. S3.4a) and therefore net metabolism (Fig. S3.4e) was also quite stable in Lac Croche (40 of 49 days were heterotrophic). Though seasonal NEP was more variable in Lac Simoncouche (Fig. S3.4f), it was actually stable enough over daily to multi-day periods to provide a snapshot of net metabolism here too. Such seasonal variability should have little effect on the conclusions we are drawing form the overall survey dataset: We emphasize that one point sample of the lake is not intended to reflect a static, season wide NEP, but even in systems such as Lac Simoncouche, it can be used at a coarse level to categorize lakes based on the sign of NEP.

Next, we explored the reliability of point isotopic samples in evaluating the metabolic balance (GPP:R) of lake surface waters using our own unpublished isotopic data from Lac Simoncouche (Fig. S3.5). During the summertime, isotopically derived GPP:R in Lac Simoncouche was consistent with published (Vachon and del Giorgio 2014), high frequency-derived GPP:R estimates, and the metabolic balance of each data point agrees in sign with that of point estimated NEP in Fig. S3.4f. From this, we can say with confidence that the point sampling isotopic approach is a robust and effective way to capture spatially integrative, daily to multi-day rates and balances of metabolism, and is generally consistent with other established techniques. Regarding the potential seasonal variability in GPP:R that

occurs in lakes (e.g., Fig. S3.5), we emphasize that, as for estimates of NEP, the GPP:R estimate appears to reflect daily- to weekly scale patterns of metabolism, and though these balances do shift through time, they remain consistent for a long enough period that we can assess the short-term coupling between GPP:R and CO_2 (Fig. 3.2a) in a meaningful way.

We assessed summertime CO_2 dynamics in both lakes (Fig. S3.6) as we did for DO in Fig. S3.4. From this exploration, we conclude that the point sampling approach likely captured the true direction (for daily to multi-day time periods) of both the over- or undersaturation of dissolved CO_2 (Fig. S3.6a,b) and the direction of flux (Fig. S3.6c,d). In some systems, CO_2 fluxes can indeed be quite stable throughout the summer period (as seen for Lac Croche, Fig. S3.6c). However, in cases where CO_2 fluxes do shift over multi-day to weekly periods (such as in Lac Simoncouche from DOY 205-215; Fig. S3.6d), CO_2 dynamics should remain stable enough that we can assess the coupling of NEP and CO_2 flux, from point sampling, at a daily to multi-day time scale.

Taken together, this exploration suggests that for the majority of our surveyed lakes, the sign and approximate rates of NEP and CO_2 flux should be sustained for day- to even week-long periods, providing a relatively stable period of time to assess the relationship between NEP and CO_2. Longer-term temporal shifts in gas flux that might alter the coupling of NEP and CO_2 (and change estimates of $\Delta_{emissions}$; Fig. 3.3a) should not have a major effect on our conclusions, which have all been

cautiously drawn based on coarse subdivisions of data, and robust correlations that should not be sensitive to some variability in patterns from individual lakes.

CHAPTER IV

OXIC WATER COLUMN METHANOGENESIS AS A MAJOR COMPONENT OF AQUATIC CH_4 FLUXES

Matthew J. Bogard, Paul A. del Giorgio, Lennie Boutet, Maria Carolina Garcia Chaves, Yves T. Prairie, Anthony Merante, Alison Derry

Published in *Nature Communications* (2014) 5: 5350. DOI: 10.1038/ncomms6350

Groupe de recherche interuniversitaire en limnologie, Département des Sciences Biologiques, Université du Québec à Montréal, Case Postale 8888, succursale Centre-Ville, Montréal, QC,H3C 3P8, Canada.

N.B. References cited in this chapter are presented at the end of the thesis.

4.1 ABSTRACT

Methanogenesis has traditionally been assumed to occur only in anoxic environments, yet there is mounting, albeit indirect, evidence of methane (CH_4) production in oxic marine and freshwaters. Here we present here the first direct, ecosystem-scale demonstration of methanogenesis in oxic lake waters. This methanogenesis appears to be driven by acetoclastic production, and is closely linked to algal dynamics. We show that oxic water methanogenesis is a significant component of the overall CH_4 budget in a small, shallow lake, and provide evidence that this pathway may be the main CH_4 source in large, deep lakes and open oceans. Our results challenge the current global understanding of aquatic CH_4 dynamics, and suggest a hitherto unestablished link between pelagic CH_4 emissions and surface-water primary production. This link may be particularly sensitive to widespread and increasing human influences on aquatic system primary productivity.

4.2 INTRODUCTION

Methane (CH_4) emissions currently contribute ~20% to the planet's greenhouse effect, with a large, but poorly defined fraction derived from freshwater ecosystems (Michmerhuizen et al. 1996; IPCC 2007; Bastviken et al. 2011; Kirschke et al. 2013). Accurately placing freshwaters in the global CH_4 budget requires a better understanding of the controls and contributions of CH_4 from different sources (Michmerhuizen et al. 1996; Bastviken et al. 2011; Kirschke et al. 2013; Prairie and del Giorgio 2013). In this regard, the surface waters of lakes and rivers are systematically supersaturated with CH_4, and it has been traditionally assumed that this CH_4 is derived from anoxic environments, via vertical and lateral transport from profundal and littoral sediments (Rudd and Hamilton 1978; Michmerhuizen et al. 1996; Murase et al. 2003; Bastviken et al. 2004). This assumption certainly holds for small, shallow ecosystems where the surface layers are in relatively close contact with sediments. Yet CH_4 supersaturation is also prevalent in large, deep lakes (Michmerhuizen et al. 1996; Schmidt and Conrad 1993; Schulz et al. 2001; Murase et al. 2003; Bastviken et al. 2004; Schmid et al. 2007; Hofmann 2013; Prairie and del Giorgio 2013) and oceanic surface waters (Scranton and Brewer 1978; Owens et al. 1991; Tilbrook and Karl 1995; Karl et al. 2008; Damm et al. 2010), where deeper water columns result in significantly reduced surface water exchange with anoxic sediments. Studies of CH_4 dynamics in surface waters of oceans and large lakes have indeed concluded that pelagic CH_4 supersaturation cannot be sustained either by lateral inputs from the littoral or from benthic inputs alone (Scranton and Brewer

1978; Owens et al. 1991; Schmidt and Conrad 1993; Tilbrook and Karl 1995; Schulz et al. 2001; Damm et al. 2010; Grossart et al. 2011; Tang et al. 2014).

A pelagic source of CH_4 would thus be required to sustain the observed CH_4 supersaturation, and multiple lines of evidence suggest that CH_4 is produced in oxic water columns of freshwater and marine systems. In vitro experiments point to CH_4 production in both microanoxic habitats in metazoan guts and on particles (Oremland 1979; Owens et al. 1991; De Angelis and Lee 1994; Tilbrook and Karl 1995; Beversdorf et al. 2010; Grossart et al. 2011; Ditchfield et al. 2012; Tang et al. 2014), and in particle-free oxic water (Karl et al. 2008; Damm et al. 2010; Beversdorf et al. 2010; Grossart et al. 2011; Carini et al. 2014; del Valle and Karl 2014; Tang et al. 2014), via multiple biochemical pathways. The presence (Grossart et al. 2011; Angel et al. 2011, 2012; Ditchfield et al. 2012; Paganin et al. 2013) and activity (Angel et al. 2011; Grossart et al. 2011; Ditchfield et al. 2012) of hydrogenotrophic and acetoclastic methanogenic archaea has been confirmed at the molecular level in diverse oxic environments. At the same time, marine studies suggest that the microbial decomposition of methylated compounds such as methanethiol (Damm et al. 2010) and methylphosphonate (Karl et al. 2008; Beversdorf et al. 2010; Carini et al. 2014; del Valle and Karl 2014) could be an important source of CH_4 in surface waters of the open ocean. Further, metalimnetic peaks of CH_4 are a recurrent feature in many ecosystems, which correlate positively with dissolved O_2 (DO), algal biomass and production (Owens et al. 1991; Schmidt and Conrad 1993; Schulz et al. 2001; Murase et al. 2003; Damm et al. 2010; Grossart et al. 2011; Tang et al. 2014).

However, despite past efforts, the ecological and biogeochemical significance of oxic water column methanogenesis remains speculative, and we have yet to determine the dominant biochemical pathway, its controls, and its contribution to diffusive CH_4 emissions from aquatic ecosystems.

In this study, we experimentally assessed pelagic CH_4 production in the oxygenated water column of Lac Cromwell, a typical Canadian temperate Shield lake, using floating mesocosms open to the atmosphere, but closed at the bottom and therefore uncoupled from non-pelagic sources of CH_4. The results presented herein represent the first direct, ecosystem-scale demonstration of oxic water CH_4 production, its drivers and source pathway, and the potential widespread importance of this poorly considered process.

4.3 RESULTS

4.3.1 CH_4 dynamics in experimental enclosures

The initial CH_4 concentrations in the enclosures were 4 to 10-fold lower than surrounding lake waters, due to degassing during the initial filtration and filling process, but the enclosures were nevertheless supersaturated relative to the atmosphere at the onset of the experiment (Fig. 4.1a). Vertical profiles of the enclosures (Supplementary Fig. S4.1) showed a range in DO between 45.6 - 128.6 % saturation, indicating that the entire water column remained oxic in all treatments for the duration of the experiment. Despite oxic conditions, CH_4 concentrations ranged between 0.10 – 0.53 μM throughout the entire experiment, across all treatments (Fig. 4.1a), which represents ~50 – 265-fold super-saturation relative to the atmosphere.

The observed surface CH_4 concentrations in the mesocosms represent the net balance between CH_4 production, CH_4 oxidation and CH_4 exchange with the atmosphere. In the absence of internal inputs of CH_4, the initial CH_4 supersaturation in the enclosures would have declined to atmospheric equilibrium within approximately one week (Fig. 4.1a, dotted lines), as estimated on the basis of our own empirical measurements of the gas exchange coefficient (see Methods section). Thus, an internal CH_4 source was necessary to sustain the systematic CH_4 supersaturation observed in all mesocosms throughout the experiment. Further, there was an overall significant increase in CH_4 concentrations through time across treatments (Fig. 4.1a; RM-ANOVA time effect: $p = 0.007$), with greater increases in nutrient amended

enclosures (NP, DOC-NP), and weaker increases in the DOC and control enclosures (RM-ANOVA treatment*time effect: $p = 0.04$). As a result, all enclosures emitted CH_4 to the atmosphere for the duration of the experiment, and the estimated water/air CH_4 fluxes (based on our measurements of gas transfer coefficients in the mesocosms) ranged from 0.07 – 0.36 mmol m^{-2} d^{-1} (Fig. 4.1b). Net CH_4 production in the enclosures, calculated as the sum of the observed net increase in concentration and the calculated CH_4 fluxes to the atmosphere, were on average highest in the nutrient enriched enclosures, while the DOC-only addition generated the lowest production rates (Fig. 4.1b; ANOVA: $p = 0.003$). We assessed the robustness of chamber-based calculations of CH_4 emissions by comparing chamber-derived gas exchange coefficients (k_{CH4}) to estimates based on wind speed (detailed in Supplementary Note S4.1). There was good agreement between the two approaches, and therefore we conclude that chamber-derived results yield reliable estimates of k_{CH4} and CH_4 fluxes for both the enclosures and the lake.

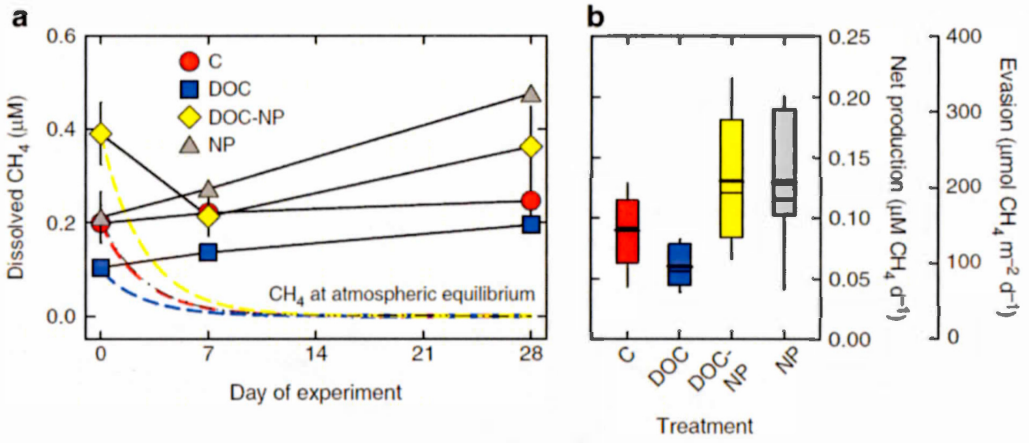

Figure 4.1. Surface water CH_4 dynamics in experimental enclosures.

Treatments include ambient untreated controls (C), addition of dissolved organic carbon (DOC), nitrogen and phosphorus (NP), or a combination of both (DOC-NP). (**a**) CH_4 concentrations (error bars $\pm$ 1 s.e.m., $n = 3$) generally increased through time, but differed between treatments (RM-ANOVA, treatment: $p = 0.004$, $F = 10.71$; time: $p = 0.007$, $F = 7.67$; treatment* time: $p = 0.04$, $F = 3.04$; Tukey HSD post-hoc grouping = NP, DOC-NP, C > C, DOC). Dashed lines show the expected declines in dissolved CH_4 due to diffusion at the air-water interface, had no methane been produced in situ. Without internal production of CH_4, concentrations would have equilibrated with the atmosphere (mean concentration at equilibrium = 0.002uM) in all treatments within 1-2 weeks. (**b**) Collectively, net CH_4 production (evasion plus water column accumulation per enclosure) and evasion rates (second y axis) displayed large differences among treatments (ANOVA, $p = 0.003$; post-hoc groups = NP & DOC-NP & C > C > C & DOC). Thick and thin horizontal lines are mean and median, respectively.

4.3.2 Linking CH_4 production to algal dynamics

The differences among treatments in water column CH_4 concentrations and fluxes were strongly linked to pelagic gross primary production (GPP) (Fig. 4.2a) and net ecosystem production (NEP = GPP-R; Fig. 4.2b). There was a 20-fold range in GPP across treatments (Fig. 4.2a), whereas there was only a 5-fold range in ecosystem respiration (R), therefore nutrient additions resulted in a strong shift in NEP (Fig. 4.2b). The average CH_4 fluxes at day 7 of the experiment were strongly positively related to average GPP rates in the enclosures (Fig. 4.2a), and to NEP, whereas the DOC addition had no positive influence relative to the control. Increases in CH_4 flux appear to have been driven mostly by increases in GPP rather than heterotrophic metabolism.

Other potential sources of CH_4 in the enclosures were also considered. The enclosures contained very little particulate organic C (POC) due to the initial filtration of the surrounding lake water prior to filling, and there was little or no accumulation of POC in the bottom of enclosures at the end of the experiment. Moreover, we estimate that zooplankton-derived CH_4, calculated from the measured zooplankton biomass in the enclosures and published production rates (Supplementary Table S4.1, Supplementary Note S4.2), contributed <10% to the estimated gross CH_4 production rates in ambient enclosures, a result that is consistent with previous studies (Miyajima et al. 1997; Schulz et al. 2001; Grossart et al. 2011; Tang et al. 2014). Membrane permeability and the resulting exchange with the surrounding lake waters was also considered as a potential cause for CH_4

supersaturation. However, the estimated contributions of CH_4 from the surrounding lake environment were on the order of < 1% of gross CH_4 production (Supplementary Methods and Supplementary Table S4.2). Finally, there was no significant development of biofilm on the walls of the enclosures during the experiment, and this is unlikely to have been a significant source of CH_4.

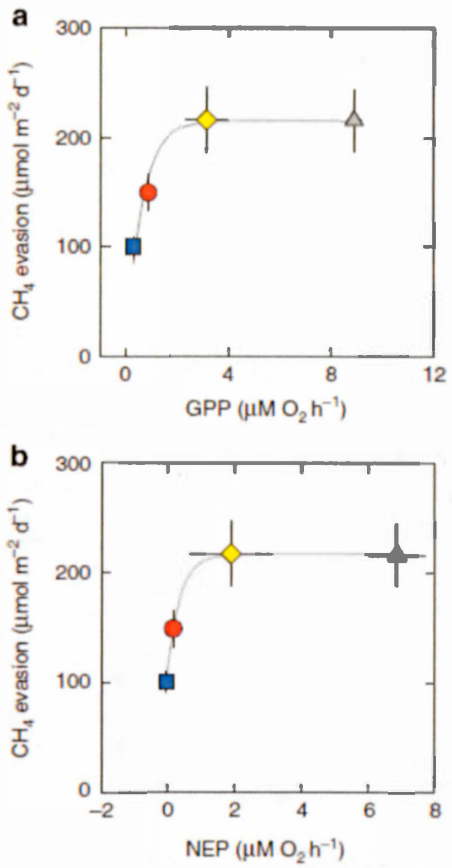

Figure 4.2. Linking pelagic ecosystem metabolism and CH_4 dynamics.

Metabolic estimates from day 7 of the experiment revealed CH_4 evasion was strongly positively correlated to (**a**) ecosystem gross primary production (GPP); ($p = 0.003$; $r^2 = 0.93$; $y = 215.3[1\text{-}e^{-1.6x}]$), and (**b**) shifts to increased net ecosystem production (NEP), which is difference between GPP and community respiration; ($p = 0.02$; $r^2 = 0.99$; $y = 111\text{-}106[1\text{-}e^{-2.6x}]$). Symbols with error bars ($\pm$ 1 s.e.m., $n = 3$) denote the different treatments, including ambient untreated controls (red circles), addition of dissolved organic carbon (blue squares), nitrogen and phosphorus (grey triangles), or a combination of both (yellow diamonds).

4.3.3 Identifying the biochemical source of CH_4

Several methanogenic pathways exist, but since acetoclastic methanogenesis is less isotopically discriminatory than CO_2 reduction or methylotrophy (Grossart et al. 2011; Angel et al. 2011, 2012), apparent fractionation factors (α_{app}; see Methods for calculation details) can be used to qualitatively distinguish whether CH_4 is produced via methanogenesis from acetate, or CO_2 reduction (Conrad 2005). Our measured α_{app} values were well within the range indicating dominance of the acetoclastic pathway (Fig. 4.3a), suggesting that acetate was the dominant source material for pelagic methanogenesis in all treatments. Since we only had one estimate of water column CH_4 oxidation (MOX) per treatment (range = 0.003 – 0.008 mmol m^{-3} h^{-1}), we used a scenario analysis with 2 extreme MOX rates (0 and 0.05 mmol m^{-3} h^{-1}; detailed in Methods section) to conservatively constrain the possible α_{app} values based on variable MOX rates and associated isotopic fractionation. In all cases α_{app} values remained well within the acetoclastic range i.e., < 1.055 (Conrad 2005; Fig. 4.3a). Acetoclastic methanogenesis was likely dominant through time, because $\delta^{13}C$-CO_2 and $\delta^{13}C$-CH_4 showed little temporal variability (Fig. 4.3b).

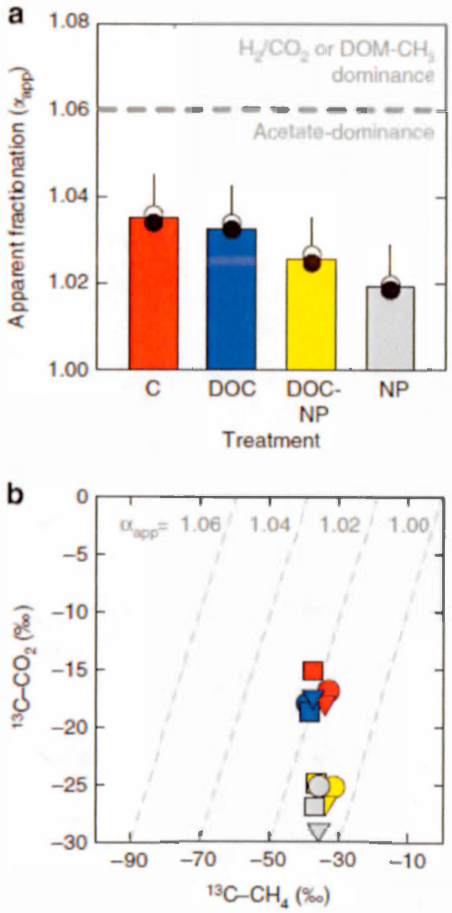

Figure 4.3. Assessing the biochemical source of pelagic CH_4.

(a) Here, patterns in the apparent fractionation (α_{app}; see methods for calculation details) during methanogenesis suggest that the acetoclastic pathway strongly dominated in all treatments, and increased in importance with the addition of nutrients. White and black circles represent values estimated using measured CH_4 oxidation rates (MOX) and a maximum and minimum associated isotopic fractionation factor, respectively. To constrain the effect of error introduced by MOX estimates, α_{app} was estimated from a highly conservative scenario analysis,

summarized here by bars and error bars (midpoint and upper potential range, respectively). Values of α_{app} were estimated for day 7 of the experiment, though isotopic signatures of CO_2 and ambient CH_4 displayed little change through time for each treatment (**b**). Red, blue, gray and yellow symbols indicate control, DOC, DOC+NP, and NP treatments, respectively, while circles, squares and triangles respectively indicate days 0, 7, and 28 of the experiment. One enclosure was followed for each treatment, and sample points represent one unreplicated measurement.

4.3.4 Rates of oxic water-column methanogenesis

The CH_4 accumulation and outgassing that we measured in the enclosures (Fig. 4.1) represent the net result of pelagic methanogenesis, gas exchange, and MOX. In order to derive a first order estimate of pelagic methanogenesis, we carried out a detailed CH_4 mass balance (described in the Methods section; summarized in Supplementary Table S4.2) for day 7 for the control enclosures. Here, we combined the measured CH_4 evasion, the change in storage corrected for cross-membrane inputs from surrounding lake water, and measured MOX. This exercise yielded rates of apparent pelagic methanogenesis on the order of 0.21 to 0.24 mmol m^{-3} d^{-1} (Table 4.1), of which ~60% was apparently oxidized and the remainder evaded to the atmosphere.

4.3.5 Oxic water methanogenesis in a whole-lake perspective

Mean pelagic CH_4 evasion from control (i.e. non-manipulated) enclosures (0.15 ± 0.03 mmol m^{-2} d^{-1}; Table 4.1) represented ~20% of the average diffusive CH_4 fluxes measured in the lake over the summer (0.78 ± 0.35 mmol m^{-2} d^{-1}), and at the whole-lake scale, were similar to CH_4 ebullitive fluxes (15.2 ± 32.5 mol d^{-1}, or 0.31 ± 0.66 mmol m^{-2} d^{-1} in lake regions < 3m deep) (Table 4.1). Further, oxic pelagic methanogenesis contributed on the order of 4% to total lake greenhouse gas (GHG) emissions (CO_2 + CH_4, expressed as CO_2 equivalents; Table 4.1). It was possible to compare fluxes directly between the enclosures and the lake because the physical conditions shaping gas exchange dynamics were quantitatively similar for each. As

shown in Supplementary Figure S4.2, floating-chamber-derived gas exchange coefficients (k_{CH4}) for the lake and the enclosures varied on a diurnal basis, but averaged 0.65 and 0.69 m d^{-1} and ranged between 0.10 – 1.91, and 0.24-1.44 m d^{-1} for the enclosures and the lake, respectively.

Table 4.1. Greenhouse gas dynamics in Lac Cromwell.

Both oxic water column production and diffusion of CH_4 in ambient (i.e., control) experimental enclosures were estimated. Mean (± 1 s.d.) summertime (June-August inclusive) areal estimates of surface emissions and ebullition were determined for Lac Cromwell alongside the experiment. In all cases, CH_4 emissions were converted to CO_2 equivalents (where 1kg CH_4 = 25kg CO_2 for a 100-yr period) to compare with areal and whole-lake CO_2 emissions. Ebullition was not detected at depths > 3m, thereby restricting contributions to whole lake flux. See Methods section for a detailed description of both enclosure and whole-lake calculations.

	CH_4 and CO_2 dynamics			
	(mmol m^{-3} d^{-1})	(mmol m^{-2} d^{-1})	(mol $lake^{-1}$ d^{-1})	(mmol CO_2eq m^{-2} d^{-1})	(mol CO_2eq $lake^{-1}$ d^{-1})
Pelagic production in enclosures	0.23 ± 0.01				
Pelagic diffusive fluxes from enclosures		0.15 ± 0.03	15.5 ± 2.6	1.4 ± 0.2	140 ± 24
Pelagic diffusive fluxes from lake		0.78 ± 0.35	79.5 ± 31.1	7.1 ± 3.2	722 ± 325
Ebullition from lake		0.31 ± 0.66	15.2 ± 32.5	2.8 ± 6.0	138 ± 295
CO_2 diffusion from lake				33.4 ± 12.4	3408 ± 1262

4.4 DISCUSSION

Here we present an ecosystem-scale, experimental demonstration of significant CH_4 production and evasion from the oxic water column of Lac Cromwell that is closely linked to algal dynamics, and which contributes a baseline flux of CH_4 that is likely present in all lakes. The relationship between CH_4 and phytoplankton observed here (Fig. 4.2) has been hypothesized before to explain both the presence of metabolically active methanogens, and the recurrent metalimnetic and near-surface CH_4 peaks in oxic lake (Schmidt and Conrad 1993; Schulz et al. 2001; Grossart et al. 2011; Tang et al. 2014) and marine (Scranton and Brewer 1977; Owens et al. 1991; Tilbrook and Karl 1995; Karl et al. 2008; Damm et al. 2010) environments. We confirm this link experimentally, and further show that it generates a significant out flux of CH_4 from the mesocosms to the atmosphere (Fig. 4.1b). These results in turn imply that factors influencing phytoplankton standing stock and GPP, such as grazing, nutrient availability, and the physical structure of the water column, will have a strong bearing on pelagic CH_4 dynamics and resulting CH_4 emissions.

To our knowledge, our results represent the first ecosystem-level estimates of methanogenesis in oxic freshwaters. For all treatments, intense CH_4 production was needed to sustain the observed patterns in CH_4 concentrations and to offset atmospheric losses. In the absence of methanogenesis, the decreases in enclosure CH_4 concentrations due solely to atmospheric evasion would have rapidly depleted the CH_4 pool (dashed lines, Fig. 4.1a). These calculations are potentially conservative, since we did not consider MOX. Considering all potential sources and

sinks, we estimate an average rate of methanogenesis of 0.23 mmol m^{-3} d^{-1} (Table 4.1; Supplementary Table S4.2). This rate is higher than previous estimates from in vitro incubations for oligotrophic Lake Stechlin, Germany (0.04 – 0.09 mmol m^{-3} d^{-1}; Grossart et al. 2011; Tang et al. 2014), but it should be noted that this estimate is very sensitive to the values of MOX used. In-situ MOX can vary dramatically across systems (Utsumi et al. 1998), with depth, diurnally, and with changes in light exposure (Grossart et al. 2011; Tang et al. 2014). Therefore it is possible that our estimates of MOX and methanogenesis may be biased by the fact that water from only one depth was used, and incubations were run in the dark (see Methods for details). Consequently, we consider our estimates of net CH_4 production (excluding MOX; Fig. 4.1b) as a lower bound for epilimnetic methanogenesis, since these estimates are analogous to methanogenesis where MOX equals zero. In the ambient enclosures, net production averaged 0.09 and ranged from 0.04 – 0.12 mmol m^{-3} d^{-1}, and is in close agreement with estimates of methanogenesis in Lake Stechlin, where MOX was shown to be extremely low throughout the epilimnion (Grossart et al. 2011; Tang et al. 2014). The fact that our approximation of pelagic methanogenesis based on mass balance (Fig. 4.1b; Table 4.1) is in good agreement with in vitro (Grossart et al. 2011; Tang et al. 2014) estimates is very promising, and suggests that both approaches could be incorporated into future detailed studies of CH_4 dynamics for other systems.

Our conclusion that acetate consumption supplied most CH_4 in the enclosures, based on estimates of α_{app}, is particularly sensitive to changes in the rate of MOX. Given the potential variability in MOX discussed above, estimates of α_{app} may be biased by our limited MOX measurement. However, scenario analyses estimating α_{app} from extreme hypothetical MOX rates (see Methods for calculations) were all well within the range of acetoclastic dominance (Fig. 4.3a). This supports our conclusion that acetate supplied the majority of CH_4 across our treatments, likely for the duration of the experiment (Fig. 4.3b). Consistent with this conclusion, observations of enriched surface $\delta^{13}C$-CH_4 in numerous lakes (Miyajima et al. 1997; Schulz et al. 2001; Murase et al. 2003; Bastviken et al. 2008; Tang et al. 2014) have been hypothesized to indicate dominance of acetoclastic methanogenesis in oxic freshwater pelagic zones (Tang et al. 2014), and both known acetoclastic genera (*Methanosaeta* and *Methanosarcina*) have recently been detected in oxic freshwater (Grossart et al. 2011; Paganin et al. 2013) and terrestrial (Angel et al. 2011, 2012) environments. Furthermore, acetoclastic dominance was enhanced with the addition of nutrients and increased algal production (Fig. 4.3a). This pattern parallels that from anoxic environments, where increased abundance of biologically-young, high-quality algal material promotes acetoclastic- over hydrogenotrophic methanogenesis, the latter instead supported by lower quality, aged terrestrial DOC (Conrad 2005). Finally, cyanobacteria were near absent in the mixed layer of our enclosures (< 3.5% relative abundance, as biomass, estimated from one enclosure per treatment on day 7

in all treatments), ruling out major contributions of diazotroph-derived water-column H_2 for hydrogenotrophic methanogenesis (Grossart et al. 2011), and cyanobacterial methanogenesis during DOM demethylation (Beversdorf et al. 2010). Taken together, it appears that acetoclastic methanogenesis linked to *in-situ*, algal DOC production, potentially plays a central role in supporting water column CH_4 production in oxic freshwaters.

The potential importance of acetate for oxic water methanogenesis is intriguing, since acetate concentrations are typically extremely low in oxic surface waters (Wright and Hobbie 1966; Allen 1968; Ho et al. 2002; Tang et al. 2014), and the presence of oxygen may inhibit acetate consumption (Angel et al. 2011). Yet past reports based on radioactive substrate additions have unequivocally demonstrated extremely rapid turnover of actetate in oxic environments across fresh and marine surface waters (Wright and Hobbie 1966; Allen 1968; Sepers 1977; Ho et al. 2002), suggesting active production of acetate from multiple metabolic pathways (Thauer et al. 1989) in oxic environments, as well as very efficient uptake (Wright and Hobbie 1966; Allen 1968; Sepers 1977; Ho et al. 2002). Fermentative metabolism by diverse and widespread facultative anaerobic bacteria in particle-associated microanoxic zones could be the main source of water column acetate (Riemann and Azam 2002; Alonso and Pernthaler 2005; Tada and Grossart 2013), and such microhabitats could be directly associated to algae or to particles (Grossart et al. 2011), yet in vitro work as well as our own results further suggest that methanogenesis proceeds even when these potential sites are removed (Grossart et al. 2011; Tang et al. 2014). One

possibility that should be further explored is that fermentative bacteria themselves create the conditions for anoxic methanogenesis through syntrophic interactions with acetoclastic methanogens in mixed cell aggregates (Stams and Plugge 2009).

Is oxic water methanogenesis a significant component of the CH_4 budget of Lac Cromwell? We have combined our estimated rates of oxic water methanogenesis and CH_4 emissions in the ambient enclosures with measurements of diffusive and ebullitive CH_4 fluxes from the surrounding lake waters (summarized in Table 4.1), and conclude that methanogenesis in the oxic pelagic zone may potentially contribute ~20% of mean summertime CH_4 diffusive fluxes, approximately the same magnitude as ebullitive fluxes measured for the entire lake. Careful extrapolation of our absolute emissions rates (Fig. 4.1b, Table 4.1) to other ecosystems should be made, since previously overlooked, system-specific differences in gas exchange coefficients (k_{CH4}) and non-Fickian fluxes will introduce error to conventional cross-system flux comparisons (see Supplementary Note S4.3 for extended coverage of this potential problem). Though oxic water methanogenesis contributed ~4% to Lac Cromwell's summertime GHG footprint, it is conceivable that this pathway could have greater relative importance in more nutrient-rich, productive ecosystems, and in hardwater environments where low to negative (i.e., net CO_2 uptake) CO_2 emissions are common (Finlay et al. 2010; Raymond et al. 2013; McDonald et al. 2013).

Within Lac Cromwell, it is interesting to note that oxic water methanogenesis contributed a significant component of whole-lake emissions, despite the fact that it is a small (0.1 km^2), relatively shallow (~3.5m mean depth) lake with an extensive

littoral area, and a CH_4-rich anoxic hypolimnion, all of which are typically major sources of CH_4. A corollary is that in large, deep lakes, and open ocean sites where surface waters are increasingly decoupled from benthic or littoral sources of CH_4, surface CH_4 concentrations should be mostly driven by pelagic methanogenesis and therefore a function of algal biomass and metabolism. In this regard, whereas chlorophyll *a* does not explain the large scale patterns in surface CH_4 across lakes in general (Rasilo et al. 2015), the relationship we observed between surface water CH_4 and chlorophyll *a* in our isolated enclosures ($\log_{10}[CH_4] = 0.46\log_{10}[\text{chl } a] + 0.68$, $r = 0.68$, $n = 4$) generally agrees with observations specifically from large lakes, extending all the way to ultraoligotrophic open ocean regions (Fig. 4.4; $\log_{10}[CH_4] = 0.99\log_{10}[\text{chl } a] - 1.63$, $r^2 = 0.73$). This continuity suggests that algal-linked pelagic CH_4 production may explain much of the ambient CH_4 dynamics observed in large and deep aquatic ecosystems, regardless of the fact that different mechanisms have been identified as potentially important in marine (i.e., methylphosphonate or methanethiol catabolism; Karl et al. 2008; Damm et al. 2010; Beversdorf et al. 2010; Carini et al. 2014; del Valle and Karl 2014) versus freshwater (hydrogenotrophic or acetoclastic methanogenesis; Fig. 4.3; Grossart et al. 2011; Tang et al. 2014). There are clearly a number of potential sources of CH_4 in oxic pelagic waters, and though it remains unknown how each pathway differs in relative importance across these diverse aquatic environments, our results highlight a consistent relationship between open-water phytoplankton dynamics and the regulation of oxic pelagic CH_4.

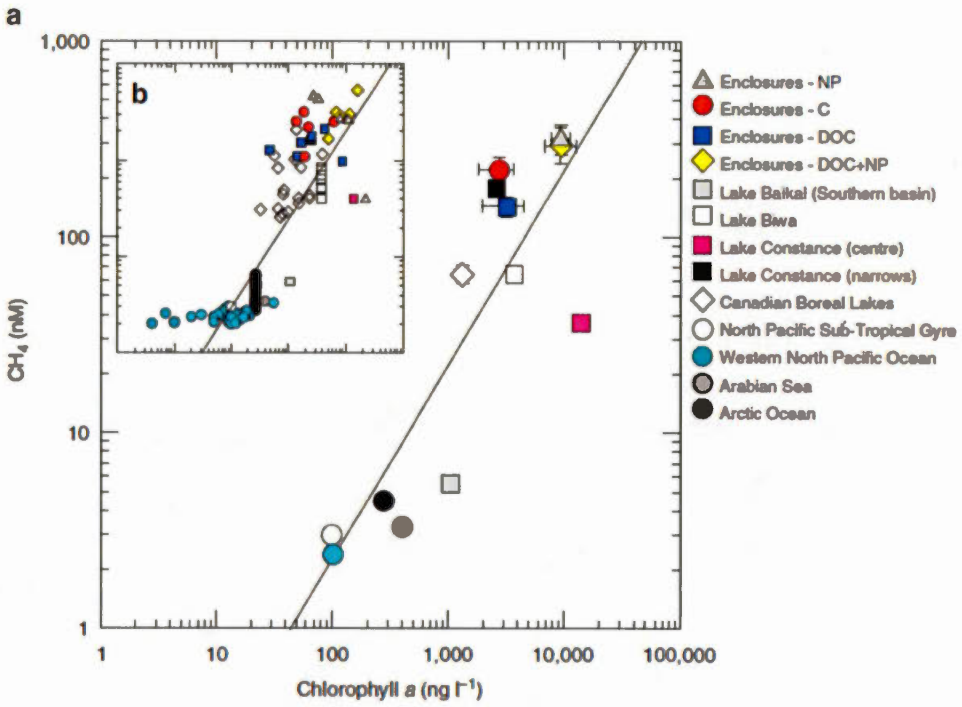

Figure 4.4. Linking dissolved CH_4 and algal biomass across diverse open-water aquatic ecosystems.

Here we combine experimental data from this study with literature-derived measurements from large (> 10 km^2), deep (> 10m maximum depth) lakes and marine environments where both CH_4 and chlorophyll *a* samples were simultaneously measured. A strong positive relationship between CH_4 and chlorophyll *a* exists across systems: (a) averaged data ($[\log_{10}x] = 0.993[\log_{10}y] - 1.630$, $r^2 = 0.73$, $p < 0.0001$), where error bars represent $\pm$1 s.e.m. (b) raw data ($[\log_{10}x] = 0.855[\log_{10}y] - 1.166$, $r^2 = 0.72$, $p < 0.0001$). Guidelines for meta-analysis are discussed in the Methods section, and raw data are available in Supplementary Table S4.3.

Taken together, our findings suggest that pelagic CH_4 production in oxic environments may be widespread, and likely supports a baseline evasion of CH_4 from all oxic water columns. In small and shallow ecosystems, such as Lac Cromwell, this pathway will be quantitatively significant but secondary relative to anoxic littoral and benthic sources. In large and deep aquatic environments, however, this pathway could become the single dominant source fueling CH_4 supersaturation and fluxes to the atmosphere. It should be emphasized that consideration of oxic water column methanogenesis does not necessarily lead to higher flux estimates for lakes, since the CH_4 derived from this process is already included in routine measurements of surface water pCH_4 and CH_4 surface fluxes (Rudd and Hamilton 1978; Michmerhuizen et al. 1996; Bastviken et al. 2004, 2008, 2011; Ortiz-Llorente and Alvarez-Cobelas 2012; Kirschke et al. 2013; Prairie and del Giorgio 2013). Incorporating the origin of the CH_4 that outfluxes to the atmosphere from these lakes, however, is critical to our understanding of the regulation of these fluxes and our capacity to predict their future change. In this regard, there are potentially large global implications for algal-driven oxic-water methanogenesis. CH_4 emissions from surface waters, particularly from freshwaters (Michmerhuizen et al. 1996; Bastviken et al. 2011; Kirschke et al. 2013), are a major element of the global atmospheric CH_4 budget, and we suggest here that the algal-mediated baseline flux is not only a major contributor to these overall aquatic CH_4 emissions, but one that is also particularly sensitive to environmental change. As such, widespread and intensifying human- and climate-driven changes in pelagic nutrient availability (Carpenter et al. 1998a; Schindler 2006; Moss 2012),

terrestrial DOC inputs (Schindler et al. 1997; Monteith et al. 2007), and physical structure of the water column (Schindler et al. 1997; Schindler 2006; Moss 2012), which strongly shape aquatic algal dynamics (Jones 1992; Schindler et al. 1997; Carpenter et al. 1998b; Schindler 2006; Taranu et al. 2012), may have major, but previously unconsidered consequences for oxic water methanogenesis and aquatic CH_4 emissions.

4.5 METHODS

4.5.1 Study site

Lac Cromwell is located at the Station de Biologie des Laurentides, a field research facility of the Université de Montréal. The lake turns over in spring and fall, is relatively shallow and small (mean depth = 3.5m, max depth = 9.5m, surface area of 0.11 km^2, volume of 3 x 10^5 m^3), and is oligo-mesotrophic, with little phytoplankton biomass (~6.0 μg chl *a* L^{-1}; Den Heyer and Kalff 1998).

4.5.2 Experimental design

Here, twelve, 1m diameter, 6m deep, 4712-L polyethylene enclosures were attached to floating wooden frames anchored in the middle of the lake (~8m depth). On June 5th, 2012, bags were filled by pumping epilimnetic water sequentially across two mesh screens of 110 and 45 μm to remove zooplankton, and three mesocosms each received N+P, DOC, N+P+DOC additions, or no addition (control). Both KH_2PO_4 and $NaNO_3$ additions were made to reach target concentrations of 50 and 700 μg P and N L^{-1}, respectively. For DOC, Superhume brand humic slurry was added to reach a target concentration of 15 mg DOC L^{-1}. For a full review of Superhume properties and applicability to freshwater experimentation, see Lennon et al. (2013). The mesocosms were allowed to stabilize for 1 week before initial sampling and re-stocking zooplankton at ambient lake concentrations. Zooplankton

were collected from Lac Cromwell by vertical tows using a 54-μm Nitex net, and immediately released into mesocosms after each haul.

4.5.3 Limnological measurements

All limnological samples were gathered at ~12pm on days 0, 7, and 28 of the experiment (June 13th, 19th, and July 10th , 2012, respectively; Supplementary Fig. S4.3). Dissolved oxygen (DO) and temperature were measured at 0.5m depth in all bags, while water column profiles were taken from one enclosure per treatment using a YSI combination probe (Supplementary Fig. S4.1). On all 3 dates, water was collected at 0.5m depth, filtered to 0.45μm, and chlorophyll *a* was measured spectrophotometrically in ethanol filter extracts. Dissolved CH_4 concentrations at 25cm depth were measured in triplicate for each mesocosm following Prairie and del Giorgio (2013). Partial pressures were converted to concentrations using Henry's constant corrected for temperature. On day 7, dark incubations to estimate MOX using unfiltered surface water were conducted in the lab at room temperature, lasting 96h (Supplementary Fig. S4.4). Incubations began at ~ noon on June 9th, day 6 of the experiment; samples for measurement of CH_4 oxidation (MOX) were collected from one mesocosm per treatment, at 25 cm depth, into 12 ml precombusted vials. Samples were capped to exclude any air with a gastight, 3mm-thick, butyl rubber lined plastic cap, then incubated in the dark at 20°C. Ambient CH_4 measured in the mesocosms was used as a time 0 concentration, and samples were subsequently killed

every 24hr by injection of $HgCl_2$, and stored at 4°C in the dark until analysis. Upon analysis, 5 ml of water was displaced with ambient air, and the remaining sample was equilibrated with the air by physically shaking the vials. Headspace equilibration and gas chromatography analysis were performed as for ambient CH_4. Respiration rates were determined by dark, *in-situ*, 24hr incubations on experiment days 6 and 7 in all enclosures, using unfiltered water in 4-L cubitainers. Initial and final samples of DO were collected and measured by membrane inlet mass spectrometry (Bouvier and del Giorgio 2002).

4.5.4 CH_4 chamber flux estimates

Air-water CH_4 fluxes in the mesocosms and the surrounding lake were calculated by combining the measured surface water pCH_4 and the CH_4 gas exchange coefficient (k_{CH4}), the latter derived from the measured gas exchange coefficient for CO_2 (k_{CO2}) in mesocosms supersaturated in CO_2. k_{CO2} was measured in one mesocosm per treatment, 3-5 times daily during days 6-7 and 27-28 of the experiment, using the floating chamber method following Vachon et al. (2010). Briefly, chambers were connected via a closed loop system to an EGM-4 infrared gas monitor (PP Systems, Boston, MA). Fluxes were calculated as the rate of change of chamber pCO_2 min^{-1} during a 15 minute interval. Diel sampling periods were spaced to obtain flux estimates from the morning, afternoon and nighttime periods, and mean values were used for daily flux estimates. Dissolved CO_2 samples were taken prior to all chamber measurements using the same headspace technique as for CH_4, but with

direct injection of the equilibrated gas into the EGM-4 in the field. The gas exchange coefficient for CH_4 was then calculated from k_{CO2} using equation (4.1), following Jahne et al. (1987):

$$k_{CH4} = k_{CO2} * (Sc_{CH4} * Sc_{CO2}^{-1})^{-2/3} \qquad (4.1)$$

where Sc is the Schmidt number of CO_2 and CH_4, respectively (Wanninkhof 1992). To calculate CH_4 fluxes, we used these average k_{CH4} values, the measured pCH_4, and the temperature dependent solubility of the gas following equation (4.2):

$$F = k_{gas} * K_h * \Delta_{gas} \qquad (4.2)$$

where F is flux of CH_4 (mmol m^{-2} d^{-1}), K_h is the temperature-corrected Henry's constant, and Δ_{gas} is the difference in partial pressures between the air and the water partial pressures of CH_4. We assumed an atmospheric partial pressure of CH_4 of 1.75 ppm.

4.5.5 Isotopic analyses

Isotope compositions are reported in delta notation following equation (4.3):

$$\delta^{13}C \text{ or } \delta^{18}O = ((R_{sample} / R_{standard}) - 1) * 1000 \qquad (4.3)$$

where R is the ratio of heavy to light isotope, $\delta^{13}C$ represents $\delta^{13}C$-CH_4 or $\delta^{13}C$-DIC, $\delta^{18}O$ represents $\delta^{18}O$-O_2 or $\delta^{18}O$-H_2O , and $R_{standard}$ is the $\delta^{13}C$ or $\delta^{18}O$ signature of Vienna Pee Dee Belemnite (VPDB) or standard mean ocean water (SMOW), respectively. All samples were taken at ~25 cm depth. Samples for $\delta^{18}O$-O_2 and $\delta^{13}C$-CH_4 were stored in 12-ml precombusted borosilicate vials, preserved with

$HgCl_2$, and air-free samples capped with a gastight rubber lined plastic cap. $\delta^{18}O\text{-}O_2$ samples were analyzed at the University of Ottawa Stable Isotopes Laboratory, and $\delta^{13}C\text{-}CH_4$ samples were measured at the University of Waterloo, both using standard laboratory methods. A single sample for $\delta O^{18}\text{-}H_2O$ was collected from the lake prior to filling enclosures, analyzed with a Picarro L230i isotopic water analyzer, and assumed representative for all enclosures for the duration of the experiment. $\delta^{13}C$-DIC samples were collected in acid-washed, 40ml vials with both Teflon and rubber-lined gas-tight plastic caps, and measured at the Colorado Plateau Stable Isotopes Laboratory using standard methods. Day 7 respiration (R), $\delta^{18}O\text{-}O_2$, and $\delta^{18}O\text{-}H_2O$ were used to estimate GPP and NEP following Quiñones-Rivera et al. (2009).

4.5.6 Numerical methods

We used repeated measures analysis of variance (RM-ANOVA) to compare the effects of treatments, and treatment by time interactions, on ambient CH_4. One-way ANOVA was used to assess differences between treatments for grouped data, and $\log_{10}(x+1)$ transformations applied to maintain the homogeneity of variances, followed by Bonferroni post-hoc pairwise comparisons of treatment means. All regression analyses were performed using Sigmaplot v. 12, and ANOVAs were computed with SPSS v. 16. We used ordinary least squares regression to quantify the link between GPP or NEP and CH_4 evasion. To estimate rates of MOX, the loss of CH_4 through time was fitted with a polynomial function, the derivative was taken,

and the slope at time 0 was calculated (Supplementary Fig. S4.4). This approach was deemed more accurate in quantifying the slope at time 0, since traditional methods, such as log transformations followed by visual selection of the linear portion of the dataset (Utsumi et al. 1998), can introduce large errors in the slope of the regression line when deciding which points to fit and which to exclude. Though MOX was estimated only once, our estimates are within the range of pelagic MOX (0.170 – 0.250 mmol m^{-3} d^{-1}) previously reported (Utsumi et al. 1998; Bastviken et al. 2002, 2008), particularly for boreal lakes of similar trophic condition (Bastviken et al. 2002).

4.5.7 Apparent isotopic fractionation of methanogenesis

We estimated the apparent fractionation factor (α_{app}) during methanogenesis following Conrad (2005). The apparent fractionation factor is defined using equation (4.4) as

$$\alpha_{app} = (\delta^{13}C\text{-}CO_2 + 10^3) / (\delta^{13}C\text{-}CH_{4source} + 10^3) \qquad (4.4)$$

where $\delta^{13}C\text{-}CH_{4source}$ is the isotopic signature of source CH_4, and $\delta^{13}C\text{-}CO_2$ was calculated from measured δ^{13}C-DIC following Stumm and Morgan (1996), using fractionation factors from Mook et al. (1974). Since we measured ambient δ^{13}C-CH_4 ($\delta^{13}C\text{-}CH_{4ambient}$), we estimated $\delta^{13}C\text{-}CH_{4source}$ by correcting for the isotopic fractionation effects of MOX and evasion to the atmosphere using an open-system, steady state model for isotope fractionation (Fry 2006), as defined in equation (4.5):

$$\delta^{13}C\text{-}CH_{4source} = f(\delta^{13}C\text{-}CH_{4ambient} - \Delta_{evasion}) + (1\text{-}f)(\delta^{13}C\text{-}CH_{4ambient} - \Delta_{MOX}) \quad (4.5)$$

where f and $1\text{-}f$ are the fractions of CH_4 loss, standardized to daily rates for the entire enclosure, estimated respectively as evasion and MOX rates divided by the sum of each. Δ is the isotopic effect of each loss pathway. In cases such as ours where $\Delta <$ 100‰, Δ can be approximated using equation (4.6):

$$\Delta = (1 - \alpha)10^3 \qquad (4.6)$$

where α is the fractionation factor of a given reaction. Literature derived values of α were used for both loss pathways. For evasion, an α value of 0.9992 was used (Knox et al. 1992), and for MOX, the range reported by Bastviken et al. (2002; i.e., 0.9816 to 0.9792) was used.

To better constrain the potential range of α_{app} estimated on day 7 of our experiment, we performed a scenario analysis by varying combinations of MOX rates and isotopic fractionation values, to determine the sensitivity of our estimates of α_{app} to potential variability in MOX. For this analysis, we chose two very conservative, extreme (for oxic pelagic freshwaters) values in MOX rates (0 and 0.05 mmol m^{-3} h^{-1}) and paired each rate with both minimum and maximum values reported for isotopic fractionation during MOX (Bastviken et al. 2002; 18.4 and 20.8‰). Because the MOX rate of zero did not have associated isotopic fractionation, we calculated 3 different combinations of extreme parameters; no oxidation with no fractionation, high oxidation with low fractionation, and high oxidation rates with high associated fractionation. We then took the maximum and minimum estimates of α_{app}, based on

this analysis, as upper and lower bounds for α_{app} estimated using our actual measurements of MOX.

4.5.8 Mesocosm mass balances

To quantify methanogenesis in the oxic mixed layer of ambient enclosures, mass balances from the ambient control treatment enclosures were constructed (Supplementary Table S4.2) for comparison with other lake based CH_4 fluxes using equation (4.7):

$$CH_{4gross} = \Delta_{CH4} + E + O - M \qquad (4.7)$$

Here, rates of methanogenesis (CH_{4gross}) are estimated by summing the rate of change in storage (Δ_{CH4}), defined as the rate of increase in the ambient CH_4 pool, with the rates of CH_4 evasion (E) and oxidation (O), minus the horizontal influx of external CH_4 via diffusion across the walls of the enclosures (M; detailed in the Supplementary Methods). In all cases, mass balance terms were first standardized to the entire mixed layer or surface of the enclosure (as mmol enclosure^{-1} day^{-1}) in order to combine aerial (E and M) and volumetric (Δ_{CH4} and O) processes on each sampling date.

The enclosure mixed layer average depth of 1.68m (Supplementary Fig. S4.1) was used to calculate both mixed layer volume, and the surface area of the enclosure wall that contributed to CH_4 influx from the surrounding lake environment. The change in storage (Δ_{CH4}) was calculated as the rate of change in ambient CH_4

concentrations in each bag as a function of time using the slope of the regression line as determined by least-squares regression analysis, then averaged and adjusted volumetrically to the enclosure scale (mmol enclosure^{-1} d^{-1}; Supplementary Table S4.2). The rate of MOX (*O*) for day 7 of the experiment was used for all calculations. Finally, estimates of CH_{4gross} were converted to units of mmol m^{-3} d^{-1} for comparison with other lake based measurements (Table 4.1).

4.5.9 Whole-Lake CH_4 dynamics

Enclosure measurements and mass balance results were compared with the surrounding Lac Cromwell environment. To quantify summertime rates of ebullition in Lac Cromwell (Table 4.1), bubble traps were fixed at five permanent sampling sites along a transect from the littoral to pelagic at ~1, 2, 3, 5, and 7m depths. Bubble traps were left in place over the entire sampling period and collected monthly in June, July and August 2012. Traps consisted of an inverted funnel (63.5cm diameter) suspended at 0.5m below the surface of the water (0.25m at the shallowest sample site). A graduated 1-L glass bottle was attached to the funnel by gluing the sides of the bottle cap to the neck of the funnel to make a gas tight seal. The bottles were covered with aluminum foil to prevent overheating or light exposure of the collected gas. Bottles were filled with water upon deployment, so the gas accumulated by displacing water in the bottle. Bottles were collected once a month or until a volume greater than 250 ml of gas was detected. All gas was carefully removed by displacement with ambient water using a stopcock cap fitted with 2 syringes. A

subset of the gas was injected in 30 ml saline vials, and analyzed upon return to the laboratory by gas chromatographic analysis as detailed for enclosure samples. Since the majority of samples sat in the bottles for up to a month before collection, we assumed that the composition of CH_4 in bubbles was 0.6 atm, or 60%, based on a subset of samples analyzed that were collected within days of sedimentary release. This assumption is consistent with literature estimates of bubble CH_4 concentration (Bastviken et al. 2008).

Diffusive evasion of lake CH_4 was estimated by first measuring concentrations of CH_4 on a monthly basis near each bubble trap site along the transect. Concentrations ranged between 0.63 – 2.09 with an average of 1.21 μM, and did not vary across sites (ANOVA, $p = 0.98$, $F = 0.10$). As detailed above for the enclosure mass balance, atmospheric fluxes were estimated by applying the average 24hr gas exchange coefficient measured at 7m depth along the transect (mean k_{CH4} = 0.65 m day^{-1}, Supplementary Fig. S4.2).

Whole lake CH_4 and CO_2 diffusive fluxes were calculated by applying average areal estimates of diffusion to the entire lake surface area (102,000 m^2). Since ebullition was only detected at depths < 3m, average rates of ebullition (0.31 + 0.66 mmol m^{-2} d^{-1}) were applied to the lake surface < 3m in depth (49,166 m^2). This area was estimated by determining the area of the lake <3m in depth from a hypsographic curve for Lac Cromwell (Livingstone and Imboden 1996), and existing bathymetric information for Lac Cromwell (Carignan 2010).

4.5.10 Data compilation for meta-analysis

To assess the relationship between algal dynamics and CH_4 in open water environments, we compared the results from our experimental enclosures with directly obtained results from large (> 10 km^2), deep (> 10 m maximum depth) boreal lakes[46] and other freshwater and marine data from the literature (raw data and selection methods tabulated in Supplementary Table S4.3). Literature data includes only studies where CH_4 and chlorophyll *a* were measured simultaneously, except for Lake Baikal, where detailed studies of CH_4 and chl *a* were made independently, but overlapped temporally and thus were included. To remain consistent with the sampling approach from our study, and sampling of boreal lakes, only near-surface, open-water results from the center of the lake or furthest from the coastal environment (in marine studies) were used. Summertime results were taken if seasonal data were presented. If surface water results were given as a range, the midpoint of that range was chosen. If multiple samples were taken at one site, then results were averaged.

4.6 CONCLUDING NOTES

4.6.1 Acknowledgements

Simon Gauthier-Fautaux, Juan Pablo Nino Garcia, Cynthia Soued, Marilyne Robidoux, and Ryan Hutchins provided field and laboratory assistance. Jean-Francois Lapierre, Dominic Vachon, Adam Heathcote, and David Bastviken provided conceptual and methodological advice. Annick St. Pierre, Alice Parks and the employees of the Station de biologie des Laurentides de l'Université de Montréal provided logistical support. Terhi Rasilo and Tonya Del Sontro revised an early version of the manuscript. M.J.B. was supported by a doctoral scholarship from the National Science and Engineering Research Council of Canada (NSERC). This project is part of the program of the NSERC / HQ Industrial Research Chair in Carbon Biogeochemistry in Boreal Aquatic Systems (CarBBAS), and was co-funded by grants from NSERC (to P.A.d.G. and A.D.) Hydro-Québec (to P.A.d.G.), and a Fonds de recherche Québec – Nature et technologie award from the government of Québec (to A.D.).

4.6.2 Author contributions

M.J.B, P.A.d.G., and A.D. designed the study; M.J.B., L.B., M.C.G.C., and A.M. performed field and lab work; M.J.B. and Y.T.P. analyzed the data; M.J.B. and P.A.d.G. wrote the paper; all authors revised the paper; A.D. and P.A.d.G. contributed materials.

4.6.3 Competing Financial Interests

The authors declare no competing financial interests.

4.7 SUPPLEMENTARY INFORMATION

4.7.1 Supplementary Figures

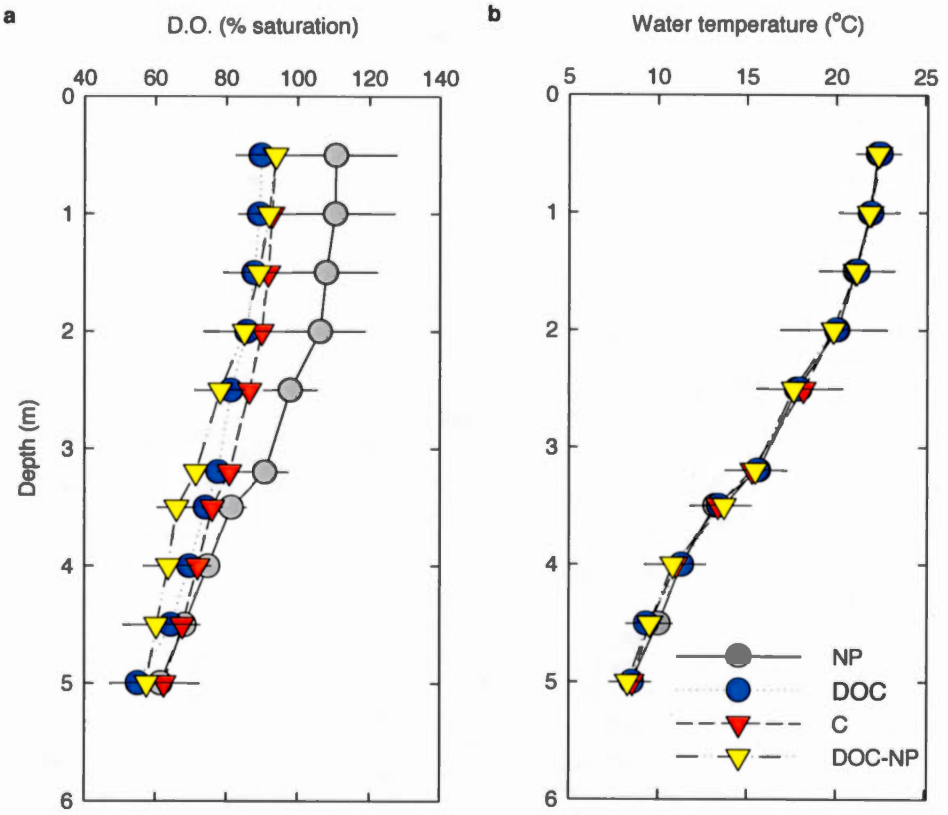

Figure S4.1. Mesocosm water-column profiles.

(**a**) dissolved oxygen (D.O.) saturation and (**b**) temperature were measured in one experimental enclosure per treatment and are averaged here for days 0, 7, and 28 (n = 3, error bars = $\pm$ 1 s.d.). Mean ($\pm$ 1 s.d.) mixed layer depth for the entire experimental duration was calculated from temperature profiles to be 1.68 $\pm$ 0.3m,

and this mixed layer depth value was applied to all enclosure-level volumetric calculations.

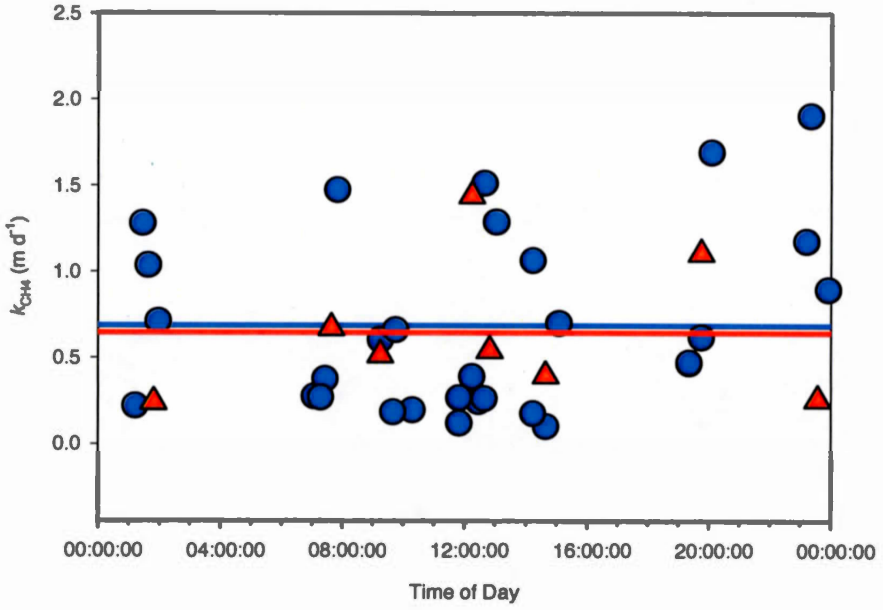

Figure S4.2. Daily atmospheric gas-exchange dynamics for the mesocosms and the lake.

Estimated CH_4 exchange coefficients (k_{CH4}) were derived from the measured k_{CO2}, as a function of time for experimental enclosures (blue circles) and for the lake (red triangles). Horizontal lines indicate mean daily values of k_{CH4}, plotted in blue and red for the enclosures and the lake, respectively (mean $\pm$ 1s.d. = 0.69 $\pm$ 0.52 and 0.65 $\pm$ 0.42 m d^{-1}, respectively).

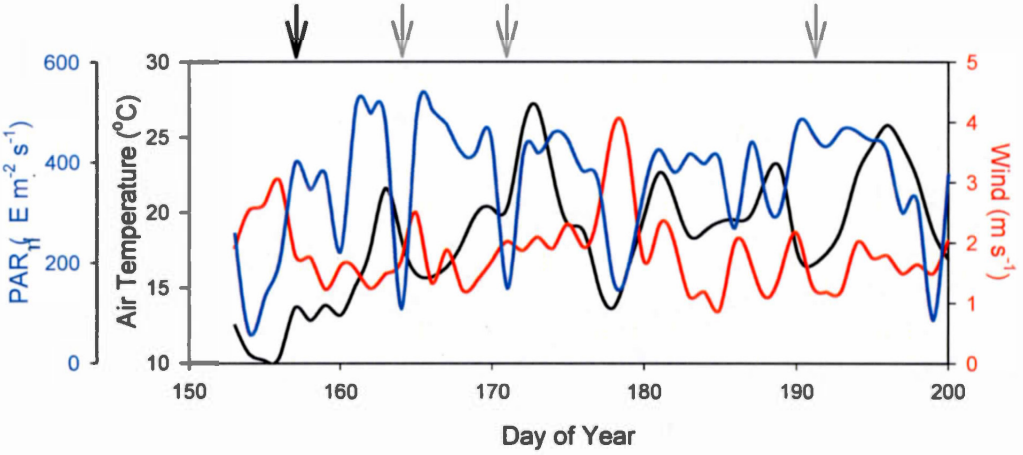

Figure S4.3. Daily average weather patterns recorded at the field station near Lac Cromwell.

Data include average wind speed (red line), average air temperature (black line) and photosynthetically active radiation (PAR, blue line). The black arrow indicates the enclosure filling date and chemical additions on June 5th, 2012 (DOY 157). Grey arrows show limnological sampling periods at noon on June 13th, June 19th, and July 10th (DOY 164, 171, 192). Note that diel gas flux estimates began at midday on the days preceding sampling. Average meteorological conditions (± 1 s.d.) are, for air temperature, PAR, and wind speed respectively; 19.1 ± 3.5 °C, 378 ± 107 μE m^{-2} s^{-1}, and 1.8 ± 0.6 m s^{-1}.

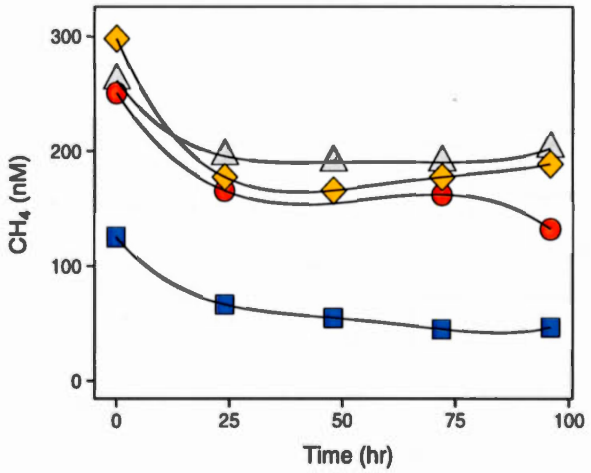

Figure S4.4. Mesocosm methane oxidation (MOX) dynamics.

Rates of MOX were quantified at day 7 of the experiment, as detailed below, from a dark incubation of vials in the lab at near ambient lake temperatures. One incubation series was run per treatment, and a polynomial was fit to the time series; control (red circles): $y= -0.0007x^3 + 0.1129x^2 - 5.86x + 250.49$, $r^2=1$, DOC (blue squares): $y = -0.0002x^3 + 0.0457x^2 - 3.254x + 124.64$, $r = 0.99$), DOC-NP (gold triangles): $y = -0.0007x^3 + 0.1306x^2 - 7.5998x + 297.41$, $r = 0.1$, NP (gray triangles): $y = -0.0003x^3 + 0.0622x^2 - 3.8812x + 260.38$, $r = 0.99$.

4.7.2 Supplementary Tables

Table S4.1. Estimates of zooplankton CH_4 release in ambient enclosures.

Estimates of zooplankton CH_4 release from the control enclosures using min- and maximum of individual emission rates (4 and 20 nmol CH_4 individual^{-1} d^{-1}) presented in De Angelis and Lee (1994), combined with our empirical determinations of zooplankton biomass in the enclosures.

Day	Zooplankton biovolume (ind. m^{-3})	Std. Error (ind. m^{-3})	Minimum zooplankton CH_4 release (nmol m^{-3} d^{-1})	Maximum zooplankton CH_4 release (nmol m^{-3} d^{-1})
Calanoids				
0	70	0.1	0.2	1.4
7	257	0.4	0.8	5.1
28	237	0.4	0.7	4.7
Cladocerans				
0	119	0.4	0.4	2.4
7	496	0.6	1.5	9.9
28	514	0.1	1.5	10.3
Cyclopoids				
0	200	0.1	0.6	4.0
7	247	0.0	0.7	4.9
28	214	1.0	0.6	4.3

Day	Summed-min	Summed-max
0	1.2	7.8
7	3.0	20.0
28	2.9	19.3

Table S4.2. Mass balance estimates of methanogenesis in ambient enclosures.

All terms in units of mmol enclosure^{-1} d^{-1}. One sample for CH_4 oxidation was analyzed so s.d. was not calculated.

	Symbol	mean	± 1 s.d.
Membrane Influx	M	0.0021	0.0001
Atmospheric Evasion	E	0.12	0.02
Oxidation	O	0.19	n.a.
Change in storage	ΔCH_4	0.0016	0.0061
Gross methanogenesis	CH_{4gross}	0.30	0.02

Table S4.3. Raw data and assembly methods for open-water CH_4 and chlorophyll *a* (chl *a*) meta-analysis.

note	site/treatment	(chl *a* - ng/L)				(CH_4 - nM)			
		range	conc.	mean or midpt.	s.e.m.	reported range	conc.	mean or midpt.	s.e.m.
[1]	C-mesocosms		1381	2730	913		250	222.1	33.8
[1]	C-mesocosms		1841				314		
[1]	C-mesocosms		1841				108		
[1]	C-mesocosms		2245				221		
[1]	C-mesocosms		6343				247		
[1]	DOC-mesocosms		460	3214	1236		125	144.3	16.9
[1]	DOC-mesocosms		1475				109		
[1]	DOC-mesocosms		1704				149		
[1]	DOC-mesocosms		2600				178		
[1]	DOC-mesocosms		4211				206		
[1]	DOC-mesocosms		8834				99		
[1]	DOCNP-mesocosms		5046	9466	1722		164	317.8	54.1
[1]	DOCNP-mesocosms		6768				315		
[1]	DOCNP-mesocosms		8430				282		
[1]	DOCNP-mesocosms		11303				298		
[1]	DOCNP-mesocosms		15783				530		
[1]	NP-mesocosms		2761	9321	2797		456	310.7	64.0
[1]	NP-mesocosms		3375				493		
[1]	NP-mesocosms		8130				261		
[1]	NP-mesocosms		10511				266		
[1]	NP-mesocosms		11322				286		
[1]	NP-mesocosms		19826				103		
[2]	Lac Nord-Est		729	1325	119		26	64.7	6.4
[2]	Lac Buad		2365				40		
[2]	Lac Buad		997				29		
[2]	Lac David		3955				116		
[2]	Lac Pentecôte		575				111		
[2]	Lac Grand Caotibi		844				49		
[2]	Lac Iron Arm		326				31		
[2]	Lac Lamotte		1678				84		
[2]	Lac Walker		818				44		
[2]	Réservoir SM2		1381				207		
[2]	Lac Kénogami		2378				43		
[2]	Lac Kénogami		1294				102		
[2]	Lac Astrey		665				83		
[2]	Réservoir Menehek		671				31		
[2]	Lac Albanel		1510				40		
[2]	Lac Albanel		1534				36		
[2]	Lac Mistassini		805				28		

[3] Lake Biwa	2200-5500		3800			52	63.8	5.34
[3] Lake Biwa						70		
[3] Lake Biwa						40		
[3] Lake Biwa						64		
[3] Lake Biwa						70		
[3] Lake Biwa						51		
[3] Lake Biwa						78		
[3] Lake Biwa						85		
[4] L. Constance (cent.)	10000-18000		14000			40	40.0	
[4] L. Constance (narrows)		2500	2500			168	168	
[5] L. Baikal (S. Basin)							5.5	
[6] L. Baikal (S. Basin)			1070					
[7] NW Pacific Ocean		560	100.3	15.4		3.3	2.4	0.05
[7] NW Pacific Ocean		210				2.4		
[7] NW Pacific Ocean		180				2.6		
[7] NW Pacific Ocean		100				2.3		
[7] NW Pacific Ocean		180				2.4		
[7] NW Pacific Ocean		160				2.4		
[7] NW Pacific Ocean		120				2.3		
[7] NW Pacific Ocean		130				2.5		
[7] NW Pacific Ocean		70				2.4		
[7] NW Pacific Ocean		50				2.4		
[7] NW Pacific Ocean		20				2.4		
[7] NW Pacific Ocean		30				2.5		
[7] NW Pacific Ocean		80				2.5		
[7] NW Pacific Ocean		70				2.5		
[7] NW Pacific Ocean		90				2.1		
[7] NW Pacific Ocean		90				2.8		
[7] NW Pacific Ocean		120				2.5		
[7] NW Pacific Ocean		70				2.4		
[7] NW Pacific Ocean		180				2.7		
[7] NW Pacific Ocean		140				2.2		
[7] NW Pacific Ocean		100				2.0		
[7] NW Pacific Ocean		100				2.0		
[7] NW Pacific Ocean		70				2.7		
[7] NW Pacific Ocean		80				2.6		
[7] NW Pacific Ocean		60				2.5		
[7] NW Pacific Ocean		50				2.3		
[7] NW Pacific Ocean		50				2.1		
[7] NW Pacific Ocean		90				2.6		
[7] NW Pacific Ocean		100				2.4		
[7] NW Pacific Ocean		80				2.9		
[7] NW Pacific Ocean		90				3.0		
[7] NW Pacific Ocean		190				2.7		
[7] NW Pacific Ocean		170				2.3		
[7] NW Pacific Ocean		0				2.2		
[7] NW Pacific Ocean		4				2.0		
[7] NW Pacific Ocean		7				2.6		
[7] NW Pacific Ocean		10				2.1		
[7] NW Pacific Ocean		10				2.1		
[7] NW Pacific Ocean		120				2.0		

[8] N Pacific Sub Trop. Gyre	50-150		100		2-4	3.0	3	
[9] Arctic Ocean	60-480	270	270			2.9	4.3	0.20
[9] Arctic Ocean						4.3		
[9] Arctic Ocean						4.1		
[9] Arctic Ocean						3.6		
[9] Arctic Ocean						3.5		
[9] Arctic Ocean						3.3		
[9] Arctic Ocean						3.3		
[9] Arctic Ocean						3.1		
[9] Arctic Ocean						2.8		
[9] Arctic Ocean						2.8		
[9] Arctic Ocean						3.5		
[9] Arctic Ocean						3.5		
[9] Arctic Ocean						3.1		
[9] Arctic Ocean						3.1		
[9] Arctic Ocean						3.2		
[9] Arctic Ocean						3.6		
[9] Arctic Ocean						3.3		
[9] Arctic Ocean						3.1		
[9] Arctic Ocean						3.3		
[9] Arctic Ocean						3.6		
[9] Arctic Ocean						4.1		
[9] Arctic Ocean						4.6		
[9] Arctic Ocean						4.6		
[9] Arctic Ocean						4.8		
[9] Arctic Ocean						4.9		
[9] Arctic Ocean						5.0		
[9] Arctic Ocean						5.3		
[9] Arctic Ocean						5.1		
[9] Arctic Ocean						5.4		
[9] Arctic Ocean						5.1		
[9] Arctic Ocean						5.4		
[9] Arctic Ocean						6.3		
[9] Arctic Ocean						6.4		
[9] Arctic Ocean						6.6		
[9] Arctic Ocean						6.0		
[9] Arctic Ocean						5.9		
[9] Arctic Ocean						5.8		
[9] Arctic Ocean						6.5		
[10] Arabian Sea			400				3.3	

[1]measured in present study

[2]Rasilo et al. (2015): Surface measurements reported for CH_4 and chl *a*

[3]Miyajiima et al. (1997): range of chl a from text; digitized surface CH_4 values from figure 2

[4]Schulz et al. (2001): Central data; midpoint of summertime chl a range in text, central summertime CH_4 surface values from figure 2; Narrows data; digitized surface values from figure 7

[5]Schmid et al (2007): Digitized summer median surface value from figure 2a

[6]Fietz et al. (2005): Average chl a value reported in text

[7]Watanabe et al (1995): Surface measurements of CH_4 and chl a reported in appendix

[8]Karl et al. (2008): ranges of CH_4 and chl a reported in table 1.

[9]Damm et al. (2010): chl a range reported in text; CH_4 data digitized from figure 3.

[10]Owens et al. (1991): surface measurements of CH_4 and chl a digitized from figure 3, stn. 9.

4.7.3 Supplementary Notes

Note S4.1. Assessing the robustness of chamber flux and k_{600} estimates.

In some cases, chamber measurements can yield gas exchange coefficients greater than wind-based estimates (Vachon et al. 2010). However wind-based estimates may be less accurate in small ecosystems where gas transfer additionally depends on atmospheric heat exchange, rain, or surface-film dynamics, particularly in systems heavily sheltered by forests or topography (Vachon and Prairie 2013, and references therein), which is certainly the case for our mesocosms. To further validate our use of flux chamber k_{CH4} estimates, we compared chamber estimates of k_{CH4} to those we would have obtained based on wind speed following equation 5 of Cole and Caraco (1998). We used the average ($\pm$ 1 s.d.) wind speed of 1.8 ± 0.6 m s^{-1} recorded at the meteorological station near the lake, for the duration of the experiment (Supplementary Fig. S4.3), adjusted to a height of 10m following equation 5 of Vachon et al. (2010). These calculations yielded a wind-based estimate of $k_{CH4} = 0.69$ m d^{-1}, and a range of 0.63 – 0.78 m d^{-1} when the $\pm$ 1 s.d. wind speeds were used in our calculations. These estimates are very close to those obtained from the chambers (Supplementary Fig. S4.2; mean $\pm$ 1s.d. chamber-based $k_{CH4} = 0.69 \pm 0.52$). We therefore conclude that chamber-derived estimates for k_{CH4} provided reasonable estimates of CH_4 fluxes for both the enclosures and the lake.

Note S4.2. Quantification of potential CH_4 inputs from zooplankton.

Here we have estimated the potential contribution of zooplankton to the observed CH_4 concentrations in experimental enclosures (Supplementary Table S4.1). Our results are likely over-estimates, since we have applied the reported rates for copepod emissions per individual to all zooplankton present in the enclosures, despite the fact that not all zooplankton species have been found to emit CH_4 (De Angelis and Lee 1994). We calculated rates of zooplankton emissions in ambient enclosures, since we had already used this treatment to estimate methanogenesis in Lac Cromwell pelagic waters (Table 4.1) via a mass balance outlined in the Methods section. Gross methanogenesis in ambient enclosures was estimated to be 0.23 mmol m^{-3} d^{-1}, and our calculations zooplankton appear to contribute little (< 10%) to this production, despite the fact that we have likely overestimated zooplankton emission rates for CH_4.

Note S4.3. Extrapolation of our CH_4 emissions estimates to other systems.

Careful extrapolation of our absolute emissions rates should be taken for two reasons. 1) Differences in lake size, shape, and wind direction can complicate cross-system comparisons of gas flux for any given wind speed (Vachon and Prairie 2013). We use this reasoning to highlight the large differences between emissions from our ambient enclosures (mean 0.15, range = 0.07 – 0.22 mmol m^{-2} d^{-1}; Fig. 1b, Table 1) and those for open waters in oligotrophic Lake Stechlin, Germany (0.12 – 5 mmol m^{-2} d^{-1}), where it was shown most CH_4 emissions were derived from the oxic pelagic zone (Tang et al. 2014). Lake Stechlin has 40 times greater surface area than Lac Cromwell, so though it had comparable dissolved CH_4 concentrations (~0.4μM) and mean wind speed (~2 m s^{-1}), the wind generated much smaller fluxes from Cromwell than from Stechlin. 2) We calculated emissions using a Fickian diffusive flux model that does not account for the non-Fickian, micro-bubble mediated flux of CH_4 (Prairie and del Giorgio 2013). To put this into a general context, we used equation 5 of Prairie and del Giorgio (2013) to estimate the quantity of CH_4 that microbubble fluxes could have added an additional ~0.5 (range of 0.2-0.7) mM m^{-2} d^{-1} to our emissions estimates for ambient enclosures. Both points collectively show that more work is needed to refine our estimates of surface water CH_4 emissions in general (Prairie and del Giorgio 2013), not just from the oxic environment.

4.7.4 Supplementary Methods: Estimates of cross-membrane CH_4 flux.

The permeability of the mesocosm lining to gas influx from the surrounding CH_4-rich lake environment (Lac Cromwell surface CH_4 for May to August, inclusive; mean = 803, range = 451 – 1320 μatm) was assessed for the surface mixed layer in experimental enclosures and applied to the enclosure mass balance (Supplementary Table S4.2). To do this we first estimated membrane permeability to CH_4 in the laboratory by conducting a 15-day incubation experiment.

In the lab, we added 30ml of 99% CH_4 gas to a 4L Erlenmeyer flask filled with distilled deionized water, shook the bottle for 5min to ensure equilibration between the gas and water, then added the water to acid washed, 250ml glass Mason jars, covered them with pieces of the mesocosm wall material, and capped them (with the ring but not the seal) while submerged in the excess CH_4-saturated water to prevent air influx into the jars. In the end, the membrane material was the only barrier between the CH_4 enriched water and the outside environment. In parallel, to correct for chemical losses of CH_4 we incubated the same CH_4-rich water in gas tight, acid washed 250ml incubation bottles. To eliminate the presence of dissolved O_2 (DO) and prevent the oxidation of CH_4, we added an O_2-scavenging agent (Na_2SO_3) to the enriched water before filling of all jars. All containers were incubated underwater in an open aquarium that was continuously bubbled with ambient air to prevent the buildup of CH_4 following evasion from membrane-capped jars. Jars were sampled with the same headspace technique and GC analysis as for all other CH_4

samples (see Methods section for details). The daily change in partial pressure of CH_4 in sealed and membrane-covered jars was tracked for 15 days, and the loss rates were then used to calculate gas exchange patterns across the enclosure walls.

Before we could quantify enclosure CH_4 fluxes into the mesocosms from the lake, we estimated the gas exchange coefficient for the enclosure membrane material using the area and volume of containers, plus the net rate of CH_4 loss across the membrane, which is the rate from the membrane-covered jars ($\ln[pCH_4] = -0.0004$[incubation time] + 11.666, r^2 adj. = 0.45, $p = 0.0015$), minus the rate of loss due to chemical CH_4 oxidation in the sealed jars ($\ln[pCH_4] = -0.0020$[incubation time] + 11.087, r^2 adj. = 0.71, $p < 0.0001$). For the incubations, the change in CH_4 through time is given by equation (S4.1);

$$V * (dpCH_4 / dt) = -(k_{memb}) * A * (\Delta pCH_4) \qquad \text{(S4.1)}$$

where (k_{memb}) is the gas exchange coefficient for the enclosure membrane material, ($dpCH_4 / dt$) is the net daily rate of decline in pCH_4, A and V are the area of the mouth, and the volume of the membrane covered jar,respectively, and (ΔpCH_4) is the cross-membrane difference in pCH_4. Putting all terms in equation (1) containing pCH_4 on the left and time on the right, and integrating gives equation (S4.2);

$$\Delta pCH_{4t} = \Delta pCH_{4t0} * e^{\left(\frac{-k_{memb} * A}{V}\right) * t} \qquad \text{(S4.2)}$$

where $\left(\frac{-k_{memb} * A}{V}\right)$ corresponds to the log-linear net slope. Knowing the net slope, or rate of change (ΔpCH_{4t}), A, and V, we solved the equation for k_{memb}. At room temperature, $k_{memb} = 0.013$ m d^{-1}.

Since the lab and field experimental temperatures were similar, we applied this gas exchange coefficient for membrane material directly to the entire mixed layer of ambient mesocosms, and knowing the concentration gradient across the membrane, we quantified the rate of cross-membrane lake inputs to the bags and included this information in an enclosure mass balance of CH_4 (see Methods and Supplementary Table S4.2 for details).

GENERAL CONCLUSIONS

5.1 Key contributions

The overall aim of this thesis was to improve our mechanistic understanding of northern lake food web functioning and C cycling by investigating the rates and drivers of lake metabolism and metabolic connections to greenhouse gas (GHG) fluxes. We explored these connections through a combination of methodological approaches (i.e., *in-vitro* and mesocosm incubations, whole-lake assessments, high- and low-frequency metabolic analyses through space and time), generating a number of unique and exciting findings that should help fill a number of gaps in our understanding of northern lake functioning and C cycling.

First, using free-water metabolic measurements (chapters I, II), we showed that ecosystem level patterns and regulation of gross primary production (GPP) and respiration (R) can deviate widely from the community-scale patterns that form the basis of much of our understanding of northern lake functioning. Despite the oligo- to mesotrophic status of most lakes studied, rates of GPP and R measured here using the oxygen isotopic approach (chapters I, II) were comparable to those reported globally in lakes of much greater trophic status, far exceeding previous reports established using *in-vitro* incubation techniques. This observation was surprising, for GPP in particular, since it is commonly assumed that metabolic rates are severely restricted by the oligotrophic nature of, and reduced light availability (linked to

elevated terrestrial organic matter inputs) in many northern lakes (e.g., Jansson et al. 2003; Karlsson et al. 2009; Seekell et al. 2015). Instead, our rates of ecosystem GPP and R actually increased in darker, DOC-rich waters, and deviated widely from expectations based on metabolic theory and cellular-level responses to temperature gradients (Allen et al. 2005; Yvon-Durocher et al. 2010). These deviations point to the potential importance of cross-habitat feedbacks in shaping the rates and ecosystem-level regulation of lake metabolism. Although the role of habitat interactions in shaping northern lake metabolic patterns are currently poorly understood (Vasconcelos et al. 2016), our findings based on the oxygen isotopic approach (which integrate patterns across habitats and incorporate such effects) represent an important step toward better understanding northern lake metabolism and C cycling.

The second major contribution from this study was the observation that the coupling of lake net ecosystem production (NEP = GPP-R) and CO_2 dynamics can vary dramatically across lakes, with potentially major implications for landscape-level C budgets. Until recently, the vast majority of northern lakes were assumed to be net heterotrophic; in part because of extrapolations of pelagic community scale measurements (direct ecosystem NEP estimates were rare for northern lakes), but also because of the fact they are almost exclusively supersaturated in CO_2. By directly estimating NEP alongside CO_2 fluxes, our findings help to refine this assumption: The wide range in lake GPP:R and rates of NEP (chapters II and III) deviated from previous observations based on community-level assessments, and were more closely

in line with the range of ecosystem NEP found in global lake datasets (chapter II). Further, the observation of simultaneous CO_2 supersaturation and net autotrophic metabolism (GPP > R) in roughly a third of the sampled lakes (chapter III) sheds light on the underappreciated summertime C sink effect of many northern lake food webs. By demonstrating a wide range in coupling of NEP and CO_2 fluxes over such a large geographic scale, our results help to reconcile the contrasting results from previous studies conducted at the lake- or regional scale, which have shown that lake biota can be both major- and minor drivers of CO_2 emissions.

Third, chapters III and IV highlight the potentially diverse and underappreciated roles that anaerobic processes play in shaping both CO_2 and CH_4 fluxes in lakes: Multiple lines of evidence (chapter III) suggest that the widespread decoupling of CO_2 emissions from aerobic lake metabolism cannot always be sustained by catchment inputs alone, and that anaerobic CO_2 production may be more important to sustaining CO_2 emissions from lakes than previously thought (Chapter III). Anaerobic CO_2 contributions were potentially most important in hydrologically disconnected lakes with autotrophic NEP. At the same time, our experimental results suggest that anaerobic production of CH_4 in oxic surface waters, which also scaled positively with measurements of NEP, may be an important, but overlooked pathway driving lake CH_4 emissions, especially in larger, pelagically-dominated water bodies (Chapter IV). Taken together, these findings emphasize the importance of anaerobically-mediated GHG fluxes, which are often intricately linked to aerobic metabolic dynamics, but seldom considered.

Fourth, by sampling lakes at such a broad (~10^6 km^2) spatial scale, we were able to explore the landscape-level regulation of lake metabolism and its coupling to CO_2 dynamics. Previous reports have paired direct metabolic estimates with those of GHG flux at local (e.g., Vachon et al. 2014, 2016; Wilkinson et al. 2016), and global scales (e.g., Duarte and Prairie 2005), but few studies have explored how lake metabolic properties (and connections to GHG flux) vary as a function of intermediate, inter-regional scale environmental variability (Lapierre et al. 2015). In chapter II, we found that rates of biotic CO_2 cycling (i.e., NEP) vary among lakes across the landscape both as a function of ambient air and water temperature, but also through more complex interactions between climate (temperature and precipitation) and catchment structure (topography, vegetation, water cover and hydrology). At the same time, NEP displayed a wide range in coupling to actual rates of air-water CO_2 flux, indicating that although internal lake CO_2 production and consumption might shift across the landscape, this will not necessarily result in important changes in lake CO_2 emissions. Positive decoupling (where CO_2 flux > NEP) was prevalent in steeper, forested catchments with less standing water and shorter hydrologic residence, suggesting that sensitivity of NEP may be of less consequence to overall GHG dynamics in lakes found in these areas, but more important in flatter, water-rich regions with longer hydrologic residence.

Finally, the exploration of the strengths and limitations to assessing ecosystem metabolism from point sampled, ecosystem level oxygen dynamics (chapters I, III) represents an important methodological contribution that should help guide future

applications of the oxygen isotopic approach. Here, we have tested the technique in a number of settings (chapter I), and have placed the results into a broader context alongside those from other studies (chapters I, II, III). In most cases we found agreement between oxygen isotopic-, and other free-water metabolic results, suggesting that the approach yields very reasonable metabolic estimates. This work demonstrates that it is possible to incorporate ecosystem metabolic measurements to sampling programs with minimal additional effort. Hopefully, this will encourage further metabolic assessments of lakes in remote regions of the world for which aquatic metabolic data have been traditionally difficult to obtain.

5.2 Implications

The response of northern lake metabolism and food web functioning to simultaneously occurring environmental pressures is poorly defined, particularly with respect to simultaneous ecosystem warming, hydrologic shifts, and altered solute delivery (nutrients and DOC) (Kritzberg et al. 2014; Solomon et al. 2015; Rodriguez et al. 2016). Here, our findings agree with previous reports suggesting that autotrophic growth and food web autochthonous resource availability may actually increase in many lakes: Paleolimnological observations of increased organic carbon (OC) burial rates and autotrophic growth and productivity since A.D. ~ 1850 have been documented for northern lakes, which are hypothesized to be in part due to increased air temperatures and longer growing seasons, and increased deposition of reactive nitrogen (Michelutti et al. 2005; Holtgrieve et al. 2011; Heathcote et al.

2015; Summers et al. 2016). This trend generally agrees with our documented, positive relationship between rates of GPP and both temperature and N availability (chapter II), and suggests that food web rresource availability may increase into the future under the combination of increased warming and atmospheric deposition of reactive materials. At the same time, the observed positive relationship between rates of GPP and lake DOC content (chapter II) is consistent with recent whole-lake manipulations (Zwart et al. 2016) suggesting that increases in terrestrial OC delivery to lakes may additionally favor increased surface water GPP and OC production in many cases, particularly in lakes with presently low DOC concentrations (Prairie et al. 2002; Hanson et al. 2003; Seekell et al. 2015). Overall, heterogeneous changes in lake physico-chemical conditions across the landscape (e.g., Leavitt et al. 2009; Zhang et al. 2010; O'Rielly et al. 2015) make it difficult to predict how resource availability and functional responses of lake food webs might shift across northern regions in the future, yet our findings represent an important step toward disentangling this issue.

Although lake GHG emissions are an important component of regional and continental C budgets (Benoy et al. 2007; Tranvik et al. 2009; Butman et al. 2016), it is also unclear how future patterns and rates of GHG flux will respond to aforementioned shifts in lake physico-chemical characteristics. By exploring the controls of lake NEP (and hence net biotic CO_2 production or consumption) and its coupling to GHG dynamics, we provide mechanistic information to help resolve this issue: Boreal lake NEP varied widely among lakes, shifting toward elevated

(autotrophic) NEP across lakes as a function of water temperature, but negatively toward heterotrophy as a function of increasing DOC concentrations (chapter II). If these spatial patterns do indeed translate into expected future responses of individual lakes, then in many cases, where lakes experience both warming and browning (i.e., increased terrestrial OC concentrations) these drivers may offset one another and dampen any shifts in NEP and food web CO_2 cycling. Conversely, lakes predominantly experiencing one or the other major ecosystem change (warming or increased DOC loading) may show the greatest response in NEP and biotic CO_2 cycling. In all cases, any changes in NEP should be taken into context with other drivers of lake CO_2. Results from chapter III indicate that biotic coupling with air-water CO_2 flux can vary strongly along topographic and hydrologic gradients, which may in turn enhance, or diminish the effect of shifting NEP on the GHG budget of a given lake.

Finally the strong connection between lake autotrophic growth and GHG production (inferred for CO_2 flux in chapter III, and experimentally established for CH_4 in chapter IV) suggests that anaerobic processes may importantly alter the C sink strength of many lakes. If we do indeed observe shifts in northern lakes toward elevated GPP (as discussed above), our findings suggest concomitant increases in anaerobic GHG flux may occur, even in aerobic habitats. Anaerobic dynamics may have important implications for the C cycle of some lakes, and where elevated GPP supports net autotrophic NEP, anaerobic GHG production may play an important role

in restricting the C-sink capacity of lakes, but this hypothesis requires further testing to confirm.

In northern regions where the density of lakes is among the highest on the planet (Downing et al. 2006), freshwater ecosystems importantly shape the global C cycle through the production, mineralization, storage, and transformation of C (Cole et al. 2007; Battin et al. 2009; Tranvik et al. 2009). The paucity of direct, ecosystem level metabolic data for northern lakes has, however, limited our mechanistic understanding of northern lake C cycling. In this thesis, the use of the oxygen isotopic technique to assess lake metabolism in a number of different settings, alongside measurements of CO_2 and CH_4 dynamics, represents a novel contribution that helps to establish more accurate baseline information on food web functioning and C cycling in boreal lakes. Looking forward, this information should improve our understanding of how lakes function, and how they are responding to ongoing shifts in physico-chemical conditions linked to widespread (Brandt et al. 2013; Gauthier et al. 2015) environmental change.

REFERENCES

Algesten G, Sobek S, Bergstrom AK, et al (2004) Role of lakes for organic carbon cycling in the boreal zone. Glob Chang Biol 10:141–147.

Algesten G, Sobek S, Bergström AK, et al (2005) Contribution of sediment respiration to summer CO_2 emission from low productive boreal and subarctic lakes. Microb Ecol 50:529–535.

Allen AP, Gillooly JF, Brown JH (2005) Linking the global carbon cycle to individual metabolism. Funct Ecol 19:202–213.

Allen HL (1968) Acetate in fresh water: Natural substrate concentrations determined by dilution bioassay. Ecology 49:346–349.

Alonso C, Pernthaler J (2005) Incorporation of glucose under anoxic conditions by bacterioplankton from coastal North Sea surface waters. Appl Environ Microbiol 71:1709–1716.

Angel R, Claus P, Conrad R (2012) Methanogenic archaea are globally ubiquitous in aerated soils and become active under wet anoxic conditions. ISME J 6:847–62.

Angel R, Matthies D, Conrad R (2011) Activation of methanogenesis in arid biological soil crusts despite the presence of oxygen. PLoS One 6:e20453.

Ask J, Karlsson J, Jansson M (2012) Net ecosystem production in clear-water and brown-water lakes. Global Biogeochem Cycles 26:1–7.

Barkan E, Luz B (2005) High precision measurements of $^{17}O/^{16}O$ and $^{18}O/^{16}O$ ratios in H_2O. Rapid Commun Mass Sp19: 3737-3742

Barth JA, Tait A, Bolshaw M (2004) Automated analyses of $^{18}O/^{16}O$ ratios in dissolved oxygen from 12-mL water samples. Limnol Oceanogr Meth 2: 35-41

Bastviken D, Cole J, Pace M, Tranvik L (2004) Methane emissions from lakes: Dependence of lake characteristics, two regional assessments, and a global estimate. Global Biogeochem Cycles 18:GB4009.

Bastviken D, Cole JJ, Pace ML, Van de Bogert MC (2008) Fates of methane from different lake habitats: Connecting whole-lake budgets and CH_4 emissions. J Geophys Res 113:G02024.

Bastviken D, Ejlertsson J, Tranvik L (2002) Measurement of methane oxidation in lakes: A comparison of methods. Environ Sci Technol 36:3354–3361.

Bastviken D, Tranvik LJ, Downing J, et al (2011) Freshwater methane emissions offset the continental carbon sink. Science 331:50.

Battin TJ, Luyssaert S, Kaplan LA, et al (2009) The boundless carbon cycle. Nat Geosci 2:598–600.

Bender M, Grande K, Johnson K, et al (1987) A comparison for determining of four methods planktonic community production. Limnol Oceanogr 32:1085–1098.

Bender ML, Grande KD (1987) Production, respiration, and the isotope geochemistry of O_2 in the upper water column. Global Biogeochem Cycles 1:49–59.

Bender ML (1990) The $\delta^{18}O$ of dissolved O_2 in seawater: A unique tracer of circulation and respiration in the deep sea. J Geophys Res-Oceans 95: 22243-22252.

Bender M, Orchardo J, Dickson ML, Barber R, Lindley S (1999) In vitro O_2 fluxes compared with ^{14}C production and other rate terms during the JGOFS Equatorial Pacific experiment. Deep-Sea Res Pt I 46: 637-654

Benoy G, Cash K, McCauley E, Wrona F (2007) Carbon dynamics in lakes of the boreal forest under a changing climate. Environ Rev 15:175–189.

Benson BB, Krause D (1984) The concentration and isotopic fractionation of oxygen dissolved in freshwater and seawater in equilibrium with the atmosphere. Limnol Oceanogr 29:620–632.

Berg A, Lindblad P, Svensson BH (2013) Cyanobacteria as a source of hydrogen for methane formation. World J Microbiol Biotechnol. doi: 10.1007/s11274-013-1463-5

Berggren M, Lapierre J-F, del Giorgio P a (2012) Magnitude and regulation of bacterioplankton respiratory quotient across freshwater environmental gradients. ISME J 6:984–93.

Berggren M, Laudon H, Jansson M (2009) Aging of allochthonous organic carbon regulates bacterial production in unproductive boreal lakes. Limnol Oceanogr 54:1333–1342.

Beversdorf LJ, White a. E, Björkman KM, et al (2010) Phosphonate metabolism by Trichodesmium IMS101 and the production of greenhouse gases. Limnol Oceanogr 55:1768–1778.

Bocaniov SA, Schiff SL, Smith REH (2012) Plankton metabolism and physical forcing in a productive embayment of a large oligotrophic lake: insights from stable oxygen isotopes. Freshw Biol 57:481–496.

Bocaniov SA, Schiff SL, Smith RE (2015) Non steady-state dynamics of stable oxygen isotopes for estimates of metabolic balance in large lakes. J Great Lakes Res 41: 719-729

Bogard MJ, del Giorgio PA (2016) The role of metabolism in modulating CO_2 fluxes in boreal lakes. Global Biogeochem Cycles 30:1509–1525.

Borges A, Delille B, Schiettecatte LS, Gazeau F, Abril G, Frankignoulle M (2004) Gas transfer velocities of CO_2 in three European estuaries (Randers Fjord, Scheldt and Thames). Limnol Oceanogr 49: 1630–1641

Bouvier TC, del Giorgio PA (2002) Compositional changes in free-living bacterial communities along a salinity gradient in two temperate estuaries. Limnol Oceanogr 47:453–470.

Brandt JP, Flannigan MD, Maynard DG, et al (2013) An introduction to Canada's boreal zone: ecosystem processes, health, sustainability, and environmental issues 1. Environ Rev 21:207–226.

Brothers S, Vadeboncoeur Y, Sibley P (2016) Benthic algae compensate for phytoplankton losses in large aquatic ecosystems. Glob Chang Biol 1:3865–3873.

Buffam I, Turner MG, Desai AR, et al (2011) Integrating aquatic and terrestrial components to construct a complete carbon budget for a north temperate lake district. Glob Chang Biol 17:1193–1211.

Butman D, Stackpoole S, Stets E, et al (2016) Aquatic carbon cycling in the conterminous United States and implications for terrestrial carbon accounting. Proc Natl Acad Sci 113:58–63.

Cantin A, Beisner BE, Gunn JM, Prairie YT, Winter JG (2011) Effects of thermocline deepening on lake plankton communities. Can J Fish Aquat Sci 68: 260-276

Carignan R (2010) Station de biologie des Laurentides – Université de Montréal. http://www.sbl.umontreal.ca/territoire-cartes/cartes/index.html.

Carini P, White AE, Campbell EO, Giovannoni SJ (2014) Methane production by phosphate-starved SAR11 chemoheterotrophic marine bacteria. Nat Commun 5:4346.

Carpenter SR, Caraco NF, Correll DL, et al (1998a) Nonpoint pollution of surface waters with phosphorus and nitrogen. Ecol Appl 8:559–568.

Carpenter SR, Cole JJ, Kitchell JF, Pace ML (1998b) Impact of dissolved organic carbon, phosphorus, and grazing on phytoplankton biomass and production in experimental lakes. Limnol Oceanogr 43:73-80.

Chomicki KM, Schiff SL (2008) Stable oxygen isotopic fractionation during photolytic O_2 consumption in stream waters. Sci Total Environ 404:236–44.

Cole JJ, Caraco NF (1998) Atmospheric exchange of carbon dioxide in a low-wind oligotrophic lake measured by the addition of SF6. Limnol Oceanogr 43:647–656.

Cole JJ, Caraco NF, Kling GW, Kratz TK (1994) Carbon dioxide supersaturation in the surface waters of lakes. Science 265:1568–70.

Cole JJ, Pace ML, Carpenter SR, Kitchell JF (2000) Persistence of net heterotrophy in lakes during nutrient addition and food web manipulations. Limnol Oceanogr 45:1718–1730.

Cole JJ, Prairie YT, Caraco NF, et al (2007) Plumbing the Global Carbon Cycle: Integrating Inland Waters into the Terrestrial Carbon Budget. Ecosystems 10:172–185.

Conrad R (2005) Quantification of methanogenic pathways using stable carbon isotopic signatures: a review and a proposal. Org Geochem 36:739–752.

Cory RM, Ward CP, Crump BC, Kling GW (2014) Sunlight controls water column processing of carbon in arctic fresh waters. Science 345:925–928.

Cotner JB, Biddanda BA (2002) Small Players, Large Role: Microbial Influence on Biogeochemical Processes in Pelagic Aquatic Ecosystems. Ecosystems 5:105–121.

Craig H (1961) Isotopic Variations in Meteoric Waters. Science 133: 1702–1703.

Cross WF, Hood JM, Benstead JP, et al (2015) Interactions between temperature and nutrients across levels of ecological organization. Glob Chang Biol 21:1025–1040.

Damm E, Helmke E, Thoms S, et al (2010) Methane production in aerobic oligotrophic surface water in the central Arctic Ocean. Biogeosciences 7:1099–1108.

Dansgaard W (1964) Stable isotopes in precipitation. Tellus 16:436–468.

de Angelis MA, Lee C (1994) Methane production during zooplankton grazing on marine phytoplankton. Limnol Oceanogr 39:1298–1308.

del Giorgio PA, Peters RH (1994) Patterns in planktonic P:R ratios in lakes: Influence of lake trophy and dissolved organic carbon. Limnol Oceanogr 39:772–787.

del Giorgio PA, Peters RH (1993) Balance between phytoplankton production and plankton respiration in lakes. Can J Fish Aquat Sci 50:282–289.

del Giorgio PA, Williams PJB (2005) The global significance of respiration in aquatic ecosystems: from single cells to the biosphere. In: del Giorgio PA, Williams PJB (eds) Respiration in aquatic ecosystems. Oxford, New York, NY, USA, pp 267–303

DelSontro T, Boutet L, St-Pierre A, del Giorgio PA, Prairie YT (2016) Methane ebullition and diffusion from northern ponds and lakes regulated by the interaction between temperature and system productivity. Limnol Oceanogr 61(S1): S62–S77.

del Valle D, Karl D (2014) Aerobic production of methane from dissolved methylphosphonate in the water column and sinking particles collected in the North Pacific Subtropical Gyre. Aquat Microb Ecol 1–36.

Demars BOL, Gíslason GM, Ólafsson JS, et al (2016) Impact of warming on CO_2 emissions from streams countered by aquatic photosynthesis. Nat Geosci 9:758–761.

den Heyer C, Kalff J (1998) Organic matter mineralization rates in sediments : A within- and among-lake study. Limnol Oceanogr 43:695–705.

Ditchfield A, Wilson S, Hart M, et al (2012) Identification of putative methylotrophic and hydrogenotrophic methanogens within sedimenting material and copepod faecal pellets. Aquat Microb Ecol 67:151–160.

Downing JA, Rath LC (1988) Spatial patchiness in the lacustrine sedimentary environment. Limnol Oceanogr 33: 447-458

Downing JA, et al (2006) The global abundance and size distribution of lakes, ponds, and impoundments. Limnol Oceanogr 51: 2388-2397

Duarte CM, Prairie YT (2005) Prevalence of Heterotrophy and Atmospheric CO_2 Emissions from Aquatic Ecosystems. Ecosystems 8:862–870.

Dubois K, Carignan R, Veizer J (2009) Can pelagic net heterotrophy account for carbon fluxes from eastern Canadian lakes? Appl Geochemistry 24:988–998.

Falkowski P, et al (2000) The Global Carbon Cycle: A Test of Our Knowledge of Earth as a System. Science 290:291–296.

Fee EJ, Shearer JA, DeBruyn ER, Schindler EU (1992) Effects of Lake Size on Phytoplankton Photosynthesis. Can J Fish Aquat Sci 49:2445–2459.

Ferland M-E, del Giorgio PA, Teodoru CR, Prairie YT (2012) Long-term C accumulation and total C stocks in boreal lakes in northern Québec. Global Biogeochem Cycles 26:GB0E04.

Fietz S, Kobanova G, Izmest'eva L, Nicklisch A (2005) Regional, vertical and seasonal distribution of phytoplankton and photosynthetic pigments in Lake Baikal. J Plankton Res 27:793–810.

Finlay K, Leavitt PR, Patoine A, Wissel B (2010) Magnitudes and controls of organic and inorganic carbon flux through a chain of hard-water lakes on the northern Great Plains. Limnol Oceanogr 55:1551–1564.

Finlay K, Leavitt PR, Wissel B, Prairie YT (2009) Regulation of spatial and temporal variability of carbon flux in six hard-water lakes of the northern Great Plains. 54:2553–2564.

Florez-Leiva L, Damm E, Farías L (2013) Methane production induced by dimethylsulfide in surface water of an upwelling ecosystem. Prog Oceanogr 112–113:38–48.

Forget MH, Carignan R, Hudon C (2009) Influence of diel cycles of respiration, chlorophyll, and photosynthetic parameters on the summer metabolic balance of temperate lakes and rivers. Can J Fish Aquat Sci 66: 1048-1058

Fry B (2006) Stable Isotope Ecology. Springer New York

Gat JR (1996) Oxygen and hydrogen isotopes in the hydrologic cycle. Annu Rev Earth Pl Sc 24: 225-262

Gauthier S, Bernier P, Kuuluvainen T, et al (2015) Boreal forest health and global change. 819–822.

Goldman JA, Kranz SA, Young JN, Tortell PD, Stanley RH, Bender ML, Morel FM (2015) Gross and net production during the spring bloom along the Western Antarctic Peninsula. New Phytol 205: 182-191

Gorham E (1991) Northern peatlands: Role in the carbon cycle and probable responses to climatic warming. Ecol Appl 1:182–195.

Graneli W, Lindell M, Tranvik L (1996) Photo-oxidative production of dissolved

inorganic carbon in lakes of different humic content. Limnol Oceanogr 41:698–706.

Grossart HP, Frindte K, Dziallas C, et al (2011) Microbial methane production in oxygenated water column of an oligotrophic lake. Proc Natl Acad Sci USA 108:19657–61.

Gu B, Schelske CL, Hodell DA (2004) Extreme ^{13}C enrichments in a shallow hypereutrophic lake: Implications for carbon cycling. Limnol Oceanogr 49:1152–1159.

Guillemette F, McCallister SL, del Giorgio PA (2013) Differentiating the degradation dynamics of algal and terrestrial carbon within complex natural dissolved organic carbon in temperate lakes. J Geophys Res -Biogeo 118: 963-973

Guy RD, Fogel ML, Berry JA (1993) Photosynthetic Fractionation of the Stable Isotopes of Oxygen and Carbon. Plant Physiol 101:37–47.

Hanson PC, Carpenter SR, Armstrong DE, et al (2006) Lake dissolved inorganic carbon and dissolved oxygen: Changing drivers from days to decades. Ecol Monogr 76:343–363.

Hanson PC, Bade DL, Carpenter SR, Kratz TK (2003) Lake metabolism: Relationships with dissolved organic carbon and phosphorus. Limnol Oceanogr 48: 1112-1119

Hanson PC, Carpenter SR, Kimura N, Wu C, Cornelius SP, Kratz TK (2008) Evaluation of metabolism models for free-water dissolved oxygen methods in lakes. Limnol Oceanogr-Meth 6: 454-465

Harrell FE (2014) Hmisc: Harrell Miscellaneous. R package version 3.14-3. http://CRAN.R-project.org/package=Hmisc.

Heathcote AJ, Anderson NJ, Prairie YT, Engstrom DR, del Giorgio PA (2015) Large increases in carbon burial in northern lakes during the Anthropocene. Nature Comm 6: 10016.

Heathcote AJ, Giorgio PA, Prairie YT (2015) Predicting bathymetric features of lakes from the topography of their surrounding landscape. Can J Fish Aquat Sci 650:643–650.

Ho T-Y, Scranton MI, Taylor GT, et al (2002) Acetate cycling in the water column of the Cariaco Basin: Seasonal and vertical variability and implication for carbon cycling. Limnol Oceanogr 47:1119–1128.

Hoellein TJ, Bruesewitz D a., Richardson DC (2013) Revisiting Odum (1956): A

synthesis of aquatic ecosystem metabolism. Limnol Oceanogr 58:2089–2100.

Hofmann H (2013) Spatiotemporal distribution patterns of dissolved methane in lakes: How accurate are the current estimations of the diffusive flux path? Geophys Res Lett 40:2779–2784.

Holtgrieve GW, Schindler DE, Branch TA, A'mar ZT (2010) Simultaneous quantification of aquatic ecosystem metabolism and reaeration using a Bayesian statistical model of oxygen dynamics. Limnol Oceanogr 55: 1047-1063

Holtgrieve GW, Schindler DE, Hobbs WO, et al (2011) A coherent signature of anthropogenic nitrogen deposition to remote watersheds of the northern hemisphere. Science 334: 1545-1548.

Hotchkiss ER, Hall RO (2014) High rates of daytime respiration in three streams: Use of $\delta^{18}O\text{-}O_2$ and O_2 to model diel ecosystem metabolism. Limnol Oceanogr 59:798–810.

Hotchkiss ER, Hall RO, Sponseller RA, et al (2015) Sources of and processes controlling CO_2 emissions change with the size of streams and rivers. Nat Geosci 8:696–699.

Humborg C, Mörth CM, Sundbom M, et al (2010) CO_2 supersaturation along the aquatic conduit in Swedish watersheds as constrained by terrestrial respiration, aquatic respiration and weathering. Glob Chang Biol 16:1966–1978.

IPCC (2007) Climate Change 2007: The physical science basis. Contribution of Working Group I to the Fourth Assessment Report of the Intergovernmental Panel on Climate Change. Cambridge University Press, New York, NY, USA

Jahne B, Munnich Otto K, Boilnger R, et al (1987) On the Parameters Influencing Air-Water Gas Exchange. J Geophys Res 92:1937–1949.

Jankowski K, Schindler DE, Lisi PJ (2014) Temperature sensitivity of community respiration rates in streams is associated with watershed geomorphic features. Ecology 95:2707–2714.

Jansson M, Karlsson J, Blomqvist P (2003) Allochthonous organic carbon decreases pelagic energy mobilization in lakes. Limnol Oceanogr 48:1711–1716.

Jansson M, Persson L, De Roos AM, et al (2007) Terrestrial carbon and intraspecific size-variation shape lake ecosystems. Trends Ecol Evol 22:316–322.

Jobin VO, Beisner BE (2014) Deep chlorophyll maxima, spatial overlap and diversity in phytoplankton exposed to experimentally altered thermal stratification. J Plankton Res 36: 933-942

Jones RI (1992) The influence of humic substances on lacustrine planktonic food chains. In: Dissolved Organic Matter in Lacustrine Ecosystems: Energy Source and System Regulator. Springer Netherlands, Dordrecht, pp 73–91

Jones RI, Grey J, Quarmby C, Sleep D (2001) Sources and fluxes of inorganic carbon in a deep, oligotrophic lake (Loch Ness, Scotland). Global Biogeochem Cycles 15:863–870.

Jonsson A, Meili M, Bergstrom AK, Jansson M (2001) Whole-lake mineralization of allochthonous and autochthonous organic carbon in a large humic lake (Ortrasket, N . Sweden). Limnol Oceanogr 46:1691–1700.

Kankaala P, Lopez Bellido J, Ojala A, et al (2013) Variable Production by Different Pelagic Energy Mobilizers in Boreal Lakes. Ecosystems 16:1152–1164.

Karl DM, Beversdorf L, Björkman KM, et al (2008) Aerobic production of methane in the sea. Nat Geosci 1:473–478.

Karl DM, Tilbrook BD (1994) Production and transport of methane in oceanic particulate organic matter. Nature 368:732–734.

Karlsson J, Byström P, Ask J, Ask P, Persson L, Jansson M (2009) Light limitation of nutrient-poor lake ecosystems. Nature 460: 506-509

Kelly C a., Fee E, Ramlal PS, et al (2001) Natural variability of carbon dioxide and net epilimnetic production in the surface waters of boreal lakes of different sizes. Limnol Oceanogr 46:1054–1064.

Kiddon J, Bender ML, Orchardo J, Caron DA, Goldman JC, Dennett M (1993) Isotopic fractionation of oxygen by respiring marine organisms. Global Biogeochem Cycles 7: 679-694

Kirschke S, Bousquet P, Ciais P, et al (2013) Three decades of global methane sources and sinks. Nat Geosci 6:813–823.

Knox M, Quay PD, Wilbur D (1992) Kinetic Isotopic Fractionation During Air-Water Gas Transfer of O_2, N_2, CH_4, and H_2. J Geophys Res 97:335–343.

Kortelainen P, Rantakari M, Huttunen JT, et al (2006) Sediment respiration and lake trophic state are important predictors of large CO_2 evasion from small boreal lakes. Glob Chang Biol 12:1554–1567.

Kraemer BM, Chandra S, Dell AI, et al (2016) Global patterns in lake ecosystem responses to warming based on the temperature dependence of metabolism. Glob Chang Biol.

Kritzberg ES, Granéli W, Björk J, Brönmark C, Hallgren P, Nicolle A, Persson A, Hansson LA (2014) Warming and browning of lakes: consequences for pelagic carbon metabolism and sediment delivery. Freshwater Biol 59:325-36.

Kroopnick P, Craig H (1972) Atmospheric oxygen: isotopic composition and solubility fractionation. Science 175: 54-55

Lapierre JF, del Giorgio PA (2014) Partial coupling and differential regulation of biologically and photochemically labile dissolved organic carbon across boreal aquatic networks. Biogeosciences 11: 5969-5985

Lapierre J-F, del Giorgio P a. (2012) Geographical and environmental drivers of regional differences in the lake p CO_2 versus DOC relationship across northern landscapes. J Geophys Res 117:G03015.

Lapierre JF, Seekell DA, del Giorgio PA (2015) Climate and landscape influence on indicators of lake carbon cycling through spatial patterns in dissolved organic carbon. Glob Chang Biol 21:4425–4435.

Larsen S, Andersen T, Hessen DO (2011) Climate change predicted to cause severe increase of organic carbon in lakes. Glob Chang Biol 17:1186–1192.

Lauster GH, Hanson PC, Kratz TK (2006) Gross primary production and respiration differences among littoral and pelagic habitats in northern Wisconsin lakes. Can J Fish Aquat Sci 63:1130–1141.

Leavitt PR, Fritz SC, Anderson NJ, et al (2009) Paleolimnological evidence of the effects on lakes of energy and mass transfer from climate and humans. Limnol Oceanogr 54: 2330-48.

Legendre P (2014) Lmodel2: Model II Regression. R package version 1.7-2. http://CRAN.R-project.org/package=lmodel2.

Lehmann MF, et al (2009) Aerobic respiration and hypoxia in the Lower St. Lawrence Estuary: Stable isotope ratios of dissolved oxygen constrain oxygen sink partitioning. Limnol Oceanogr 54: 2157-2169

Lennon JT, Hamilton SK, Muscarella ME, et al (2013) A source of terrestrial organic carbon to investigate the browning of aquatic ecosystems. PLoS One 8:e75771. doi: 10.1371/journal.pone.0075771

Lewitus AJ, Kana TM (1995) Light respiration in six estuarine phytoplankton species: Contrasts under photoautotrophic and mixotrophic growth conditions. J Phycol 761:754–761.

Livingstone DM, Imboden DM (1996) The prediction of hypolimnetic oxygen

profiles: a plea for a deductive approach. Can J Fish Aquat Sci 53:924–932.

Luz B, Barkan E (2000) Assessment of oceanic productivity with the triple-isotope composition of dissolved oxygen. Science 288: 2028-2031

Luz B, Barkan E, Sagi Y, Yacobi YZ (2002) Evaluation of community respiratory mechanisms with oxygen isotopes: A case study in Lake Kinneret. Limnol Oceanogr 47:33–42.

Maberly SC, Barker PA, Stott AW, et al (2013) Catchment productivity controls CO_2 emissions from lakes. Nat Clim Chang 3:391–394.

Macpherson GL (2009) CO_2 distribution in groundwater and the impact of groundwater extraction on the global C cycle. Chem Geol 264:328–336.

Magnuson JJ, Robertson DM, Benson BJ, et al (2000) Historical Trends in Lake and River Ice Cover in the Northern Hemisphere. Science 289: 1743-1746.

Marchand D, Prairie YT, del Giorgio PA (2009) Linking forest fires to lake metabolism and carbon dioxide emissions in the boreal region of Northern Quebec. Glob Chang Biol 15:2861–2873.

McCallister SL, del Giorgio PA (2008) Direct measurement of the $\delta^{13}C$ signature of carbon respired by bacteria in lakes: Linkages to potential carbon sources, ecosystem baseline metabolism, and CO_2 fluxes. Limnol Oceanogr 53:1204–1216.

McDonald CP, Stets EG, Striegl RG, Butman DE (2013) Inorganic carbon loading as a primary driver of dissolved carbon dioxide concentrations in the lakes and reservoirs of the contiguous United States. Global Biogeochem Cycles 27:285–295.

Mevik BH, Wehrens R, Liland KH (2013) pls: Partial least squares and principal component regression. R package version 2.4-3. http://CRAN.R-project.org/package=pls.

Michelutti N, Wolfe AP, Vinebrooke RD, et al (2005) Recent primary production increases in arctic lakes. Geophys Res Letters 32: 19.

Michmerhuizen CM, Striegl RG, Mcdonald ME (1996) Potential methane emission from north-temperate lakes following ice melt. Limnol Oceanogr 41:985–991.

Miyajima T, Yamada Y, Wada E, et al (1997) Distribution of greenhouse gases, nitrite, and ^{13}C of dissolved inorganic carbon in Lake Biwa: Implications for hypolimnetic metabolism. Biogeochemistry 36:205–221.

Molot LA, Dillon PJ (1996) Storage of terrestrial carbon in boreal lake sediments and evasion to the atmosphere. Global Biogeochem Cycles 10:483–492.

Molot LA, Dillon PJ (1997) Photolyric regulation of dissolved organic carbon in northern lakes. Global Biogeochem Cycles 11:357–365.

Monteith DT, Stoddard JL, Evans CD, et al (2007) Dissolved organic carbon trends resulting from changes in atmospheric deposition chemistry. Nature 450:537–40.

Mook KA (1974) Carbon isotope fractionation between dissolved bicarbonate and gaseous carbon dioxide. Earth Planet Sci Lett 22:169–176.

Moss B (2012) Cogs in the endless machine: lakes, climate change and nutrient cycles: a review. Sci Total Environ 434:130–42.

Murase J, Sakai Y, Sugimoto A, et al (2003) Sources of dissolved methane in Lake Biwa. Limnology 4:91–99.

Nurnberg GK, Shaw M (1998) Productivity of clear and humic lakes: Nutrients, phytoplankton, bacteria. Hydrobiologia 382:97–112.

O'Reilly CM, Sharma S, Gray DK, et al (2015) Rapid and highly variable warming of lake surface waters around the globe. Geophys Res Lett 42:10,773-10,781.

Obrador B, Staehr PA, Christensen JPC (2014) Vertical patterns of metabolism in three contrasting stratified lakes. Limnol Oceanogr 59:1228–1240.

Odum HT (1956) Primary Production in Flowing Waters1. Limnol Oceanogr 1:102–117.

Ojala A, Bellido JL, Tulonen T, et al (2011) Carbon gas fluxes from a brown-water and a clear-water lake in the boreal zone during a summer with extreme rain events. Limnol Oceanogr 56:61–76.

Oksanen, J, et al (2013) Vegan: Community Ecology Package. R package version 2.0-10. http://cran.r-project.org, http://vegan.r-forge.r-project.org/

Oremland RS (1979) Methanogenic activity in plankton samples and fish intestines: A mechanism for in situ methanogenesis in oceanic surface waters. Limnol Oceanogr 24:1136–1141.

Ortiz-Llorente MJ, Alvarez-Cobelas M (2012) Comparison of biogenic methane emissions from unmanaged estuaries, lakes, oceans, rivers and wetlands. Atmos Environ 59:328–337.

Ostrom NE, Russ ME, Field A, Piwinski L, Twiss MR, Carrick HJ (2005) Ratios of community respiration to photosynthesis and rates of primary production in Lake Erie via oxygen isotope techniques. J Great Lakes Res 31: 138-153.

Owens NJP, Law CS, Mantoura RFC, et al (1991) Methane flux to the atmosphere from the Arabian Sea. Nature 354:293–296.

Pace ML, Prairie YT (2005) Respiration in Lakes. In: del Giorgio PA, Williams PJLB (eds) Respiration in Aquatic Ecosystems. Oxford, New York, NY, pp 103–121

Paganin P, Chiarini L, Bevivino A, et al (2013) Vertical distribution of bacterioplankton in Lake Averno in relation to water chemistry. FEMS Microbiol Ecol 84:176–88.

Parker SR, Poulson SR, Gammons CH, DeGrandpre MD (2005) Biogeochemical controls on diel cycling of stable isotopes of dissolved O_2 and dissolved inorganic carbon in the Big Hole River, Montana. Environ Sci Technol 39: 7134-7140

Perga M-E, Maberly SC, Jenny J-P, et al (2016) A century of human-driven changes in the carbon dioxide concentration of lakes. Global Biogeochem Cycles 30:93–104.

Pollard PC (2013) In situ rapid measures of total respiration rate capture the super labile DOC bacterial substrates of freshwater. Limnol Oceanogr Methods 11:584–593.

Prairie YT, Bird DF, Cole JJ (2002) The summer metabolic balance in the epilimnion of southeastern Quebec lakes. Limnol Oceanogr 47:316–321.

Prairie YT, del Giorgio PA (2013) A new pathway of freshwater methane emissions and the putative importance of microbubbles. Inl Waters 3:311–320.

Quay PD, Emerson S, Wilbur DO, Stump C, Knox M (1993) The $\delta^{18}O$ of dissolved O_2 in the surface waters of the subarctic Pacific: a tracer of biological productivity. J Geophys Res-Oceans 98: 8447-8458

Quay PD, Peacock C, Bjrkman K, Karl DM (2010) Measuring primary production rates in the ocean: Enigmatic results between incubation and non-incubation methods at Station ALOHA. Global Biogeochem Cycles 24:1–14.

Quay PD, Wilbur D, Richey JE, et al (1995) The ^{18}O:^{16}O of dissolved oxygen in rivers and lakes in the Amazon Basin: Determining the ratio of respiration to photosynthesis rates in freshwaters. Limnol Oceanogr 40:718–729.

Quiñones-Rivera ZJ, Wissel B, Justić D (2009) Development of Productivity Models

for the Northern Gulf of Mexico Based on Oxygen Concentrations and Stable Isotopes. Estuaries and Coasts 32:436–446.

Quiñones-rivera ZJ, Wissel B, Justic D, Fry B (2007) Partitioning oxygen sources and sinks in a stratified , eutrophic coastal ecosystem using stable oxygen isotopes. Mar Ecol Prog Ser 342:69–83.

Quiñones-Rivera ZJ, Finlay K, Vogt RJ, Leavitt PR, Wissel B (2015) Hydrologic, metabolic and chemical regulation of water-column metabolism and atmospheric CO_2 exchange in a large continental reservoir during spring and summer. J Great Lakes Res 41: 144-154

R Core Team (2014) R: A language and environment for statistical computing. R Foundation for Statistical Computing, Vienna, Austria.

Rasilo T, Prairie YT, del Giorgio PA (2015) Large-scale patterns in summer diffusive CH4 fluxes across boreal lakes, and contribution to diffusive C emissions. Glob Chang Biol 21:1124–1139.

Raymond PA, Hartmann J, Lauerwald R, et al (2013) Global carbon dioxide emissions from inland waters. Nature 503:355–359.

Read JS et al (2011) Derivation of lake mixing and stratification indices from high-resolution lake buoy data. Environ Modell Softw 26: 1325-1336.

Regaudie-de-Gioux A, Duarte CM (2012) Temperature dependence of planktonic metabolism in the ocean. Global Biogeochem Cycles 26:1.

Riemann L, Azam F (2002) Widespread N-acetyl-d-glucosamine uptake among pelagic marine bacteria and its ecological implications. Appl Environ Microbiol 68:5554–5562.

Robidoux M, del Giorgio PA, Derry A (2015) Landscape-level variation among crustacean zooplankton lake populations in face of a humic stressor. Freshwater Biol 60:1263-1278

Rodríguez P, Byström P, Geibrink E, et al (2016) Do warming and humic river runoff alter the metabolic balance of lake ecosystems? Aquat Sci 78:717–725.

Roehm CL, Prairie YT, del Giorgio PA (2009) The p CO_2 dynamics in lakes in the boreal region of northern Québec, Canada. Global Biogeochem Cycles 23: GB3013.

Rosseel Y (2012) lavaan: An R Package for Structural Equation Modeling. J Stat Softw 48: 1-36.

Rudd JWM, Hamilton RD (1978) Methane cycling in a eutrophic shield lake and its effects on whole lake metabolism. Limnol Oceanogr 23:337–348.

Russ ME, Ostrom NE, Gandhi H, Ostrom PH, Urban NR (2004) Temporal and spatial variations in R:P ratios in Lake Superior, an oligotrophic freshwater environment. J Geophys Res-Oceans 109: C10.

Sand-jensen K, Staehr PA (2009) in Small Danish Net Heterotrophy Lakes : A Widespread Feature Over Gradients in Trophic Status and Land Cover. Ecosystems 12:336–348.

Schindler DW (2006) Recent advances in the understanding and management of eutrophication. Limnol Oceanogr 51:356–363.

Schindler DW (1990) Experimental Perturbations of Whole Lakes as Tests of Hypotheses concerning Ecosystem Structure and Function. Oikos 57:25–41.

Schindler DW, Bayley SE, Parker BR, et al (1996) The effects of climatic warming on the properties of boreal lakes and streams at the Experimental Lakes Area, northwestern Ontario. Limnol Oceanogr 41: 1004-10017.

Schindler DW, Curtis PJ, Bayley SE, et al (1997) Climate-induced changes in the dissolved organic carbon budgets of boreal lakes. Biogeochemistry 36:9–28.

Schmid M, De Batist M, Granin NG, et al (2007) Sources and sinks of methane in Lake Baikal : A synthesis of measurements and modeling. Limnol Oceanogr 52:1824–1837.

Schmidt U, Conrad R (1993) Hydrogen, carbon monoxide, and methane dynamics in Lake Constance. Limnol Oceanogr 38:1214–1226.

Schulz M, Faber E, Hollerbach A, et al (2001) The methane cycle in the epilimnion of Lake Constance. Arch fur Hydrobiol 151:157–176.

Scranton MI, Brewer PG (1977) Occurrence of methane in the near-surface waters of the western subtropical North-Atlantic. Deep Res 24:127–138.

Seekell DA, Lapierre JF, Ask J, et al (2015) The influence of dissolved organic carbon on primary production in northern lakes. Limnol Oceanogr 60:1276–1285.

Sepers A (1977) The utilization of dissolved organic compounds in aquatic environments. Hydrobiologia 52:39–54.

Solomon CT, Bruesewitz DA, Richardson DC, et al (2013) Ecosystem respiration: Drivers of daily variability and background respiration in lakes around the globe.

Limnol Oceanogr 58:849–866.

Solomon CT, Jones SE, Weidel BC, et al (2015) Ecosystem Consequences of Changing Inputs of Terrestrial Dissolved Organic Matter to Lakes: Current Knowledge and Future Challenges. Ecosystems. 18:376-389.

Staehr PA, et al (2010) Lake metabolism and the diel oxygen technique: state of the science. Limnol Oceanogr-Meth 8: 628-644

Staehr PA, Baastrup-Spohr L, Sand-Jensen K, Stedmon C (2012a) Lake metabolism scales with lake morphometry and catchment conditions. Aquat Sci 74:155–169. doi: 10.1007/s00027-011-0207-6

Staehr PA, Testa JM, Kemp WM, et al (2012b) The metabolism of aquatic ecosystems: History, applications, and future challenges. Aquat Sci 74:15–29.

Stams AJM, Plugge CM (2009) Electron transfer in syntrophic communities of anaerobic bacteria and archaea. Nat Rev Microbiol 7:568–77.

Striegl RG, Kortelainen P, Chanton JP, et al (2001) Carbon dioxide partial and ^{13}C content of north and boreal lakes at pressure temperate ice melt spring. Limnol Oceanogr 46:941–945.

Striegl RG, Michmerhuizen CM (1998) Hydrologic influence on methane and carbon dioxide dynamics at two north-central Minnesota lakes. Limnol Oceanogr 43:1519–1529.

Stumm W, Morgan JJ (1996) Aquatic chemistry: Chemical equilibria and rates in natural waters, 3rd edn. Wiley, Hoboken, NJ, USA

Summers JC, Kurek J, Kirk JL, et al (2016) Recent warming, rather than industrial emissions of bioavailable nutrients, is the dominant driver of lake primary production shifts across the Athabasca oil sands region. PloS one 11: e0153987.

Tada Y, Grossart H-P (2013) Community shifts of actively growing lake bacteria after N-acetyl-glucosamine addition: Improving the BrdU-FACS method. ISME J 8:1–14.

Tang KW, McGinnis DG, Frindte K, et al (2014) Paradox reconsidered: Methane oversaturation in well-oxygenated lake waters. Limnol Oceanogr 59:275–284.

Taranu ZE, Zurawell RW, Pick F, Gregory-Eaves I (2012) Predicting cyanobacterial dynamics in the face of global change: the importance of scale and environmental context. Glob Chang Biol 18:3477–3490.

Teodoru CR, del Giorgio P a., Prairie YT, Camire M (2009) Patterns in pCO_2 in

boreal streams and rivers of northern Quebec, Canada. Global Biogeochem Cycles 23:GB2012.

Thauer RK, Möller-Zinkhan D, Spormann AM (1989) Biochemistry of acetate catabolism in anaerobic chemotrophic bacteria. Annu Rev Microbiol 43:43–67.

Tilbrook BD, Karl DM (1995) Methane sources , distributions and sinks from California coastal waters to the oligotrophic North Pacific gyre. Mar Chem 49:51–64.

Tobias CR, Böhlke JK, Harvey JW (2007) The oxygen-18 isotope approach for measuring aquatic metabolism in high productivity waters. Limnol Oceanogr 52: 1439-1453

Torgersen T, Branco B (2007) Carbon and oxygen dynamics of shallow aquatic systems: Process vectors and bacterial productivity. J Geophys Res Biogeosciences 112:1–16.

Tranvik LJ, Downing JA, Cotner JB, et al (2009) Lakes and reservoirs as regulators of carbon cycling and climate. Limnol Oceanogr 54:2298–2314.

Trolle D, Staehr PA, Davidson TA, et al (2012) Seasonal Dynamics of CO_2 Flux Across the Surface of Shallow Temperate Lakes. Ecosystems 15:336–347.

Turner KW, Edwards TWD, Wolfe BB (2014) Characterising Runoff Generation Processes in a Lake-Rich Thermokarst Landscape (Old Crow Flats, Yukon, Canada) using $\delta^{18}O$, $\delta^{2}H$ and d-excess Measurements. Permafr Periglac Process 25:53–59.

Utsumi M, Nojiri Y, Nakamura T, et al (1998) Oxidation of Dissolved Methane in a Eutrophic, Shallow Lake: Lake Kasumigaura, Japan. Limnol Oceanogr 43:471–480.

Vachon D, del Giorgio PA (2014) Whole-Lake CO_2 Dynamics in Response to Storm Events in Two Morphologically Different Lakes. Ecosystems 17:1338–1353.

Vachon D, Lapierre JF, del Giorgio PA (2016) Seasonality of photochemical dissolved organic carbon mineralization and its relative contribution to pelagic CO_2 production in northern lakes. J Geophys Res Biogeo 121:864–878.

Vachon D, Prairie YT (2013) The ecosystem size and shape dependence of gas transfer velocity versus wind speed relationships in lakes. Can J Fish Aquat Sci 70:1–8.

Vachon D, Prairie YT, Cole JJ (2010) The relationship between near-surface turbulence and gas transfer velocity in freshwater systems and its implications

for floating chamber measurements of gas exchange. Limnol Oceanogr 55:1723–1732.

Vadeboncoeur Y, Vander Zanden MJ, Lodge DM (2002) Putting the Lake Back Together: Reintegrating Benthic Pathways into Lake Food Web Models. Bioscience 52:44.

Van de Bogert MC, Carpenter SR, Cole JJ, Pace ML (2007) Assessing pelagic and benthic metabolism using free water measurements. Limnol Oceanogr-Meth 5: 145-155

Vasconcelos FR, Diehl S, Rodriguez P, et al (2016) Asymmetrical competition between aquatic primary producers in a warmer and browner world. Ecology 97: 2580-2592.

Venkiteswaran JJ, Wassenaar, LI, Schiff SL (2007) Dynamics of dissolved oxygen isotopic ratios: a transient model to quantify primary production, community respiration, and air–water exchange in aquatic ecosystems. Oecologia 153: 385-398

Venkiteswaran JJ, Schiff SL, Wallin MB (2014) Large carbon dioxide fluxes from headwater boreal and sub-boreal streams. PLoS One 9:22–25.

Vesterinen J, Devlin SP, Syväranta J, Jones RI (2016) Accounting for littoral primary production by periphyton shifts a highly humic boreal lake towards net autotrophy. Freshw Biol 61:265–276.

Wang X, Depew D, Schiff S, Smith RE (2008) Photosynthesis, respiration, and stable isotopes of oxygen in a large oligotrophic lake (Lake Erie, USA-Canada). Can J Fish Aquat Sci 65: 2320-2331.

Wanninkhof (1992) Relationship Between Wind Speed and Gas Exchange Over the Ocean. J Geophys Res 97:7373–7382.

Wassenaar LI, Koehler G (1999) An on-line technique for the determination of the δ18O and δ17O of gaseous and dissolved oxygen. Anal Chem 71: 4965-4968.

Wassenaar LI (2012) Dissolved oxygen status of Lake Winnipeg: Spatio-temporal and isotopic (δ18O–O 2) patterns. J Great Lakes Res 38: 123-134.

Watanabe S, Higashitani N, Tsurushima N, Tsunogai S (1995) Methane in the western north Pacific. J Oceanogr 50:39–60.

Wetzel RG (2001) Limnology: lake and river ecosystems, 3rd edn. Academic Press, London.

Wetzel RG, Likens, GE (2000) Limnolgical analysis. W.B. Saunders Co., Philadelphia.

Weyhenmeyer GA (2001) Warmer Winters: Are Planktonic Algal Populations in Sweden's Largest Lakes Affected? Ambio 30:565–571.

Weyhenmeyer GA, Fröberg M, Karltun E, et al (2012) Selective decay of terrestrial organic carbon during transport from land to sea. Glob Chang Biol 18:349–355.

Weyhenmeyer GA, Kosten S, Wallin MB, et al (2015) Significant fraction of CO_2 emissions from boreal lakes derived from hydrologic inorganic carbon inputs. Nat Geosci 8:933–936. doi: 10.1038/NGEO2582

Weyhenmeyer GA, Meili M, Livingstone DM (2004) Nonlinear temperature response of lake ice breakup. Geophys Res Lett 31:6–9.

Wilkinson GM, Buelo CD, Cole JJ, Pace ML (2016) Exogenously produced CO_2 doubles the CO_2 efflux from three north temperate lakes. Geophys Res Lett 43: 1996–2003.

Williams PJB, del Giorgio PA (2005) Respiration in aquatic ecosystems: history and background. In: del Giorgio PA, Williams PJB (eds) Respiration in Aquatic Ecosystems. Oxford, New York, NY, USA, pp 1–17

Wright RR, Hobbie JE (1966) Use of glucose and acetate by bacteria and algae in aquatic ecosystems. Ecology 47:447–464.

Yang H, Andersen T, Dörsch P, et al (2015) Greenhouse gas metabolism in Nordic boreal lakes. Biogeochemistry 126:211–225.

Yvon-Durocher G, Caffrey JM, Cescatti A, et al (2012) Reconciling the temperature dependence of respiration across timescales and ecosystem types. Nature 487:472–6.

Yvon-Durocher G, Jones JI, Trimmer M, et al (2010) Warming alters the metabolic balance of ecosystems. Phil Trans R Soc B 365: 2117-2126.

Zwart JA, Craig N, Kelly PT, et al (2016) Metabolic and physiochemical responses to a whole-lake experimental increase in dissolved organic carbon in a north-temperate lake. Limnol Oceanogr 61:723–734.